# Influence of the St. John's Wort Extract Ze117 on the Lipidome of PBMC and on the Lateral Diffusion of ß$_1$-Adrenergic Receptors in C6 Cells

**Dissertation**

zur

Erlangung des Doktorgrades (Dr. rer. nat)

der Mathematisch-Naturwissenschaftlichen Fakultät

der Rheinischen Friedrich-Wilhelms-Universität Bonn


vorgelegt von

**Hendrik Werner Bußmann**

aus

Lingen (Ems)



Bonn 2020

Angefertigt mit Genehmigung der Mathematisch-Naturwissenschaftlichen Fakultät der Rheinischen Friedrich-Wilhelms-Universität Bonn

1. Gutachter: Prof. Dr. Hanns Häberlein

2. Gutachter: Prof. Dr. Gabriele König

Tag der mündlichen Prüfung: 07.01.2021

Erscheinungsjahr: 2021

Die vorliegende Arbeit wurde in der Zeit von November 2016 bis Juli 2020 am Institut für Biochemie und Molekularbiologie der Rheinischen Friedrich-Wilhelms-Universität Bonn unter der Leitung von Herrn Prof. Dr. Hanns Häberlein angefertigt.

*Für meine Familie*

# Abstract

Stress causes pathological changes in the signal transduction of neurotransmitter systems, which can lead to depression. Signaling relies not only on receptor-ligand interactions and subsequent regulatory processes, but also on the composition of the surrounding lipid bilayer, which has a decisive influence on the behavior of receptors.
The aim of the present study was to investigate the influence of the St. John's wort extract Ze117 on the lipid composition of cortisol-stressed peripheral blood mononuclear cells (PBMC) and on the lateral mobility of $\beta_1$-adrenergic receptors ($\beta_1$AR) in C6 cells.
The influence of Ze117 on the membrane fluidity of PBMC compared to cortisol was investigated by fluorescence anisotropy measurements. Changes in phospholipids in terms of the average number of double bounds and the average chain lengths under the influence of cortisol compared to untreated control cells were analyzed by mass spectrometry. Compared to cortisol treated cells, simultaneous incubation of cells with cortisol and Ze177 was investigated.
Influence of Ze117 on lateral mobility of SNAP-tagged $\beta_1$AR in the plasma membrane of C6 cells was analysed under both non-stimulating and isoprenaline-stimulating conditions. Single particle tracking (SPT) was used to observe the lateral diffusion of $\beta_1$AR, whereby the registered trajectories were evaluated by variational Bayesian treatment of a hidden Markov model (vbSPT) and packing coefficient (Pc) analysis with respect to diffusion coefficients, receptor state occupancies and confinement.
The results of this work show that Ze117 has a decreasing effect on membrane fluidity in PBMC compared to an increased membrane fluidity after cortisol preincubation. An increased average number of double bonds and carbon atoms in fatty acids of certain phospholipid classes in cortisol pretreated cells were reversed by Ze117.
The membrane fluidity essentially depends on the phospholipid composition. Ze117 therefore normalizes the membrane fluidity of cortisol-stressed cells. In particular, the decrease in the number of double bonds in fatty acids under Ze117 suggests an increase in membrane rigidity, which counteracts the cortisol effect.
Most likely, the membrane composition also has effects on receptor systems as demonstrated by findings of SPT experiments. In C6 cells overexpressing SNAP-tagged $\beta_1$AR (SNAP-$\beta_1$AR) three individual diffusive states for SNAP-$\beta_1$AR were detected. Each state was defined by a diffusion coefficient, a corresponding state

occupancy value and the confinement area. The states were classified as an immobile state S1, a slow diffusing state S2, and a fast diffusing state S3.

After stimulation of control cells with isoprenaline, the fraction of the immobile state S1 was more pronounced compared to unstimulated cells, whereas confinement of SNAP-$\beta_1$AR was not affected. After preincubation with Ze117 the diffusion coefficients of S1 and S2 decreased compared to control cells, indicating a hindered diffusion. Additionally, the fraction of the immobile diffusive state S1 increased and the confinement area decreased, indicating regulatory responses of the cell and altered receptor environment.

The findings of this work might contribute to new insights on the pathogenesis and treatment of depression and on a new mode of action of the herbal antidepressant St. John’s wort.

# Table of contents

# List of Figures

# List of Tables

# Abbreviations

| | |
|---|---|
| **AA** | arachidonic acid |
| **AC** | adenylyl cyclase |
| **ALA** | α-linolenic acid |
| **BG** | benzylguanine |
| **BG-$NH_2$** | $O^6$-[4-(aminomethyl-)benzyl]-guanine |
| **C6 cells** | rat glioblastoma cells |
| **Cer** | ceramides |
| **DAG** | diacylglycerols |
| **DHA** | docosahexaenoic acid |
| **DMEM/F12** | Gibco Dulbecco's Modified Eagle Medium: Nutrient Mixture F-12, phenol red |
| **DMEM/F12 no phenol red** | Gibco Dulbecco's Modified Eagle Medium: Nutrient Mixture F-12, no phenol red |
| **DMF** | dimethylformamide |
| **DMI** | desipramine hydrochloride |
| **DMSO** | dimethyl sulfoxide |
| **DPH** | 1,6-diphenyl-1,3,5-hexatriene |
| **Dy-549-NHS** | DY-549P1-NHS-ester |
| **EGFR** | epidermal growth factor receptor |
| **EMA** | European Medicines Agency |
| **EMCCD** | electron multiplying charge-coupled device |
| **EPA** | eicosapentaeonic acid |
| **Escitalopram** | escitalopram oxalate |
| **EYFP** | enhanced yellow fluorescent protein |
| **FA** | fatty acids |
| **FCS** | fetal calf serum |
| **FRAP** | fluorescence recovery after photobleaching |
| **GDP** | guanosine diphosphate |
| **GFP** | green fluorescent protein |
| **GPCR** | G-protein coupled receptors |

| | |
|---|---|
| **GTP** | guanosine triphosphate |
| **HAMD** | Hamilton Rating Scale for Depression |
| **HBSS** | Hank's Balanced Salt Solution |
| **HexCer** | hexosylceramides |
| **HMPC** | Committee on Herbal Medicinal Products |
| **HPA** | hypothalamic pituitary adrenal |
| **HPLC** | high-performance liquid chromatography |
| **LC-PUFA** | long chain polyunsaturated fatty acids |
| **LPC** | lyso-phosphatidylcholines |
| **MALDI-TOF** | flight mass spectrometry |
| **MAO** | monoamine oxidase |
| **MDD** | major depressive disorders |
| **MβCD** | methyl-β-cyclodextrin |
| **NHS** | N-hydroxysuccinimide |
| **NRI** | noradrenaline reuptake inhibitors |
| **PBMC** | peripheral blood mononuclear cells |
| **PBS** | phosphate-buffered saline |
| **PC** | phosphatidylcholines |
| **Pc** | packing coefficient |
| **PC O** | phosphatidylcholine ethers |
| **PCA** | principal component analysis |
| **PDA** | 1-pyrenedecanoic acid |
| **PE** | phosphatidylethanolamines |
| **PE O** | phosphatidylethanolamine ethers |
| **PEI** | polyethylenimine |
| **PG** | phosphatidylglycerols |
| **Ph.Eur.** | European Pharmacopoeia |
| **PI** | phosphatidylinositols |
| **PLA2** | phospholipase A2 |
| **PPARγ** | peroxisome proliferator-activated receptor γ |
| **PS** | phosphatidylserines |
| **PTSD** | posttraumatic stress disorder |
| **PUFA** | polyunsaturated fatty acids |

| | |
|---|---|
| **RPMI** | Roswell Park Memorial Institute 1640 Medium |
| **SJW** | St. John's wort |
| **SNAP-$\beta_1$AR** | SNAP-tagged-$\beta_1$AR receptors |
| **SNR** | signal to noise ratio |
| **SPT** | single particle tracking |
| **SREBP** | sterol regulatory element binding-protein |
| **SSNRI** | selective serotonin-noradrenaline reuptake inhibitors |
| **SSRI** | selective serotonin reuptake inhibitors |
| **TAG** | triacylglycerols |
| **TCA** | tricyclic antidepressants |
| **vh** | vertical and horizontal |
| **vv** | vertical and vertical |
| **WHO** | World Health Organisation |
| **Ze117** | Ze117, Hypericum perforatum extract, batch-no. V803900 |
| **$\beta_1$AR** | $\beta_1$-adrenergic receptor |
| **$\beta_2$AR** | $\beta_2$-adrenergic receptor |

# 1 Introduction

Depressive disorders are mental disorders characterized by a state of clearly low mood as well as reduced interest and drive over a longer period of time. This is often associated with a wide range of physical complaints, such as cardiovascular diseases [1]. Patients with depressive disorders are usually affected by their illness in their entire life. They are often not able to cope with everyday tasks, they suffer from strong self-doubt, concentration problems and a tendency to worry. More than almost any other disease, depression is accompanied by a high level of suffering, as this disease has a central impact on the well-being and self-esteem of affected patients [2].

Depression is one of the most common diseases, but at the same time the most underestimated one in terms of its individual and social significance. The annual incidence of depressive disorders in Germany is one or two cases per 100 persons [2]. The risk of developing some form of depressive disorder during the course of a lifetime is 16 to 20%, both nationally and internationally [3,4]. According to a current study on the health of adults in Germany (DEGS1), the lifetime risk of being diagnosed with depression is 11.6% [5]. According to this study, about 8.1% of the population between the ages of 18 and 79 are currently suffering from depressive symptoms. The number of people in Germany who have suffered from unipolar depression over a period of 12 months is approximately 6.2 million [6]. According to numerous studies, women are more often affected by depressive disorders than men [2]. With a 12-month prevalence of unipolar depression of 10.6%, their risk of developing the disease is twice as high as that of men with 4.8% [7]. Also, recent studies suggest that there is especially a higher risk of depressive episodes for girls and young women compared to their male counterparts [8]. Girls are probably more exposed to risk factors before the beginning of adolescence such as consequences of their upbringing or experiences of abuse, which in view of the many changes and challenges in adolescence may favor the development of depression [9]. Alarmingly, 15- to 19-year-old women have the highest rate of attempted suicide [2]. Nevertheless, in general it can be said that depression occurs at any age. Both the time of the initial illness and the course of the depression vary greatly from person to person. However, 50% of all depressive patients in Germany fall ill with depression for the first time before the age of 31 [2]. Unfortunately, depression often leads to one or more secondary diseases. Above all, other

psychological disorders such as anxiety or eating disorders, or medication and drug abuse must be mentioned [2]. In addition, depressive patients show an increased risk of somatic diseases. A study by the World Health Organisation (WHO) showed that the risk of developing a physical impairment is 1.8 times higher one year after a depressive illness [10].

Depression does not comprise a homogeneous clinical picture. Explanatory hypotheses can be assigned to simplified biological and psychological models, although none of these approaches has so far been able to provide a convincing monocausal explanation [2,9]. The heterogeneity of the symptoms of depressive disorders also makes it unlikely that one factor alone is responsible for the development of depression. Therefore, it is assumed that depression arises due to an interaction of biological and psychosocial factors. The significance of the different factors can vary considerably from patient to patient. In this respect, the concept of depression covers a broad spectrum of mental disorders, ranging from biologically determined diseases to a combination of different factors and psychosocially determined diseases [2].

However, it is generally accepted that many cases of depressions are to some sort due to disorders in the brain monoaminergic system. Pharmacological findings with the antihypertensive drug reserpine led to the monoaminergic theory of depression that a lack of monoaminergic neurotransmitters in the synaptic cleft is responsible for depressive behavior. The mechanism of action of reserpine is based on the reduced store of biogenic amines such as the neurotransmitters dopamine, serotonin and noradrenaline. Patients with high blood pressure who had not suffered from depression prior therapy with reserpine, showed depressive symptoms after being treated with the drug. This hypothesis was supported by findings that first tricyclic antidepressants (TCA) and monoamine oxidase (MAO) inhibitors caused short term increase in synaptic concentrations of monoamines, which resulted in attenuated symptoms of depression [11].

It is therefore not surprising that today's pharmacological therapy of depressions mainly affects the monoaminergic transmitter system. The German therapeutic S3 guideline for "Unipolar Depression" divides antidepressants into six groups: TCA, selective serotonin reuptake inhibitors (SSRI), MAO inhibitors, other antidepressants, lithium salts and phytotherapeutics [2].

TCA inhibit the reuptake of serotonin, norepinephrine and dopamine [12]. Compared to SSRI, TCA have a higher potential for side effects and are therefore no longer first-line therapeutics [13]. In cases of severe depression where therapy with SSRI is not successful TCA are still used. SSRI prevent the reuptake of released serotonin at the presynaptic membrane. MAO inhibitors block the enzyme MAO, which degrades the neurotransmitters serotonin, noradrenaline, and dopamine in the central nervous system. Accordingly, blocking this enzyme increases the concentration of these neurotransmitters in the brain [14]. Under "other antidepressants", various substance groups with different mechanisms of action are summarized, e.g. the selective serotonin-noradrenaline reuptake inhibitors (SSNRI), tetracyclic antidepressants and noradrenaline reuptake inhibitors (NRI). Lithium salts are mainly used in the phase of prophylaxis of recurrent depression as well as for the augmentation of an inadequate therapy with an antidepressant [2].

The German therapeutic S3 guideline also recommends phytopharmaceutical St. John's wort (SJW) extracts for a first therapeutic attempt in mild and moderate depressive episodes [2]. The monograph of the European Pharmacopoeia (Ph. Eur.) defines Hyperici herba as the above-ground parts of *Hypericum perforatum* L., harvested during the flowering period [15]. For the dried drug a minimum content of 0.08% total hypericins is required, calculated as hypericin. For extraction methanol (50 to 80%) or ethanol (50 to 80%) are used as extracting agents. The extract must have a minimum content of 0.1 to 0.3% of total hypericins, expressed as hypericin and 6% flavonoids, expressed as rutin and must not exceed a maximum content of 6% hyperforin.

SJW is one of the phytopharmaceuticals with the best clinical evidence. In the past decades, many clinical studies have been carried out to prove the antidepressant effectiveness of SJW extracts. In a prospective, randomized, double-blind, parallel grouped, placebo-controlled study, Schrader et al. (1998) found out that 56% of the patients responded to a 6-week treatment with the standardized SJW extract Ze117, compared to 15% in the placebo group [16].

Woelk et al. (2000) found in a prospective, randomized, double blind, parallel group-controlled trial that Ze117 was equivalent to imipramine in its effectiveness in treating mild to moderate depression. Ze117 was also better tolerated [17].

In another randomized, controlled, double-blind trial, 70 patients suffering from mild to moderate depression received one tablet of either a commercially available SJW extract (Calmigen®, Denmark) or fluoxetine hydrochloride (Prozac®, United States of America) twice a day for 6 weeks [18]. Depressive symptoms were evaluated using the Hamilton Rating Scale for Depression (HAMD). Both therapies significantly improved depressive symptoms. The authors of the study concluded that the Hypericum preparation was therapeutically equivalent to fluoxetine and therefore represented a rational alternative to synthetic antidepressants.

A Cochrane review based on 29 trials with 5489 patients in total showed that SJW preparations are as effective as synthetic antidepressants, but show fewer adverse effects [19]. Thus, SJW extract, which has been traditionally mainly used in German speaking countries was as well included in therapeutic guidelines of other countries: SJW extract is recommended in the USA as a drug for patients with mild to moderate depression who prefer not to use conventional synthetic antidepressants [20]. The Canadian therapeutic guideline speaks of Level 1 evidence to support the first-line use of SJW as monotherapy in mild to moderate major depressive disorders (MDD) [21].

Pharmacological preclinical research supports the clinically observed antidepressant effects of SJW [22]. The efficacy of SJW seems to be based on a number of parallel mechanisms of action, which in turn are triggered by different ingredients. Confirmation of antidepressive effects was found *in vivo* in rodent models such as a forced swimming test, an open field test, a tail suspension test or a model of stress-related reduced memory performance [22]. However, the overall effect could not be assigned to a single ingredient or substance class identified in the extract. The efficacy of SJW is therefore obviously defined by a range of parallel mechanisms of action, triggered by different constituents. Thus, compared to synthetic active ingredients, the extract has the potential to act on multiple targets via multiple ingredients.

The mode of action of SJW has been in part elucidated by many *in vitro* studies. In a study by Chang et al. (2010) the effect of hypericin, a major active constituent of SJW, on the glutamate release from nerve terminals purified from rat cerebral cortex was examined [23]. Hyperfunction of the central glutamate system can occur in depression and it is known that antidepressant effects can be achieved by the reduction of central glutamate neurotransmission. The authors demonstrated that hypericin inhibited the release of glutamate.

*In vitro* studies have also shown that SJW inhibits the reuptake of serotonin, noradrenalin and dopamine into the presynaptic neuron. This has been shown in a study with rat cortical brain slices and radio-labeled neurotransmitters [24]. As a result, the concentration of neurotransmitters in the synaptic cleft increases and intensifies the signal transduction to the postsynaptic neuron. These mechanisms are similar to those of synthetic antidepressants and target the hypothesized neurotransmitter deficiency in depression patients.

Another mode of action is the post-synaptic downregulation of β-adrenergic receptors (βAR). This means that βAR are less expressed on the cell surface and can not interact with the neurotransmitters in the synaptic cleft. In a study by Kientsch et al. (2001), it was shown that a seven-day incubation of C6 cells with desipramine resulted in a reduction of βAR numbers to 65 ± 6%. Similarly, Ze117 led to a downregulation of βAR of 56 ± 9% compared to untreated control cells [25]. In post-synaptic neurons, the diminution of β-adrenoreceptors reduces the “adrenergic stress” and mediates effects that naturally oppose serotonin-mediated effects. Reduction of sympathic inflow on neurotransmission is likely to contribute to decrease depressive symptoms.

Another study by Prenner et al. (2007) examined the influence of SJW constituents hyperforin and hyperoside on $\beta_2$-adrenergic receptor ($\beta_2$AR) ligand binding by fluorescence correlation spectroscopy (FCS). They found that preincubation with both constituents, similar to desipramine, led to a significant reduction of ligand binding to $\beta_2$AR and a reduced formation of the second messenger cAMP, which was not due to receptor internalization. This was mainly observed in high-affinity receptor-ligand complexes with hindered lateral mobility in the cell membrane. They also observed a reduced lateral diffusion of $\beta_2$AR in C6 cells after preincubation with desipramine, hyperforin and hyperoside [26]. Jakobs et al. (2013) observed in rat C6 cells a reduced fraction of $\beta_1$-adrenergic receptors ($\beta_1$AR) diffusing with fast diffusion coefficients by FCS [27].

The $\beta_1$AR plays an important role in the pathophysiology of depressive disorders and is the most abundant adrenergic receptor subtype in the mammalian brain [28]. Several classical synthetic antidepressants such as TCA and MAO inhibitors are known to downregulate $\beta_1$AR density in certain brain regions after long-term treatment [29–32].

The $\beta_1$AR belongs to the vast group of G-protein coupled receptors (GPCRs). As their name implies, GPCRs interact with G-proteins in the plasma membrane. When a ligand binds to the binding site of a GPCR, the receptor changes its conformation. This change triggers the interaction between the GPCR and nearby G-proteins. Most G-proteins that associate with GPCRs are heterotrimeric. This means they have three different subunits: an α-subunit, a β-subunit, and a γ-subunit. The α- and γ-subunits are attached to the plasma membrane by lipid anchors. In the absence of a ligand, guanosine diphosphate (GDP) attaches to the α-subunit, and the entire G-protein-GDP complex binds to a nearby GPCR. This arrangement persists until a ligand binds to the GPCR. At this point, a change in the conformation of the GPCR activates the G-protein, and guanosine triphosphate (GTP) physically replaces the GDP bound to the α-subunit. As a result, the G-protein subunits dissociate into two parts: the GTP-bound α-subunit and a βγ-dimer. Both parts remain anchored to the plasma membrane, but they are no longer bound to the GPCR, so they can now diffuse laterally to interact with other membrane proteins. In the case of $\beta_1$AR, the receptor binds to Gαs proteins. When activated Gαs stimulates adenylyl cyclase (AC) which leads to the production of the second messenger cAMP.

$\beta_1$AR, among other GPCRs have been intensively investigated. The advent of optical methods allows us to directly investigate the dynamics of GPCR signaling in living cells. Thus, a more complex scenario than previously thought has been revealed, where GPCR accumulate in nanodomains located in biological membranes, in which they interact with their signaling partners, with each other and with their surrounding molecules [33].

A central theory in GPCR signaling is the ternary complex model [34,35]. This model describes the idea that receptors and G-proteins interact via random collisions in the absence of agonists. After ligand binding to the receptor, the so called ternary complex is stabilized and consists of an active receptor, a G-protein, and the ligand. Depending on the stability of the complex, this model allows several possible scenarios ranging from short interactions to long-lived receptor-G-protein complexes [33]. Also, whether receptor and G-protein are located in the same membrane domain or not influences the probability of interaction significantly. Thus, the membrane composition and protein distribution in it play an important role in the regulation of GPCR signaling.

Another important aspect is related to receptor dimerization. GPCR have long been considered as monomeric receptors. However, new results indicate that receptors can associate into dimers or higher-order oligomers [36,37]. This has been associated with GPCR trafficking, cell surface expression and signaling [36–38]. In addition to homomers, heterodimers of different receptors appear. In a review by Naumenko et al. (2014) the interplay between serotonin 5-HT1A and 5-HT7 receptors in depressive disorders was discussed. It was shown that 5-HT1A and 5-HT7 receptors form homo- and heterodimers both *in vitro* and *in vivo* using coimmunoprecipitation, bioluminiscence resonance energy transfer and Förster resonance energy transfer techniques. The authors came to the conclusion that heterodimerization has been shown to play an important role in regulation of receptor-mediated signaling and internalization, suggesting the implication of heterodimerization in the development and maintenance of depression [39].

With the upcoming of new microscopic methods with improved signal-to-noise ratio, sensitive cameras, and bright fluorophores, such phenomenona can also be investigated by single particle tracking (SPT) methods. They allow the investigation of GPCR signaling in living cells with single-molecule sensitivity and high spatio-temporal resolution [33].

In most SPT experiments fluorescently labeled molecules, e.g. receptors, are recorded by a fast, highly sensitive electron multiplying charge-coupled device (EMCCD) camera. The emitted fluorescence signals result in diffraction limited spots and are automatically localized by a software based on their fluorescence intensity profile (Figure 1-1). In classical microscopy the maximal resolution between two spots is about 200 nm, according to Abbe’s law, which is dependent on the used wavelength and the numeric aperture. However, the fluorescence signals appear as diffraction limited spots of which the brightness is Gaussian distributed around a maximum value in the center. The exact position of a spot can therefore be determined with higher precision via fitting a two-dimensional Gaussian distribution. The localization precision in SPT experiments is consequently typically in the range of 10 to 30 nm, which is about ten times higher than the resolution limit of light microscopy [33]. The localization of the fluorescence signals is repeated on each image of the image series. The receptors detected in this way are linked from image to image to form trajectories by automatic tracking algorithms. Finally, diffusion properties, such as diffusion coefficients and

confinement sizes can be characterized by statistically evaluating thousands of trajectories. There is not a single diffusion coefficient which describes the diffusion of the receptor best. Instead, the receptor population is characterized by different diffusion states, with different diffusion coefficients. These states reflect the heterogeneity of plasma membrane domains and the interaction of the receptor with its environment.

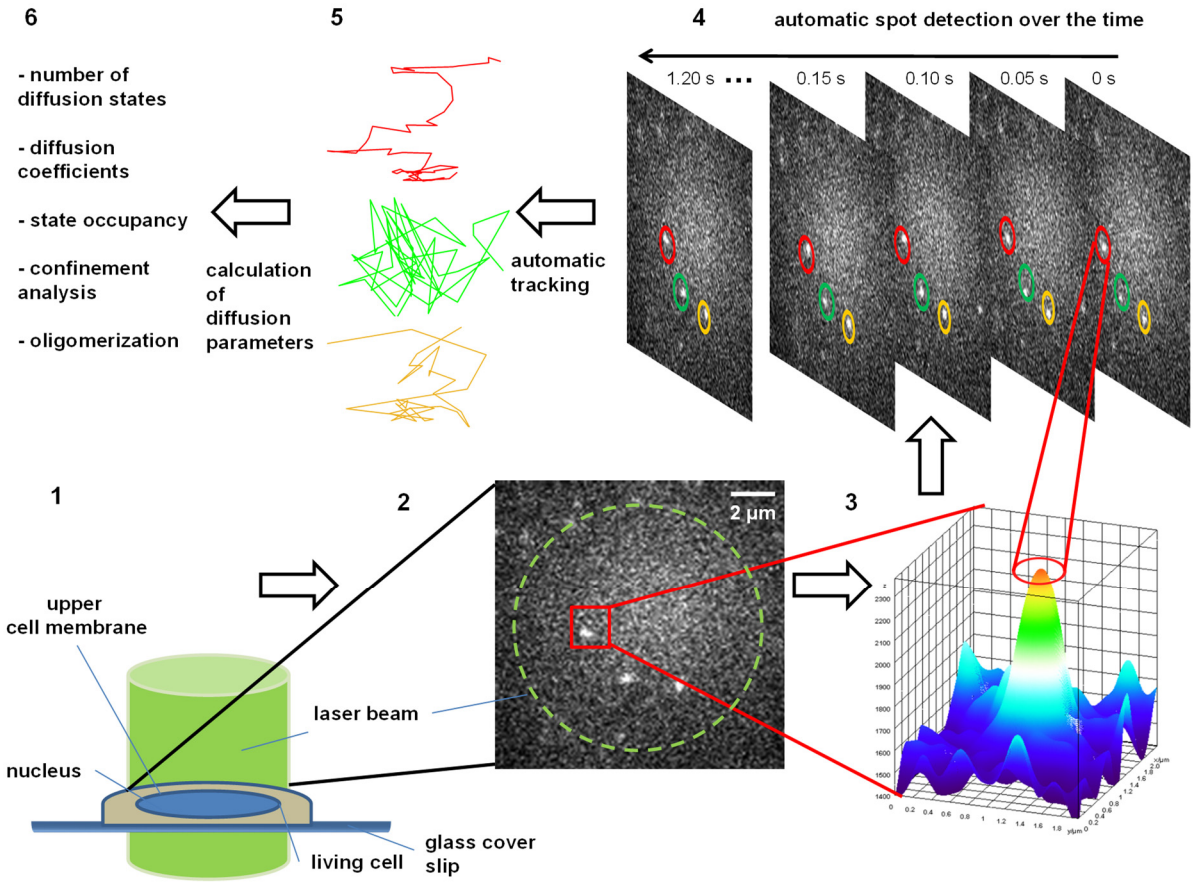


**Figure 1-1 Generation and evaluation of SPT data** 1: The upper plasma membrane of a living cell is focused under the microscope. The fluorophores coupled to the receptor are excited by a laser. 2: The emitted photons of the tagged receptors are detected by an EMCCD camera. 3: The fluorophores are automatically localized by software based on their fluorescence intensity profile. Their exact position is determined via fitting of a 2D Gaussian distribution. 4: The localization of the fluorescence signals is repeated on each image of the image series. 5: The receptors detected in this way are linked from image to image to form trajectories. 6: The diffusion properties of the receptor can be characterized by statistically evaluating thousands of trajectories.

All important steps in the signaling of GPCR from the initial ligand binding to the production of second messengers take place at the plasma membrane. Thus, interactions of GPCR with elements of the plasma membrane, such as lipids and

membrane proteins most likely influence GPCR signaling [33]. Hence, the composition of the membrane plays a key role in the development and treatment of diseases.

Recent advances in the mass spectrometric analysis of lipids (lipidomics) and the subsequent bioinformatic evaluation make it possible to obtain increasingly detailed information about the lipid composition of different cell types and tissues.

In fact, there is increasing evidence that altered lipid compositions in patients correlate with the occurrence of depressive disorders. In a meta analysis of 14 clinical studies by Lin et al. (2010) it was shown that polyunsaturated long chain fatty acid moieties of samples from red blood cells, membranes, blood phospholipids or cholesteryl esters in depressive patients were significantly altered compared to healthy subjects [40]. Knowles et al. (2017) analyzed mass-spectrometry lipidomic data of plasma samples to evaluate the genetic overlap between 23 biological distinct lipid classes and a dimensional scale of MDD. The authors found that alterations in the lipidome are not secondary to the manifestation of MDD, but rather share etiology with the illness [41]. In a review summarizing preclinical and clinical lipidomic studies Walther et al. (2018) concluded that lipidomics was emerging as a powerful approach to identify a diagnostic biomarker for MDD [42]. They described the inflammatory and glucocorticoid system to be potential pathways linking the lipidome to MDD. However, they pointed out that the current prediction power was still insufficient to extract clinically applicable lipid biomarkers for MDD and more research in this field had to be done.

One reason for the changes in lipid composition and the associated altered membrane properties could be an increased stress level. The hypothalamic pituitary adrenal (HPA) axis is hyperactivated by chronic stress resulting in increased circulation of catecholamines and glucocorticoids [43].

In healthy subjects the HPA axis mediates and regulates sustained stress response, providing metabolic support by mobilizing glucose from energy stores by glycogen degradation [44] and suppressing growth, cell maturation and the immune response [45]. However, extreme and prolonged stress exposure and subsequent chronic upregulation of glucocorticoids induce adaptive changes resulting in long-term consequences increasing overall risk on psychopathology of multiple stress-related mental illnesses like depression and posttraumatic stress disorder (PTSD) [45].

This hyperactivity is related to an increased corticotropin-releasing hormone signaling and impaired glucocorticoid receptor-mediated negative feedback. The following chronic glucocorticoid exposure has also been demonstrated to modulate membrane properties. In this context several studies have demonstrated a changed membrane fluidity after chronic preincubation with glucocorticoids using different cell types, e.g. lymphocytes, [46], HeLa cells [47], and intestinal membranes [48].

Membrane fluidity refers to the motion of the membrane bilayer and is mainly dependent on cholesterol content, the phospholipid composition and the saturation and chain length of the fatty acid moieties. Alterations in membrane fluidity are therefore a strong indication of changes in the lipid composition of the plasma membrane.

An established tool for gaining information about membrane fluidity in living cells are fluorescence anisotropy measurements. Fluorescence anisotropy is based upon the phenomenon that excitation with polarized light again results in polarized emission from the excited-state population of fluorophores. With increasing rotational mobility during the absorption transition moment, the emitted light is distributed more strongly within different polarization planes [49]. A popular approach to study membrane fluidity uses water-insoluble fluorescent probes which spontaneously partition into the membrane and gauge the movement of their surrounding microenvironment. 1,6-diphenyl-1,3,5-hexatriene (DPH) is one of the most suitable probes for polarization studies due to its low solubility and quenched emission in water [49]. Once DPH enters the hydrocarbon core of phospholipids located in the plasma membrane its fluorescence intensity increases due to the hydrophobic environment within the lipid bilayer [50,51]. The rod-like structured DPH arranges itself parallel to the alkyl chains of the phospholipids on the outer bilayer leaflet [50,51]. This orientation makes DPH very sensitive to angular reorientations of the long axis of the neighboring acyl chains [50,52].

Keksel et al. (2018) investigated the influence of cortisol on the membrane fluidity of C6 cells by fluorescence anisotropy measurements with a DPH probe [53].

They showed that plasma membrane fluidity in C6 cells increased when chronically exposed to the stress hormone cortisol. An opposite effect was seen for C6 cells chronically incubated with Ze117. The cortisol mediated effect was reversed when C6 cells were co-incubated with cortisol and Ze117 [53].

# 2 Aim and Approach

Stress causes pathological changes in the signal transduction of neurotransmitter systems which can lead to depression. Neurotransmitter signaling relies not only on receptor-ligand interactions and subsequent regulatory processes, but also on the composition of the lipid bilayer in which the receptor is embedded and which has a decisive influence on the receptor behavior. It has been shown that plasma membrane fluidity in several cell systems increases when chronically exposed to the stress hormone cortisol. There is also growing evidence that altered lipid compositions in patients correlate with the occurrence of depressive disorders. St. John's wort (SJW) preparations are widely used in the treatment of mild and moderate depressive disorders. However, the exact mode of action has not yet been elucidated.

One aim of this study was to investigate whether cortisol and the antidepressant Ze117 affect the membrane fluidity of peripheral blood mononuclear cells (PBMC) differently. Membrane fluidity was assessed by fluorescence anisotropy measurements applying DPH (1,6-diphenyl-1,3,5-hexatriene), which gauges the dynamic behavior of the surrounding lipid microenvironment of the plasma membrane.

Changes in the plasma membrane of PBMC were further investigated by a comprehensive mass spectrometric lipidome analysis (lipidomics) of cortisol and Ze117 preincubated PBMC. Quantitative lipidomic data of 893 membranous and storage lipid species were assessed. Changes in the number of double bonds and the average chain length of fatty acid moieties of phospholipids would explain alterations in membrane fluidity.

The $\beta_1$-adrenergic receptor ($\beta_1$AR) plays an important role in the development and treatment of depression. Being a G-protein coupled receptor embedded in the membrane, the activity and lateral diffusion of the $\beta_1$AR are dependent on the composition of the membrane. If Ze117 changes the composition of the plasma membrane, it is likely that it has a decisive influence on the lateral diffusion of the receptor. Thus, the lateral diffusion of $\beta_1$AR in the plasma membrane of cortisol and Ze117 pretreated cells was investigated by single particle tracking.

# 3 Material and Methods

## 3.1 Solutions

**Table 3-1 Solutions**

| Name | Abbreviation | Supplied by | Reference Number |
|---|---|---|---|
| Fetal calf serum | FCS | Gibco | 10270 |
| Gibco Dulbecco's Modified Eagle Medium: Nutrient Mixture F-12, phenol red | DMEM/F12 | Gibco | 11320-033 |
| Gibco Dulbecco's Modified Eagle Medium: Nutrient Mixture F-12, no phenol red | DMEM/ F12 no phenol red | Gibco | 21041-025 |
| Glutamax 100x | Glutamax | Gibco | 35050061 |
| Hank’s Balanced Salt Solution | HBSS | Gibco | 14025050 |
| L-glutamine | - | Gibco | 25300054 |
| Polyethyleneimine | PEI | Sigma-Aldrich, Darmstadt, Germany | 408727 |
| Penicillin-Streptomycin 10000 U/ml | P/S | Gibco | 15140122 |
| | | | |

| | | | |
|---|---|---|---|
| Roswell Park Memorial Institute 1640 Medium | RPMI | Gibco | 31870-025 |
| Trypsin EDTA 0.05 %, phenol red | Trypsin | Gibco | 25300104 |

## 3.2 Chemicals

**Table 3-2 Chemicals**

| Name | Abbreviation | Supplied by | Reference Number |
|---|---|---|---|
| 1,6-diphenyl-1,3,5-hexatriene | DPH | Sigma-Aldrich, Darmstadt, Germany | D208000 |
| $O^6$-[4 (amino-methyl)-benzyl]-guanine | BG-$NH_2$ | New England Biolabs, Ipswich, Massachusetts, USA | S9148S |
| cortisol | - | Sigma-Aldrich, Darmstadt, Germany | C-106 |
| desipramine hydrochloride | DMI | Sigma-Aldrich, Darmstadt, Germany | D3900 |
| DY-549P1-NHS-ester | Dy-549-NHS | Dyomics (MoBiTec), Jena, Germany | 549P1-01A |
| escitalopram oxalate | escitalopram | Biozol, Eching, Germany | TRC-C505010 |
| methyl-β-cyclodextrin | MβCD | Sigma-Aldrich, Darmstadt, Germany | C4555 |
| Ze117, Hypericum perforatum extract, batch-no. V803900 | Ze117 | Max Zeller Söhne AG (Romanshorn; Switzerland) | - |

## 3.3 Cell lines

**Table 3-3 Cell lines**

| Name | Abbreviation | Supplied by |
|---|---|---|
| Rat glioblastoma cells | C6 cell | Leibniz Institute DSMZ-German Collection of Microorganisms and Cell Cultures GmbH |
| Primary Peripheral Blood Mononuclear Cells (human) | PBMC | ATCC, Manassas, Virginia, USA |

## 3.4 Fluorescence anisotropy

### 3.4.1 Cell culture

Frozen aliquots of $2x10^7$ peripheral blood mononuclear cells (PBMC) were thawed in a 37 °C water bath and rinsed with 1 ml ice cold HBSS supplemented with 20% fetal calf serum (FCS). The suspension was transferred into a conical tube and was centrifuged at 4 °C at 300 g to a cell pellet. The pellet was washed with phosphate buffered saline (PBS) and then suspended in 10 ml RPMI medium supplemented with 10% FCS, 2 mM L-glutamine, 100 units/ml penicillin and 100 µg/ml streptomycin. PBMC were cultured in cell culture flasks with vented caps (Sarstedt, Nürnbrecht, Germany, reference: 83.3919.502) at 37 °C in a humid atmosphere containing 5% $CO_2$. All steps of cell cultivation and processing were performed under sterile conditions using only prewarmed (37 °C) solutions.

Chronic incubation of PBMC was performed for at least 4 days using cell culture medium enriched with 25 µg/ml Ze117 and 1 µM cortisol. To each series of chronic experiments a corresponding untreated control was prepared. Solvents were individually added to each condition and to the untreated control to reach a uniform solvent concentration of max. 0.1% MeOH and 0.25% EtOH.

After 4 days fluorescence anisotropy measurements were performed. Therefore, cell suspension was transferred into a conical tube and was centrifuged at room temperature at 300 g to pellet cells. The pellet was resuspended in HBSS containing 2.5 µM 1,6-diphenyl-1,3,5-hexatriene (DPH). Afterwards, cells were incubated for another 20 minutes at 37 °C in a humid atmosphere containing 5% $CO_2$.

Cholesterol depletion was performed by adding methyl-β-cyclodextrin (MβCD) to the cell suspension at a concentration of 1 mM 15 minutes prior to fluorescence anisotropy measurements.

### 3.4.2 Fluorescence anisotropy measurements on cells in suspension

The fluorescence anisotropy measurements were performed with a PerkinElmer LS55 fluorescence spectrometer (L-configuration). The fluorescence spectrometer was equipped with a circulation thermostat with stirring unit, which heated the cell suspension to a constant 37 °C during the measurements and ensured that the cells were evenly distributed. The absorption polarizer was fixed to vertical and the emission polarizer could be adjusted variably vertically or horizontally. Because of that the possible polarization filter configurations were vertical and vertical (vv) or vertical and horizontal (vh). For the measurement with DPH the excitation wavelength was set to $\lambda_{ex}$= 360 nm. The emission wavelength was set to $\lambda_{em}$: 430 nm.

The measurements started 5 minutes after placing the cuvette in the cuvette holder of the spectrometer. This ensures that the temperature was equalized by the heating device. For each experiment 10 individual anisotropy measurements were performed, measuring intensities *I vv* and *I vh*.

Anisotropy *r* was calculated as follows:

$$\boldsymbol{Anisotropy\ r} = \frac{\boldsymbol{I\ vv - I\ vh}}{\boldsymbol{I\ vv + 2 \cdot I\ vh}} \quad \text{(Equation 1)}$$

### 3.4.3 Data processing and statistics

Raw data were processed by Excel (Microsoft office 2013, Redmond, WA, USA). Ten fluorescence anisotropy measurements of one experiment were pooled and the mean value was calculated. At least three individual experiments were performed. For statistical analysis the unpaired t-test was performed using the Prism V.6 software (GraphPad, La Jolla, CA, USA). Results significantly different from their corresponding control groups are marked by * $p \leq 0.05$.

## 3.5 Lipidomics

### 3.5.1 Cell culture

Frozen aliquots with PBMC containing 25 million cells each were thawed in a 37 °C water bath and rinsed with 10 ml ice cold HBSS supplemented with 20% fetal calf serum (FCS). The suspension was transferred into a conical tube and was centrifuged at 4 °C at 300 g to pellet cells. The pellet was washed with PBS and cells were counted with a Neubauer counting chamber. Five million cells were suspended in 20 ml RPMI medium supplemented with 15% FCS, 2 mM L-glutamine, 100 units/ml penicillin and 100 µg/ml streptomycin. The cell suspension was transferred in an upright standing 75 $cm^2$ culture flask (Corning, USA) and cultivated at 37 °C and 5% $CO_2$.

On the first day of the experiment, five cell culture flasks with five million cells each were available. Cortisol or Ze117 was added to the medium in the respective culture flask according to the following scheme, resulting in five different conditions, namely a control condition, 1 µM cortisol, 1 µM cortisol plus 0.01 mg/ml Ze117, 1 µM cortisol plus 0.025 mg/ml Ze117, and 1 µM cortisol plus 0.05 mg/ml Ze117 (Table 3-4). Solvents were individually added to each condition and to the untreated control, to reach a uniform solvent concentration. This procedure resulted in five experimental cohorts.

**Table 3-4 Different incubation conditions prior lipidomic analysis**

| condition | cortisol | Ze117 | | |
|---|---|---|---|---|
| | [1 µM] | [0.01 mg/ml] | [0.025 mg/ml] | [0.05 mg/ml] |
| 1 | - | - | - | - |
| 2 | + | - | - | - |
| 3 | + | + | - | - |
| 4 | + | - | + | - |
| 5 | + | - | - | + |

After four days of preincubation, the cells were prepared for mass spectrometry: The cells were each washed twice in PBS and centrifuged. Then the cells were resuspended in PBS, resulting in a cell concentration of 3000 cells/µl. The cell suspensions were transferred into 1.5 ml Eppendorf vessels and shock frozen using liquid nitrogen. Until shipment the cells were stored at -80 °C.

### 3.5.2 PBMC lipids analyzed by mass spectrometry

The samples were analyzed by the commercial mass spectrometry provider Lipotype (Lipotype GmbH, Dresden, Germany). The lipidomic analysis provided by Lipotype consisted of the automated extraction of samples, an automated direct sample infusion and high-resolution Orbitrap mass spectrometry including lipid class-specific internal standards to assure absolute quantification of lipids. The software LipotypeXplorer was used for identification of lipids in the mass spectra. The equipment and software used in the study are listed in Table 3-5.

**Table 3-5 Software and equipment used for lipidomic analysis**

| Analysis step | Equipment or software |
|---|---|
| Extraction | Hamilton Robotics STARlet |
| Sample infusion | Advion Triversa Nanomate |
| Mass spectrometry | Thermo Scientific Q-Exactive |
| Lipid identification software | LipotypeXplorer |
| Data processing | Lipotype LIMS and Lipotype Zoom |

#### 3.5.2.1 Lipid extraction

Lipid extraction was performed, as explained by Eijsing et al. (2009), using chloroform and methanol mixtures [54]. Class specific internal standards were spiked to the samples before extraction. Prior to spectrometric analysis, lipid extracts were dried and suspended in a mass spectrometry acquisition mixture.

#### 3.5.2.2 Spectra acquisition

Spectra acquisition was performed on a hybrid quadrupole/Orbitrap mass spectrometer equipped with an automated nano-flow electrospray ion source in both positive and negative ion mode.

#### 3.5.2.3 Data processing and normalization

Lipid identification was performed by an inhouse software on unprocessed mass spectra. Lipid identification was either based on the molecular masses of intact molecules or by inclusion of the collision induced fragmentation of lipid molecules.

Prior to normalization and further statistical analysis of lipid species, lipid identifications were filtered according to mass accuracy, occupation threshold, noise and background. Lipid quantification was carried out using internal lipid class standards.

The amounts in pmoles of individual lipid molecules of a given lipid class were summed to yield the total amount of the lipid class. The amounts of the lipid classes were normalized to the total lipid amount yielding mol% per total lipids.

#### 3.5.2.4 Principal component analysis

For the principal component analysis (PCA) only mol% values of the lipidomic analysis were used. These were given in a master table for each test condition. The data were imported into MATLAB software (version R2016b, MathWorks, Nattic, Massachusetts, USA) for this purpose.

To generate a meaningful PCA, only lipid species whose values for each of the test conditions were above the detection limit were used. This means that lipids that were not recorded for at least one condition were not included in the PCA evaluation. For the PCA the Z-scores of the measured values were calculated using the MATLAB software. The principal components 1 and 2 were calculated using the MATLAB PCA tool. Principal components 1 and 2 were then plotted in a two-dimensional coordinate system.

#### 3.5.2.5 Average number of double bonds of fatty acid moieties

The average number of double bonds within a lipid class $DB_{av}$ was calculated by the following equation:

$$\boldsymbol{DB_{av} = \frac{DB\ mol\%}{\sum_{i=1}^{n} DB_i\ mol\%_i}} \qquad \text{(Equation 2)}$$

where DB is the number of double bonds of a lipid species within the lipid class and mol% is the mol% value of the respective lipid species.

#### 3.5.2.6 Average chain length of fatty acid moieties

The average number of the fatty acid chain length ($CL_{av}$) within a lipid class was calculated as follows:

$$\boldsymbol{CL_{av} = \frac{N_c\ mol\%}{\sum_{i=1}^{n} N_{c_i}\ mol\%_i}} \qquad \text{(Equation 3)}$$

Where $N_c$ is the number of carbon atomes of a lipid species within the lipid class and mol% is the mol% value of the respective lipid species.

#### 3.5.2.7 Volcano plots

The *p*-values and fold changes for the volcano plots were calculated using a software script based on the R software environment (R Foundation for Statistical Computing, Vienna, Austria). In order to decrease the false discovery rate, p-values were corrected according to the Benjamini-Hochberg procedure. The calculations were done by the Core Unit for Bioinformatics Data Analysis of the University of Bonn.

The values were then imported into MATLAB (version R2016b, MathWorks, Nattic, Massachusetts, USA). The volcano plots were generated using the MATLAB volcano plot tool.

#### 3.5.2.8 Statistics

Results significantly different from their corresponding control groups are marked by *p ≤ 0.05. Raw data were processed by Excel (Microsoft office 2013, Redmond, WA, USA). For statistical analysis the unpaired t-test was performed using the Prism V.6 software (GraphPad, La Jolla, CA, USA).

## 3.6 Single particle tracking

### 3.6.1 General cell culture

C6 cells were cultured in 10 cm culture dishes containing 10 ml culture medium at 37°C in a humid atmosphere containing 5% $CO_2$. The culture medium consisted of DMEM/F12, supplemented with 5% FCS, 2 mM L-glutamine, 100 units/ml penicillin and 100 µg/ml streptomycin. Cell cultivation and processing were performed under sterile conditions using prewarmed media and trypsinization solutions. The cells were splitted every three to four days in a 1:20 ratio when cell confluency reached 80 to 95%.

### 3.6.2 Synthesis of BG-Dy549

DY-549P1-NHS ester (Dyomics, Jena) was suspended in dried DMF to a concentration of 10 mM. BG-$NH_2$ was suspended in dried DMF to a concentration of 15 mM. Before starting the coupling reaction, an equimolar portion of triethylamine from a 1:100 (v / v) solution was added to the BG-$NH_2$ solution. To start the reaction, 20 µl of each the DY-549P1-NHS ester and BG-$NH_2$ solution were combined and allowed to stand overnight at 30 °C.

The reaction mixture was dried using a vacuum centrifuge, then resuspended in 100 µl of 9:1 water/acetonitrile. High-performance liquid chromatography (HPLC) was conducted to purify the desired product on an Agilent Series 1200 HPLC system

equipped with a degasser (G1322A), a quaternary pump (G1311A), an autosampler (G1329A), and a photodiode array detector (G1315D) using a LiChrospher RP-18 column (5 µm, 125 x 4 mm, Merck, Darmstadt). The following eluents were used: eluent A water/acetonitrile (22:1, v/v), adjusted to pH = 2 with phosphoric acid and eluent B acetonitrile. A linear gradient was used: initial 5% B, 0 – 15 min to 25% B, 15 – 16 min to 100% B, 16 – 25 min 100% B.

Identity of the product was confirmed by MALDI-TOF mass spectrometry. MALDI-TOF mass spectrometry was performed on an autoflex III smartbeam (Bruker Billerica, Massachusetts, USA) equipped with flexControl software. Spectra analysis was performed with the flexAnalysis software (Bruker). BG-Dy549 was again dried in a vacuum centrifuge, dissolved in DMSO (100 µM) and stored at -20 °C.

### 3.6.3 Transformation

For DNA amplification of the plasmid coding for SNAP-$\beta_1$AR (Figure 3-1), 1 ng of DNA was gently mixed with 80 µl of frozen competent XL-1 blue bacteria. The mixture was incubated on ice for 30 min. The mixture was heat shocked for 30 s at 42 °C and suddenly cooled on ice for 1 min.

Nine-hundred µl of prewarmed LB medium was added and the mixture was incubated in a shaker at 37 °C for 1 h. The suspension was centrifuged at 3500 g for 5 minutes. The pellet was resuspended in 50 µl prewarmed LB medium. Afterwards, the mixture was spread on agar-LB-medium plates (1.5 % w/v agar in LB-medium) containing ampicillin and incubated at 37 °C overnight.

Single clones arised from single bacterial cells and were picked and incubated each in 5 ml LB-medium containing 50 µg/ml ampicillin and incubated at 37 °C overnight in a shaker. The next day 500 µl of the preculture was added to 25 ml fresh, antibiotic containing LB-medium and allowed to grow for 8 h.

Plasmid DNA was isolated by a midi prep isolation kit (Qiagen®) according to the manufacturer's instructions and digested with the suitable restriction enzymes. The

correct insert size was verified by agarose gel electrophoresis in comparison to a DNA standard ladder.

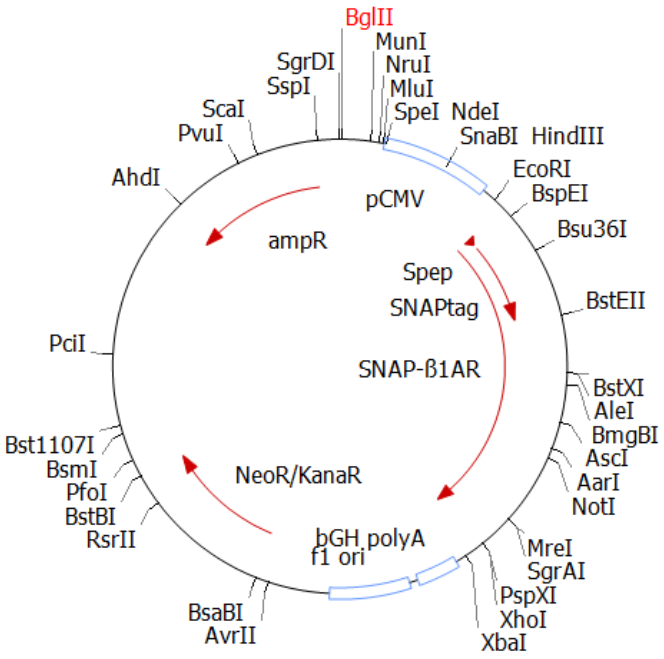


**Figure 3-1 Plasmid card of a vector encoding for a SNAP-$\beta_1$AR fusion protein.** Calebiro et al. (2013) kindly provided the plasmid [37].

### 3.6.4 Transfection

C6 cells were transfected by the polyethyleneimine (PEI) method. Cells were seeded in 12-well plates and allowed to attach for 24 h. Before transfection, the medium was changed to 1000 µl fresh fully supplemented medium. One µg of plasmid DNA and 2 µl of PEI solution (1 mg/ml) were mixed and added to cells in a 12-well plate containing 1 ml of medium.

After 24 h the medium was changed to fully supplemented medium containing G418 (600 µg/ml). After one week of selection, a single clone was picked by trypsinization in a cloning ring and seeded in a 6-well plate for further cultivation.

### 3.6.5 Fluorescence imaging

To test the plasmid and the SNAP-tag substrate BG-Dy549 a SNAP-tag staining of C6 cells transfected with a plasmid coding for SNAP-$\beta_1$AR was performed. Cells were seeded on heat sterilized round coverslips (# 1, diameter 18 mm, Marienfeld, Lauda-Königshofen) in 12 x multiwell dishes (Nunclon™, Nunc, Wiesbaden) with DMEM/F12 without phenol red, supplemented with 5% FCS, 2 mM L-glutamine, 100 units/ml penicillin and 100 µg/ml streptomycin. A number of 25.000 cells per well was chosen for a confluency of about 80 - 90% after five days. The cultivation took place in the incubator at 37 °C, 5% $CO_2$ and saturated air humidity.

The staining was performed 5 days after seeding, at a confluency of about 80%. SNAP-$\beta_1$AR over-expressed in C6 cells were fluorescently labeled by preparing a solution of 2.5 µM BG-Dy549 in clear DMEM/F12 and incubating at 37 °C and 5% $CO_2$ for 20 minutes. The cells were then washed 3 times with 500 µl PBS. The coverslip was then placed in a custom-made mounting bracket, covered with 300 µl PBS and imaged at 25 °C.

Fluorescence imaging was performed with an Axiovert® 200 M microscope equipped with a Colibri.2® LED system, LD Achroplan 40x, NA 0.60 Corr objective, AxioCamMR3® camera filter set 43 (Excitation: G 545, Beam Splitter: FT 570 Emission: BP 605/70). The system was operated with Axiovision® Rev. 4.8. All parts mentioned were from Carl Zeiss Microscopy GmbH, Jena, Germany.

### 3.6.6 SNAP staining and premeasurement procedures

For single particle tracking experiments, cells were seeded on heat sterilized round coverslips (# 1, diameter 18 mm, Marienfeld, Lauda-Königshofen) in 12 x multiwell dishes (Nunclon ™, Nunc, Wiesbaden) with DMEM/F12 without phenol red, supplemented with 5% FCS, 2 mM L-glutamine, 100 units/ml penicillin and 100 µg/ml streptomycin. A number of 25.000 cells per well was chosen for a confluency of about

80 - 90% after five days. The cultivation took place in the incubator at 37 °C, 5% $CO_2$ and saturated air humidity.

C6 SNAP-$\beta_1$AR were pretreated for 5 days with 0.25 mg/ml Ze117, 1 µM escitalopram, 1 µM desipramine, or 1 µM cortisol. In contrast, 1 mM methyl-β-cyclodextrin (MβCD) was given to the cells 30 min prior to SPT measurements. The stock solutions of Ze117, escitalopram and desipramine contained 50% ethanol. The cortisol stock solution was prepared in 100% methanol. The stock solution of MβCD was prepared in PBS. The control cells were treated with the same volume of solvents.

For appropriate spot densities and lower background signal a labeling solution of 10 nM BG-Dy549 in clear medium was freshly prepared. Cells were incubated with labeling solution for 10 minutes at 37 °C and then washed with PBS for three times. The coverslip was then placed inside a custom mounting bracket, which was filled with PBS and immediately imaged at 20 °C. To avoid photobleaching before image acquisition, cells were searched and focused to the epical membrane in transmitted light, before opening the laser shutter and starting the recording. Image sequences were acquired with a frame rate of 20 Hz. The cells on the coverslip were used no longer than 45 minutes. Within this time 10 cells were recorded. Cells showing either unusually low spot densities or areal fluorescent artifacts were generally discarded.

### 3.6.7 Single particle tracking settings

All SPT data were recorded with an EMCCD camera (iXon DV-860DCS-BV, Andor Technology), being part of a custom-built setup, which used an inverted widefild epifluorescence microscope (TE2000-S, Nikon) equipped with a water immersion objective (Plan APO VC, 60x, 1.2 NA, Nikon) and a 200-mm-focal length tube lens. Due to a 4x-magnification lens (VM Lens C-x, Nikon), the setup had an effective magnification of 240x, translating to a pixel width of 100 nm. A 532 nm continuous wave laser (LasNova GLK 2350 T01, 532 nm, 50 mW) was used. Intensity was regulated using an acousto-optic tunable filter (AA Opto-Electronic) and set to 0.733 kW/cm² in the object plane. Cells were imaged in phosphate buffered saline on 18 mm glas coverslips (# 1, diameter 18 mm, Marienfeld, Lauda-Königshofen). To avoid

photobleaching before image acquisition, cells were searched and focused to the epical membrane in transmitted light, before opening the laser shutter and starting the recording. Image sequences were acquired with a frame rate of 20 Hz.

### 3.6.8 Spot detection and tracking

The MATLAB software (version R2016b, MathWorks, Nattic, Massachusetts, USA) was used for the generation of 2-dimensional particle tracks from image data and further diffusion analysis. Images were directly imported by the u- track package [55] and processed using the following settings: 1.32 px spot radius, 3 frame rolling window time-averaging for local maxima detection, 2 frame minimum track segment length, 1 frame maximum gap length, other settings on default.

To identify discrete diffusive states from particle tracks, variational Bayes single particle tracking was applied using the vbSPT Matlab package [56]. Tracks were thereby segmented and variably classified to one of three states according to their momentary diffusion speed. Higher order models were recognized by the program but not used, since they resulted in degenerate states of insignificant occupancy and indistinct diffusion behaviour. The following settings in the *runinput*-file were used: *timestep* = 0.05, *dim* = 2, *trjLmin* = 2, *runs* = 24, *maxHidden* = 3, *bootstrapNum* = 100, *fullBootstrap* = 0.

### 3.6.9 Confinement analysis

For the analysis of confinement, the previously classified track segments were extracted and pooled by their respective diffusion states. The recently introduced packing coefficient Pc was used as a measurement of spatial confinement strength. The packing coefficient (*Pc*) at each time point *i* was calculated as

$$Pc_i = \sum_{i}^{i+n-1} \frac{(x_{i+1}-x_i)^2+(y_{i+1}-y_i)^2}{S_i^2}$$ (Equation 4).

In this equation *xi* and $y_i$ are the coordinates at time *i*. $x_{i+1}$ and $y_{i+1}$ are the coordinates at time *i + 1* and *n* is the length of the time window. $S_i$ is the surface area of the convex hull of the trajectory segment between time points *i* and *i + 1*. $S_i$ was calculated using the convhull function in MATLAB (version R2016b, MathWorks, Nattic, Massachusetts, USA) [57].

A window length of 10 points (0.5 s) was chosen, which was long enough to yield stable results and still include sufficient numbers of track segments. To determine $Pc_{80}$-values given by the 80th percentile of packing coefficients, random walk data based on the previously determined vbSPT state diffusion coefficients and segment lengths was simulated. The derived $Pc_{80}$-values were then used as a threshold to classify tracks as spatially confined. Confined tracks ($Pc > Pc_{80}$) were then compared by their average hull areas, again by averaging on the 0.5 s timescale.

### 3.6.10 Simulation

Three receptor states with diffusion coefficients of 0.016 µm²/s for S1, 0.034 µm²/s for S2, and 0.168 µm²/s for S3 were generated. For S1, S2, and S3 relative occupancy value of 0.21, 0.73, and 0.06 were simulated, respectively. The model values were based on the experimentally obtained data. 2000 trajectories were generated. To take photobleaching into account, an exponential distribution with the mean track length of 7.4 was assumed. All generated spots were subjected to a localization error by a normally distributed positional offset with σ = 20 nm in each dimension. Values for diffusion coefficients and occupancies were derived from averaged vbSPT analysis results of the real data. For the simulation of vbSPT data the track simulation algorithm provided in the vbSPT package was used.

Confinement was modeled for the respective track segments of each state with particles diffusing out of bounds being deflected towards the center. The mean

confinement size was defined as the square root of a circular confinement area specified as 80 nm for S1 and 120 nm for S2. Confinement fractions were simulated with 50, 60, 70 and 90% for each S1 and S2. The track lengths were modeled by an exponential distribution with $\mu_{D1}$ = 17.0 frames, $\mu_{D2}$ = 7.0 frames and$\mu_{D3}$ = 2.4 frames with a minimal track length of 2 frames.

### 3.6.11 Spot intensity histogram analysis

For the detection of monomers, dimers and higher order models, the spot intensities generated by uTrack were plotted as a histogram for each independent experiment. The distribution was fitted by a Gaussian mixture model using a script in MATLAB (version R2016b, MathWorks, Nattic, Massachusetts, USA). Spot intensity histogram fit was optimized by variation of the number of components.

### 3.6.12 SPT statistics

Depending on the data set the one-way ANOVA or student's t-test was performed using the GraphPad Prism V.6 software (GraphPad, La Jolla, CA, USA). Values with $p \leq 0.05$ were significantly different from their corresponding controls.

# 4 Results

## 4.1 Fluorescence anisotropy measurements

Stress causes pathological changes in the signal transduction of neurotransmitter systems, which can lead to depression [58]. Neurotransmitter signaling relies not only on receptor-ligand interactions and subsequent regulatory processes, but also on the composition of the lipid bilayer in which the receptor is embedded and which has a decisive influence on the receptor behavior [33,59]. Keksel et al. (2019) showed in their work that plasma membrane fluidity in C6 cells increased when chronically exposed to the stress hormone cortisol [53]. An opposite effect was seen for C6 cells chronically incubated with St. John´s wort extract Ze117. The cortisol mediated effect was reversed when C6 cells were co-incubated with cortisol and Ze117 (Figure 4-1) [53].

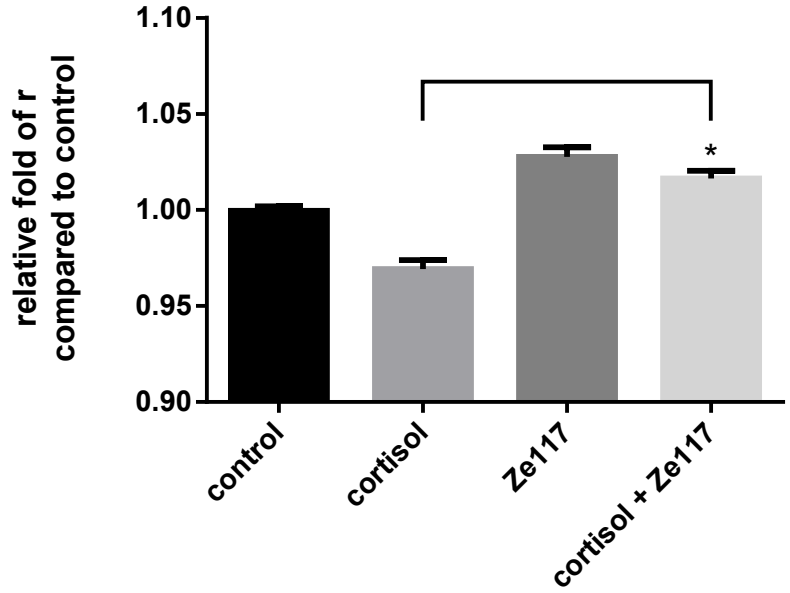


**Figure 4-1 Membrane fluidity of C6 cells:** Relative fold of fluorescence anisotropy within adherent C6 cells after chronic (6 – 8 days) exposure to 1 µM cortisol or 0.05 mg/ml Ze117 and a corresponding combination of both using 2.5 µM DPH, compared to untreated control. Results of at least 6 samples from at least 2 independent experiments were pooled and are presented as mean ± SEM. *Marked values of occupancies are significantly different from corresponding unstimulated condition with $p \leq 0.05$ determined by student's t-test. Figure from Keksel et al. [53].

Peripheral blood mononuclear cells (PBMC) are frequently used for diagnostics in clinical research. That is why it is interesting to see if changes in membrane fluidity after Ze117 or cortisol preincubation can also be observed in PBMC.

Thus, changes of the plasma membrane fluidity of commercially available PBMC chronically exposed to cortisol and Ze117 were assessed by fluorescence anisotropy measurements. For this purpose DPH (1,6-diphenyl-1,3,5-hexatriene) was applied as a fluorescent membrane probe.

### 4.1.1 Evaluation of fluorescence anisotropy measurements

In order to evaluate whether changes in membrane fluidity can generally be measured in PBMC suspension, fluorescence anisotropy was measured before and after 10 min pretreatment with 5 mM methyl-β-cyclodextrin (MβCD). MβCD causes cholesterol depletion from the plasma membrane and consequently has a strong effect on membrane fluidity, which is reflected by reduced fluorescence anisotropy values. DPH was used at a concentration of 2.5 µM. MβCD pretreatment significantly decreased the relative fluorescence anisotropy to 0.522 ± 0.011 compared to the control (Figure 4-2). Changes in membrane fluidity of PBMC were therefore detectable in suspension.

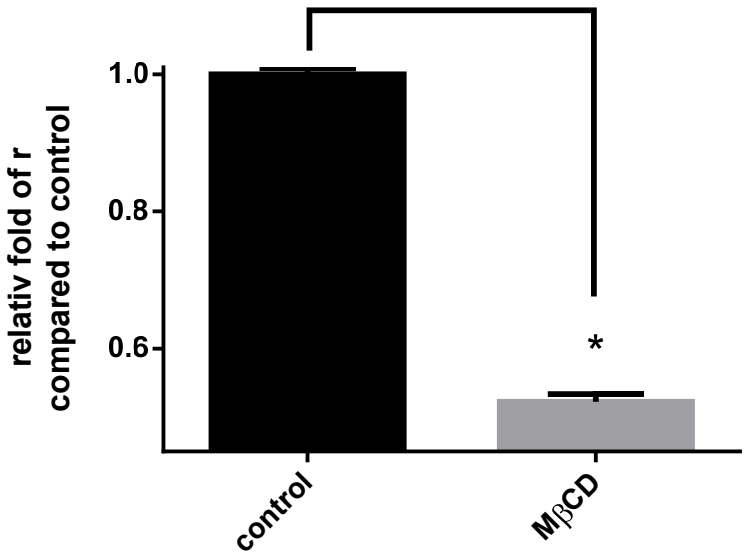


**Figure 4-2 Membrane fluidity of PBMC influenced MβCD:** Relative fold of fluorescence anisotropy of untreated PBMC (control) and after treatment with 10 mM MβCD using 2.5 µM DPH. Results of 30 samples from 3 independent experiments were pooled and are presented as mean ± standard deviation. *Marked values of occupancies are significantly different from corresponding unstimulated condition with $p \leq 0.05$ determined by student's t-test.

### 4.1.2 Changes in membrane fluidity of PBMC after cortisol and Ze117 preincubation

PBMC that were pretreated with 1 µM cortisol for 4 days showed a significant decrease in fluorescence anisotropy to 0.926 ± 0.018 compared to the control (Figure 4-3).

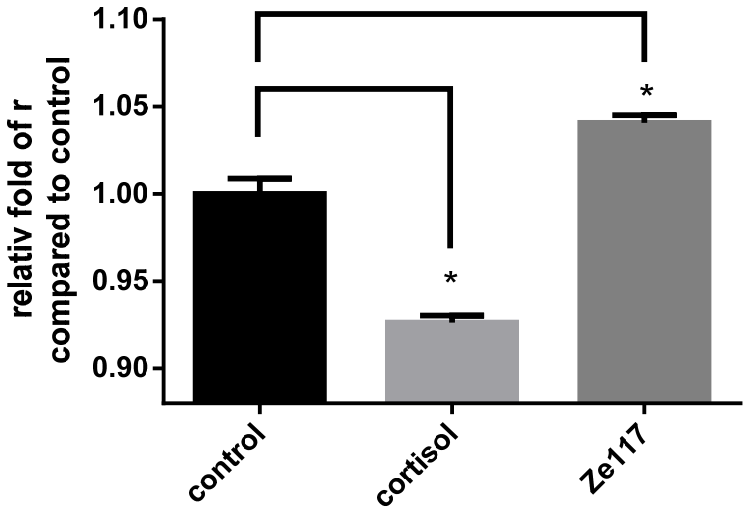


**Figure 4-3 Membrane fluidity of PBMC influenced by cortisol and Ze117:** Relative fold of fluorescence anisotropy of untreated PBMC (control) and after treatment with 1µM cortisol and 0.05 mg/ml Ze117 using 2.5 µM DPH. Results of at least 20 samples from at least 3 independent experiments were pooled and are presented as mean ± standard deviation. *Marked values of occupancies are significantly different from corresponding unstimulated condition with $p \leq 0.05$ determined by student's t-test.

An opposite effect was observed after 4 days of incubation with 0.05 mg/ml Ze117. Fluorescence anisotropy significantly increased to 1.041 ± 0.004 compared to control leading to a significant plasma membrane rigidification (Figure 4-3).

## 4.2 Changes in the lipidome of PMBC after cortisol and Ze117 preincubation

Keksel et al. (2019) demonstrated the influence of Ze117 on the membrane fluidity of C6 cells by changed molecular structures of fatty acid moieties of membranous phosopholipids [53]. In the present work this approach was further investigated by a comprehensive lipidomic analysis of cortisol and Ze117 preincubated PBMC. By co-incubation of cortisol with Ze117 it was investigated whether Ze117 counteracts a possible cortisol-induced change in the lipid composition of PBMC.

### 4.2.1 Experimental setup of lipidomic analysis

PBMC were preincubated with 1 µM cortisol for four days prior to the lipidomic analysis. In addition, PBMC were co-incubated for 4 days with 1 µM cortisol and Ze117 in concentrations of 0.01 mg/ml, 0.025 mg/ml and 0.05 mg/ml, respectively. The different incubation conditions are summarized in Table 3-4. Considering the control condition, five different experimental conditions were applied, which were repeated in five independent cohorts leading to 25 samples in total.

Mass spectrometry analyses delivered quantitative lipidomic data of membranous and storage lipid species. A list of all lipid classes analyzed in this experiment is presented in Table 4-1. In total, 893 lipid species were analysed.

**Table 4-1 Alphabetical list of analyzed lipid classes**

| | |
|---|---|
| Ceramide | Phosphatidate |
| Cholesterol esters | Phosphatidylcholine (-ether) |
| Diacylglycerol | Phosphatidylglycerol |
| Hexosylceramide | Phosphatidylinositol |
| lyso-Phosphatidylethanolamine (-ether) | Phosphatidylserine |
| lyso-Phosphatidylglycerol | Sphingomyelin |
| lyso-Phosphatidylinositol | Triacylglycerol |

### 4.2.2 Principal component analysis

In order to get a first overview of the complex data set, a principal component analysis (PCA) was performed.

PCA is a procedure of multivariate statistics. Its purpose is to structure, simplify and illustrate large data sets by approximating a large number of statistical variables – in this case 893 lipid species – by a smaller number of linear combinations. These combinations are called principal components. By definition the first principal component has the largest possible variance. Each subsequent principal component has the highest possible variance under the condition that it is orthogonal to the preceding principal components. Samples that differ greatly in their variables can often be separated by one principal component. On the other hand, if the samples differ only slightly, they will be very close to each other on the respective principal component. To cover a greater variability of the data, it is often advisable to correlate two or more principal components. This can be easily visualized in two- or three-dimensional plots.

PCA can be used to test whether samples differ due to different pretreatments or due to systematic errors. For example, if all samples with the same pretreatment scatter around one value of the principal component, it is likely that this is due to the respective pretreatment. At the same time, if samples of one of several experimental days or one

of several experimental cohorts scatter around one value of the principal component, a systematic error must be considered.

By calculating the principal components 1 and 2 of all samples of the present analysis the formation of three clusters was observed (Figure 4-4). The first cluster contained all samples of cohort 2. The second cluster contained samples of cells preincubated with Ze117. The third cluster contained samples of the control and cortisol condition.

For this reason, the samples of cohort 2 were excluded from further data analysis. PCA also revealed that preincubation with cortisol probably only had a small effect on the lipidome of PBMC. Co-incubation with cortisol and Ze117 in contrast had a more pronounced effect.

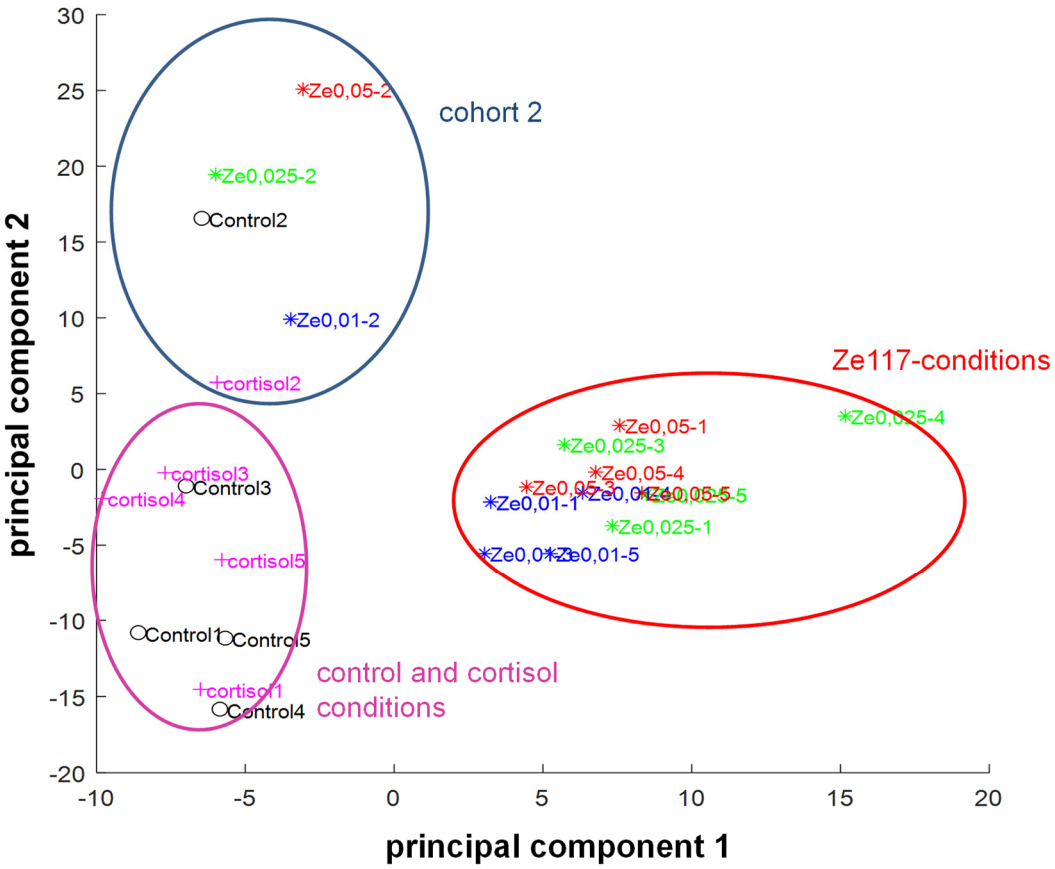


**Figure 4-4 Principal component analysis:** 2D Scatter plot with the principal components 1 and 2 of all 25 samples. The following five conditions were included in each experimental cohort: Control (o), cortisol (+) and cortisol with 0.01 mg/ml Ze117 (*), 0.025 mg/ml Ze117 (*) and 0.05 mg/ml Ze117 (*), respectively. A clustering of the samples preincubated with Ze117 was observed, which is marked with a red circle. The samples of the control and cortisol condition also form a cluster, which is circled in pink. All samples of cohort 2 form an own cluster (blue circle).

### 4.2.3 Effect of cortisol and cortisol/Ze117 combination on double bonds and chain lengths of fatty acids in lipid classes of PBMC

Changes in the fatty acid composition within lipid classes indicate species remodeling. Thus, influences of cortisol and the cortisol/Ze117 combination, respectively, on the average chain length and the number of double bonds of fatty acids were analyzed for every lipid class. The evaluation was based on quantitative values of each lipid species relative to total amounts of the respective lipid classes assessed by mass spectometry analysis. According to scientific literature both chain lengths and double bonds of fatty acids within lipidomic studies are described as robust and resilient parameters [60,61]. Hence, small differences indicate changes in the lipid metabolism of the cell. Only lipid classes containing at least 10 species above the mass spectrometric detection limit were considered for the evaluation.

#### 4.2.3.1 Phosphatidylcholines and phosphatidylethanolamines

Compared to the control, a significant increase in the average chain length from 35.31 ± 0.06 to 35.40 ± 0.02 and a significant increase in the average number of double bonds from 2.42 ± 0.010 to 2.48 ± 0.03 within phosphatidylcholines (PC) was found for cortisol treated PBMC (Figure 4-5). In contrast, the average chain length after co-incubation with 1 µM cortisol and 50 µg/ml Ze117 was brought to control level, indicating a significant counteracting effect of Ze117. In lower concentrations up to 10 µg/ml Ze117 a comparable effect was observed. A clear dose-response relationship is therefore missing. In addition, the average number of double bonds after preincubation with cortisol and 50 µg/ml Ze117, respectively, was reduced to the control level. Remarkably, with lower Ze117 concentrations the decrease in the average number of double bonds was more pronounced.

In cortisol pretreated PBMC both the average chain length and the average number of double bonds of phosphatidylethanolamines (PE) were not affected, compared to control. In contrast, after cortisol/Ze117 pretreatment the average chain length was reduced dose-dependently from 37.76 ± 0.05 to 37.63 ± 0.03 compared to cortisol

pretreated cells. Similarly, the average number of double bonds decreased dose-dependently and significantly from 3.76 ± 0.05 to 3.642 ± 0.02.

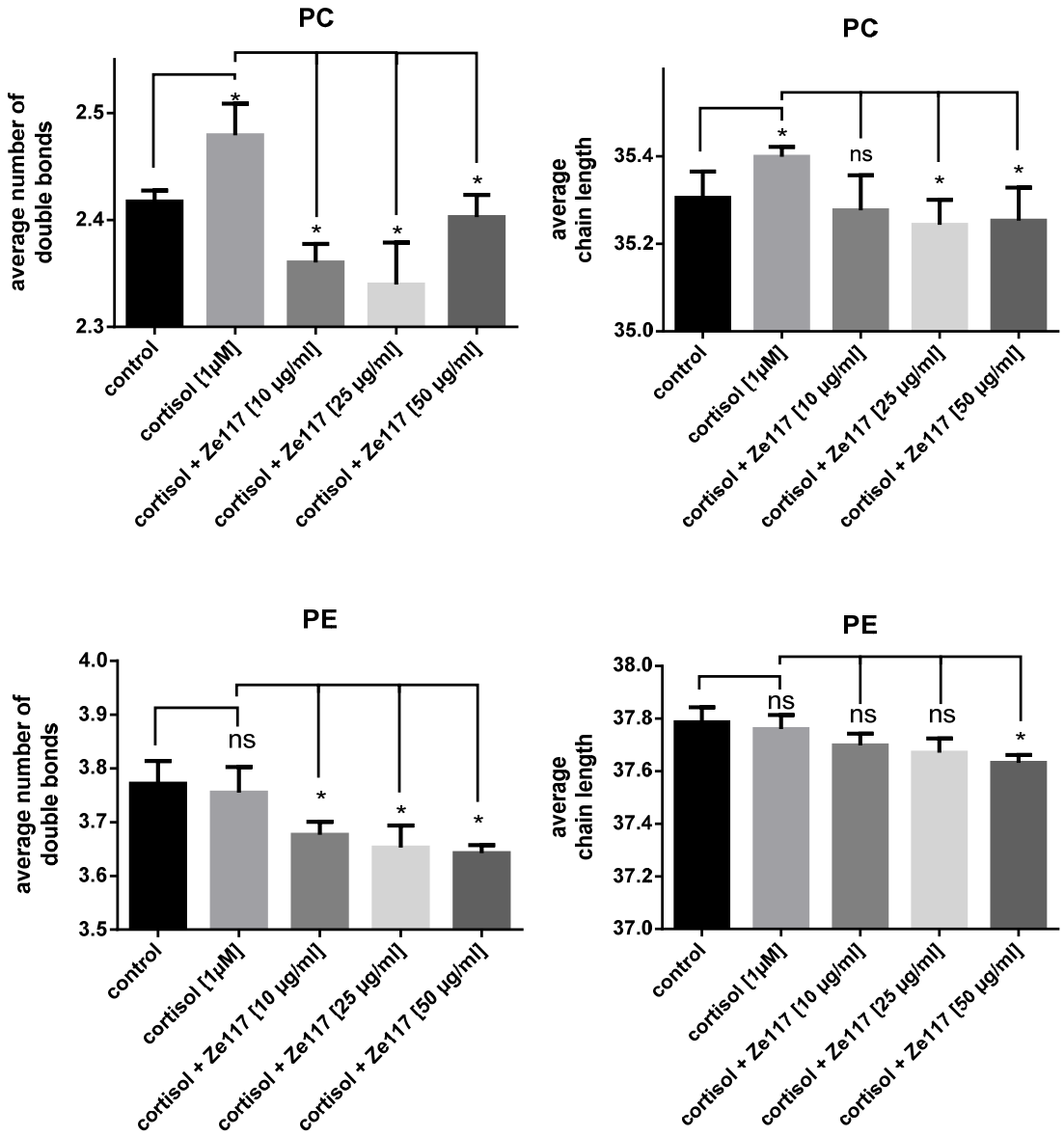


**Figure 4-5 Influence of cortisol and Ze117 on fatty acid structures of PC and PE:** Average chain length and average number of double bonds of phosphatidylcholines (PC) and phosphatidylethanolamines (PE) of PBMC after cortisol and cortisol/Ze117 preincubation, respectively. For statistical evaluation the cortisol condition was compared to the control. Average chain length and average number of double bonds of cortisol/Ze117 pretreated cells were compared to the cortisol condition. *Marked values of occupancies are significantly different from corresponding unstimulated condition with $p \leq 0.05$ determined by student's t-test (n=4).

**Table 4-2 Corresponding table to Figure** 4-5 Influence of cortisol and Ze117 on fatty acid structures of PC and PE: Average chain length and average number of double bonds of phosphatidylcholines (PC) and phosphatidylethanolamines (PE) of PBMC after cortisol and cortisol/Ze117 preincubation, respectively. For statistical evaluation the cortisol condition was compared to the control. Average chain length and average number of double bonds of cortisol/Ze117 pretreated cells were compared to the cortisol condition.

| | control | cortisol [1 µM] | cortisol [1 µM] + Ze117 | | |
|---|---|---|---|---|---|
| | | | [10 µg/ml] | [25 µg/ml] | [50 µg/ml] |
| **PC** | | | | | |
| double bonds | 2.42 ± 0.01 | 2.48 ± 0.03* | 2.36 ± 0.02* | 2.34 ± 0.04* | 2.40 ± 0.02* |
| chain length | 35.31 ± 0.06 | 35.40 ± 0.02* | 35.28 ± 0.08 | 35.24 ± 0.06* | 35.25 ± 0.08* |
| **PE** | | | | | |
| double bonds | 3.77 ± 0.04 | 3.76 ± 0.05 | 3.68 ± 0.02* | 3.65 ± 0.04* | 3.642 ± 0.02* |
| chain length | 37.79 ± 0.06 | 37.76 ± 0.05 | 37.70 ± 0.05 | 37.67 ± 0.06 | 37.63 ± 0.03* |

#### 4.2.3.2 Phosphatidylethanolamine ethers and phosphatidylcholine ethers

Neither cortisol alone nor co-incubation with Ze117 had an impact on the average number of double bonds and the average chain length of fatty acids in the phosphatidylethanolamine ethers class (PE O) (Figure 4-6).

Cortisol alone did not alter the fatty acid composition in the phosphatidylcholine ethers class (PC O). After co-incubation with Ze117 a significant and dose-dependent decrease in the average chain length of fatty acids within the PC O class was found. The average chain length decreased from 36.19 ± 0.11 to 35.84 ± 0.07 after co-incubation with 1 µM cortisol and 50 µg/ml Ze117, compared to cortisol pretreated cells. The same effect was observed for the average number of double bonds which dose-dependently decreased from 3.85 ± 0.12 to 3.50 ± 0.09.

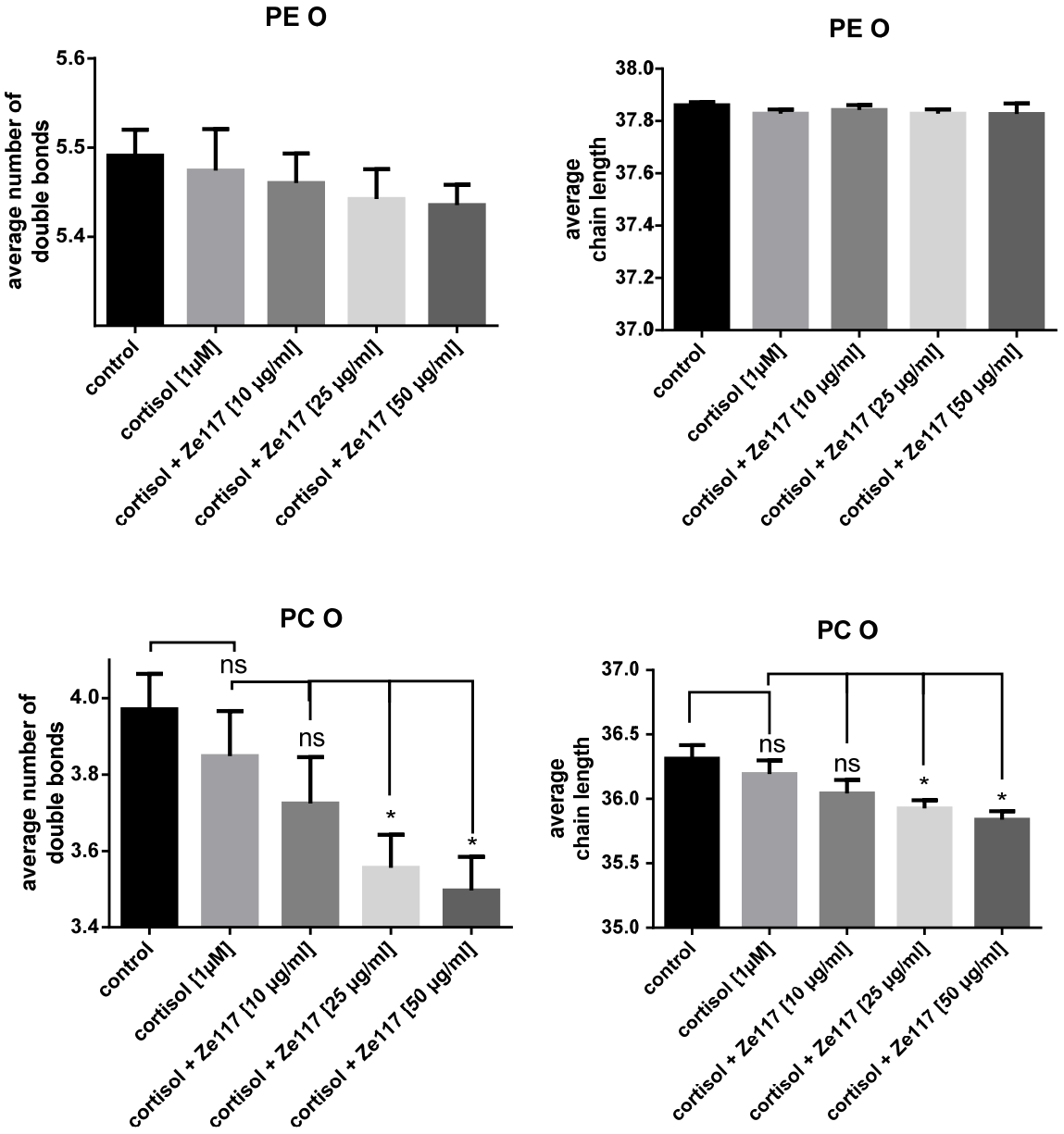


**Figure 4-6 Influence of cortisol and Ze117 on fatty acid structures of PC-O and PE-O:** Average chain length and average number of double bonds of phosphatidylcholine ethers (PC O) and the phosphatidylethanolamine ethers (PE O) species after cortisol and cortisol/Ze117 preincubation, respectivly. For statistical evaluation the cortisol condition was compared to the control. Average chain length and average number of double bonds of cortisol/Ze117 pretreated cells was compared against the cortisol condition. *Marked values are significantly different from corresponding unstimulated condition with $p \leq 0.05$ determined by student's t-test (n=4).

**Table 4-3 Corresponding table to Figure 4-6** Influence of cortisol and Ze117 on fatty acid structures of PC-O and PE-O: Average chain length and average number of double bonds of phosphatidylcholine ethers (PC O) and the phosphatidylethanolamine ethers (PE O) species after cortisol and cortisol/Ze117 preincubation, respectivly. For statistical evaluation the cortisol condition was compared to the control. Average chain length and average number of double bonds of cortisol/Ze117 pretreated cells was compared against the cortisol condition. *Marked values are significantly different from corresponding unstimulated condition with $p \leq 0.05$ determined by student's t-test (n=4).

| | control | cortisol [1 µM] | cortisol [1 µM] + Ze117 | | |
|---|---|---|---|---|---|
| | | | [10 µg/ml] | [25 µg/ml] | [50 µg/ml] |
| **PE O** | | | | | |
| double bonds | 5.49 ± 0.03 | 5.47 ± 0.05 | 5.46 ± 0.03 | 5.44 ± 0.03 | 5.44 ± 0.02 |
| chain length | 37.86 ± 0.01 | 37.83 ± 0.02 | 37.84 ± 0.02 | 37.83 ± 0.02 | 37.83 ± 0.04 |
| **PC O** | | | | | |
| double bonds | 3.97 ± 0.10 | 3.85 ± 0.12 | 3.72 ± 0.12 | 3.56 ± 0.09* | 3.50 ± 0.09* |
| chain length | 36.31 ± 0.11 | 36.19 ± 0.11 | 36.04 ± 0.11 | 35.93 ± 0.06* | 35.84 ± 0.07* |

### 4.2.3.3 Phosphatidylinositols and phosphatidylserines

As shown in Figure 4-7 the average chain length of fatty acids within the phosphatidylinositol (PI) class was significantly increased after cortisol treatment from 37.99 ± 0.02 to 38.02 ± 0.02 compared to control cells. Co-incubation with 50 µg/ml Ze117 counteracted the cortisol induced effect by a significant decrease of the average chain length from 38.02 ± 0.02 to 37.78 ± 0.06, which remarkably was below control level. This was also oberserved for co-incubation with cortisol and 10 µg/ml Ze117 and 25 µg/ml Ze117, respectively, but to a lesser extent (Figure 4-7).

No effect was seen for the average number of double bounds for cortisol treated cells. Co-incubation with Ze117, however, reduced the average number of double bounds within the PI class significantly and dose-dependently from 4.00 ± 0.06 in cortisol preincubated cells to 3.78 ± 0.01 in PBMC pretreated with 1 µM cortisol and 50 µg /ml Ze117.

Neither cortisol nor cortisol/Ze117 co-incubation had a significant effect on average chain length and average number of double bonds in phosphatidylserines (PS).

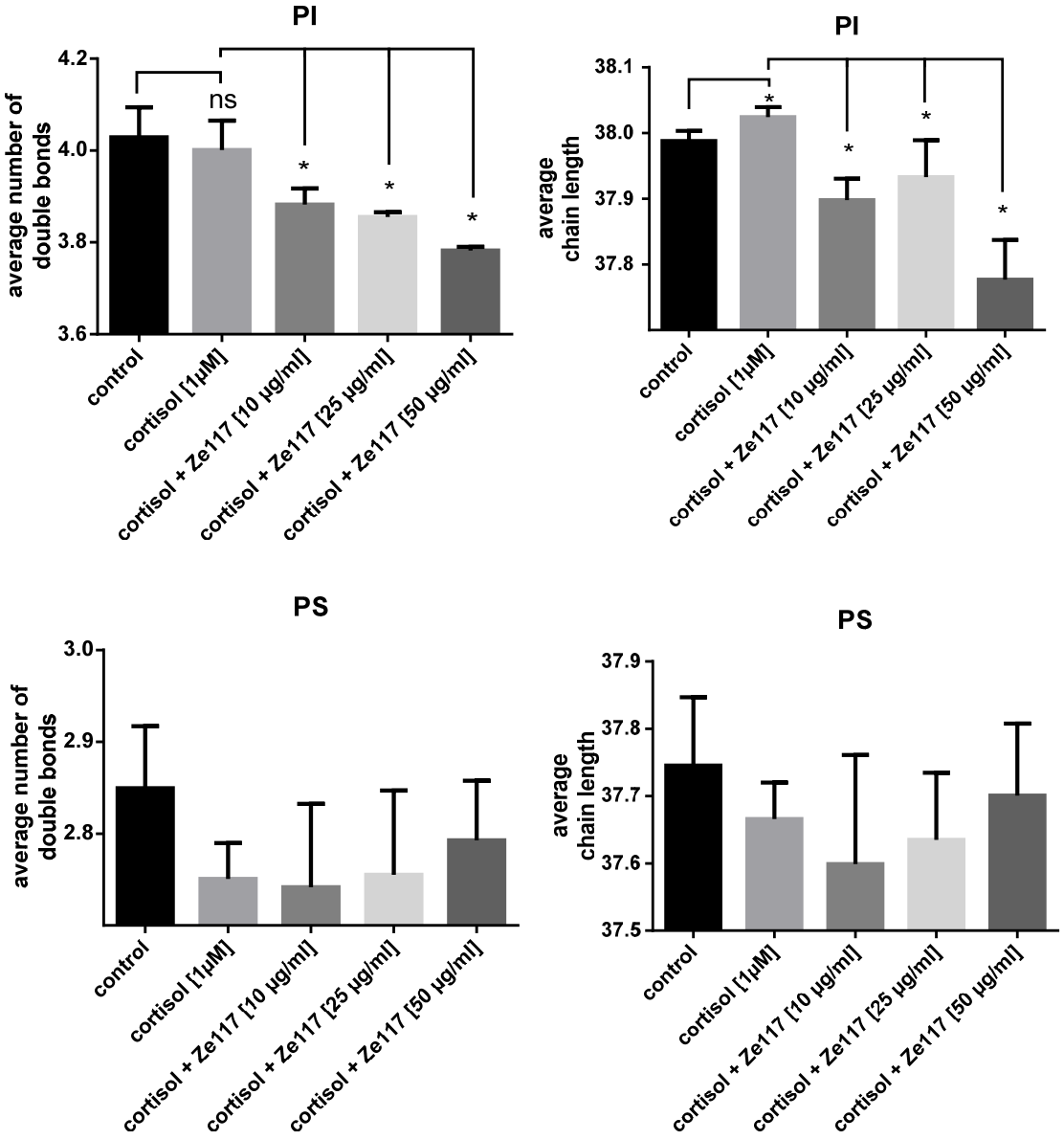


**Figure 4-7 Influence of cortisol and Ze117 on fatty acid structures of PC-O and PE-O:** Average chain length and average number of double bonds of the lipid classes of phoshpatidylinositols (PI) and phosphatidylserines (PS) after cortisol and cortisol/Ze117 preincubation, respectively. For statistical evaluation the cortisol condition was compared to the control. Average chain length and average number of double bonds of cortisol/Ze117 pretreated cells were compared with the cortisol condition. *Marked values are significantly different from corresponding unstimulated condition with $p \leq 0.05$ determined by student's t-test (n=4).

**Table 4-4 Corresponding table to Figure 4-7** Influence of cortisol and Ze117 on fatty acid structures of PC-O and PE-O: Average chain length and average number of double bonds of the lipid classes of phoshpatidylinositols (PI) and phosphatidylserines (PS) after cortisol and cortisol/Ze117 preincubation, respectively. For statistical evaluation the cortisol condition was compared to the control. Average chain length and average number of double bonds of cortisol/Ze117 pretreated cells were compared with the cortisol condition. *Marked values are significantly different from corresponding unstimulated condition with $p \leq 0.05$ determined by student's t-test (n=4).

| | control | cortisol [1 µM] | cortisol [1 µM] + Ze117 | | |
|---|---|---|---|---|---|
| | | | [10 µg/ml] | [25 µg/ml] | [50 µg/ml] |
| **PI** | | | | | |
| double bonds | 4.029 ± 0.07 | 4.001 ± 0.06 | 3.88 ± 0.04* | 3.86 ± 0.011* | 3.78 ± 0.01* |
| chain length | 38.00 ± 0.015 | 38.02 ± 0.02 | 37.90 ± 0.03* | 37.93 ± 0.06* | 37.78 ± 0.06* |
| **PS** | | | | | |
| double bonds | 2.850 ± 0.07 | 2.75 ± 0.04 | 2.74 ± 0.09 | 2.76 ± 0.092 | 2.79 ± 0.065 |
| chain length | 37.75 ± 0.10 | 37.67 ± 0.05 | 37.60 ± 0.16 | 37.63 ± 0.01 | 37.70 ± 0.11 |

#### 4.2.3.4 Triacylglycerols and diacylglycerols

One micromolar cortisol alone did neither have an effect on average chain length nor on the average number of double bonds of fatty acids of triacylglycerols (TAG) and diacylglycerols (DAG).

Compared to cortisol pretreated PBMC the average chain length of TAG decreased significantly from 55.60 ± 0.43 to 54.44 ± 0.22 after co-incubation with 50 µg/ml Ze117. Similar significant effects were observed after co-incubation with 10 µg/ml and 25 µg/ml Ze117 (Figure 4-8).

The average number of double bonds of TAG decreased significantly after co-incubation with 10µg/ml Ze117 from 5.60 ± 0.29 to 4.73 ± 0.09. Again, similar significant effects were observed after co-incubation with 10 µg/ml and 25 µg/ml Ze117.

Within DAG no significant effect on the average chain length after cortisol/Ze117 co-incubation was observed. Only co-incubation with cortisol and 10 µg/ml and 50 µg/ml Ze117 reduced the average number of double bonds significantly from 3.37 ± 0.01 to

3.08 ± 0.14 and 3.16 ± 0.08, respectively, whereas 25 µg/ml Ze117 did not show any effect.

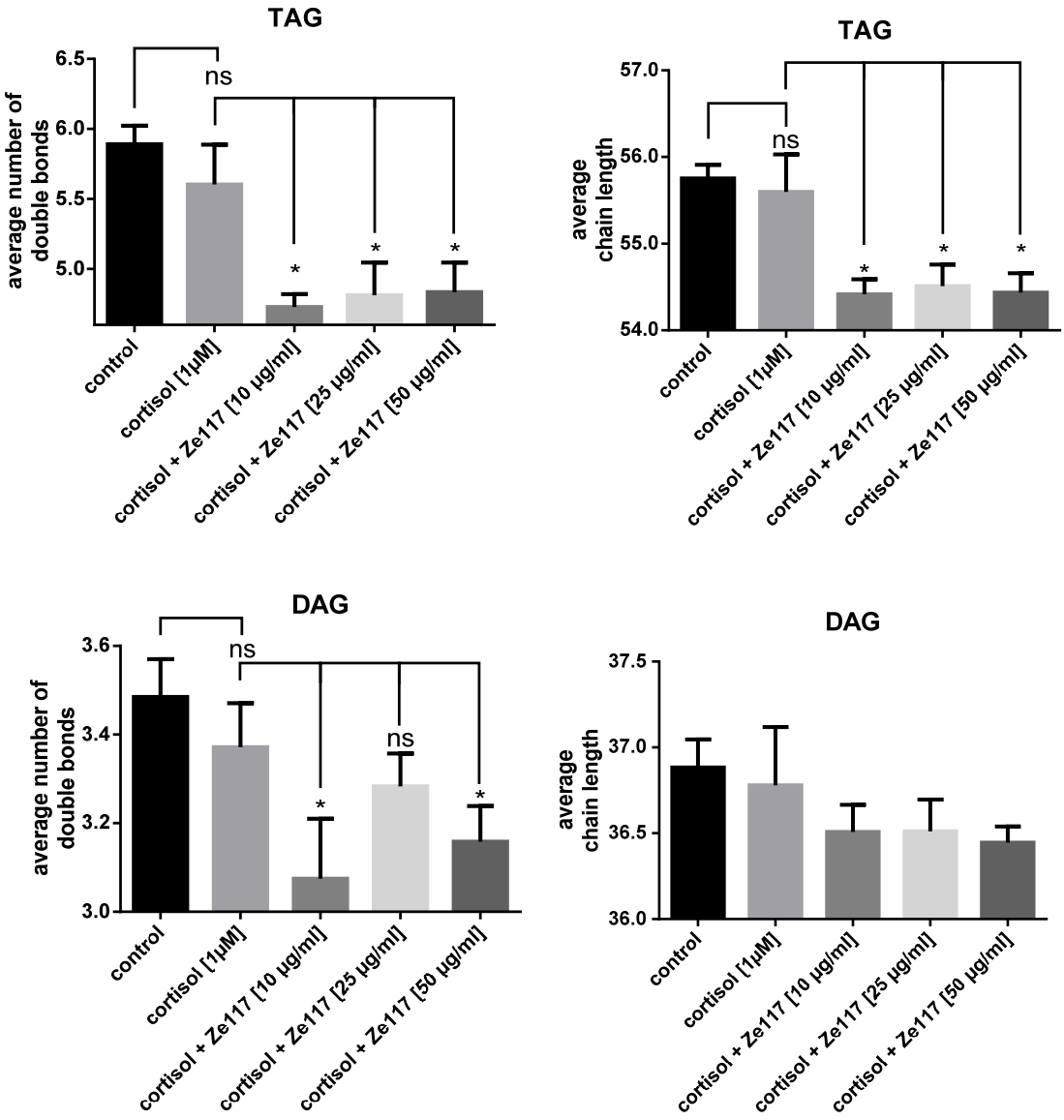


**Figure 4-8 Influence of cortisol and Ze117 on fatty acid structures of TAG and DAG:** Average chain length and average number of double bonds of triacylglycerols (TAG) and diacylglycerols (DAG) after cortisol and cortisol/Ze117 preincubation, respectively. For statistical evaluation the cortisol condition was compared to the control. Average chain length and average number of double bonds of cortisol/Ze117 pretreated cells were compared with the cortisol condition. *Marked values are significantly different from corresponding unstimulated condition with $p \leq 0.05$ determined by student's t-test (n=4).

**Table 4-5 Corresponding table to Figure 4-8** Influence of cortisol and Ze117 on fatty acid structures of TAG and DAG: Average chain length and average number of double bonds of triacylglycerols (TAG) and diacylglycerols (DAG) after cortisol and cortisol/Ze117 preincubation, respectively. For statistical evaluation the cortisol condition was compared to the control. Average chain length and average number of double bonds of cortisol/Ze117 pretreated cells were compared with the cortisol condition. *Marked values are significantly different from corresponding unstimulated condition with $p \leq 0.05$ determined by student's t-test (n=4).

| | control | cortisol [1 µM] | cortisol [1 µM] + Ze117 | | |
|---|---|---|---|---|---|
| | | | [10 µg/ml] | [25 µg/ml] | [50 µg/ml] |
| **TAG** | | | | | |
| double bonds | 5.89 ± 0.13 | 5.60 ± 0.29 | 4.73 ± 0.09* | 4.81 ± 0.23* | 4.83 ± 0.212* |
| chain length | 55.75 ± 0.156 | 55.60 ± 0.433 | 55.60 ± 0.172* | 54.51 ± 0.247* | 54.44 ± 0.224* |
| **DAG** | | | | | |
| double bonds | 3.49 ± 0.09 | 3.37 ± 0.10 | 3.08 ± 0.14 | 3.28 ± 0.08 | 3.16 ± 0.081 |
| chain length | 36.88 ± 0.16 | 36.78 ± 0.34 | 36.51 ± 0.16* | 36.51 ± 0.19 | 36.45 ± 0.093* |

#### 4.2.3.5 Ceramides and phosphatidylglycerols

Neither cortisol alone nor co-incubation with Ze117 had an impact on the average number of double bonds and the average chain length of fatty acids in the ceramide class (Figure 4-9).

Cortisol alone did not alter the fatty acid composition in the phosphatidylglycerol (PG) class. After co-incubation with Ze117 a significant and dose-dependent decrease in the average chain length of fatty acids within the PG class was found. The average chain length decreased from 38.51 ± 0.55 to 37.41 ± 0.44 after co-incubation with 1 µM cortisol and 50 µg/ml Ze117, compared to cortisol pretreated cells. The same effect was observed for the average number of double bonds which dose-dependently decreased from 5.58 ± 0.55 to 4.45 ± 0.47.

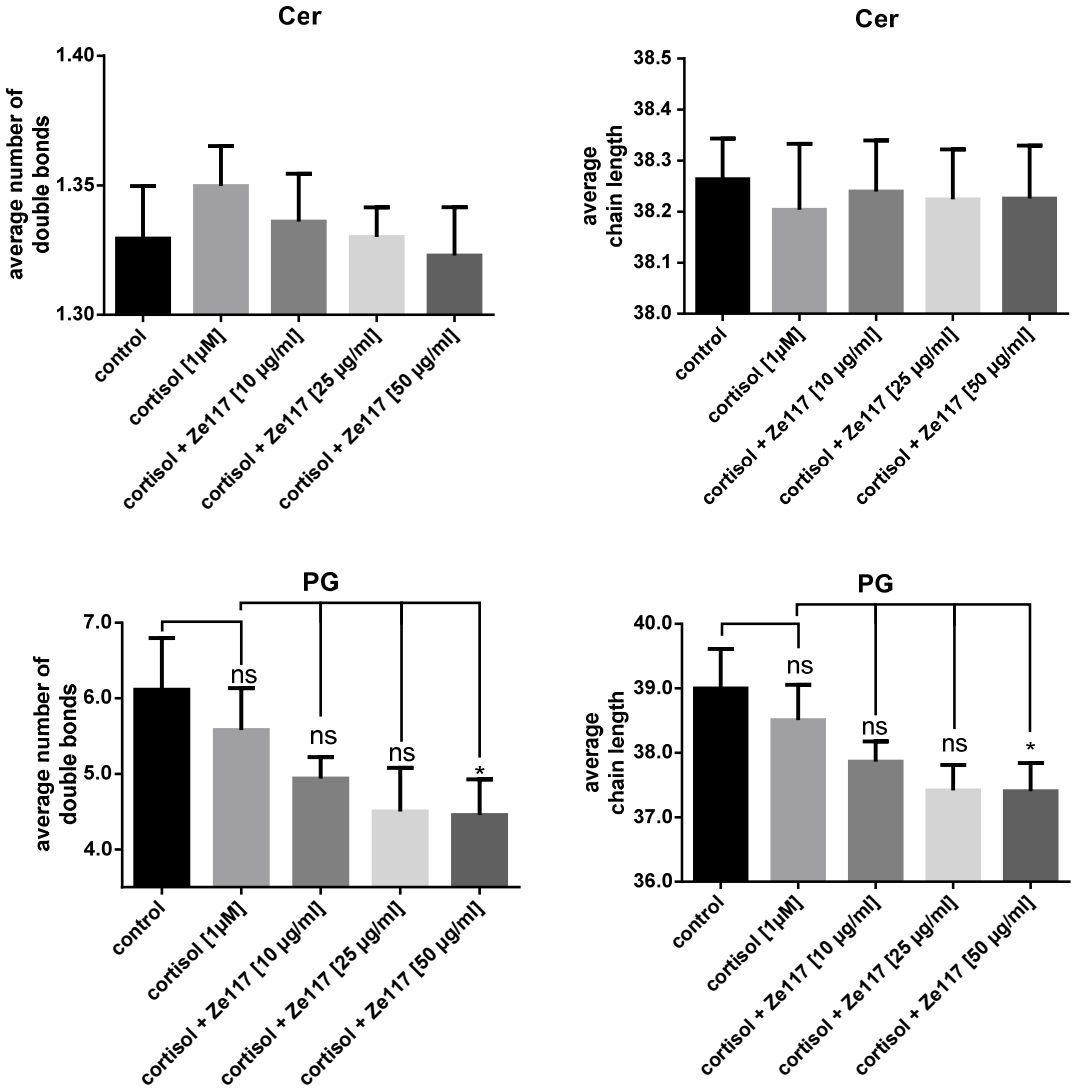


**Figure 4-9 Influence of cortisol and Ze117 on fatty acid structures of CER and PG:** Average chain length and average number of double bonds of ceramides (Cer) and phosphatidylglycerol (PG) after cortisol and cortisol/Ze117 preincubation, respectively. For statistical evaluation the cortisol condition was compared to the control. Average chain length and average number of double bonds of cortisol/Ze117 pretreated cells were compared with the cortisol condition. *Marked values are significantly different from corresponding unstimulated condition with $p \leq 0.05$ determined by student's t-test (n=4).

**Table 4-6 Corresponding table to Figure 4-9** Influence of cortisol and Ze117 on fatty acid structures of CER and PG: Average chain length and average number of double bonds of ceramides (Cer) and phosphatidylglycerol (PG) after cortisol and cortisol/Ze117 preincubation, respectively. For statistical evaluation the cortisol condition was compared to the control. Average chain length and average number of double bonds of cortisol/Ze117 pretreated cells were compared with the cortisol condition. *Marked values are significantly different from corresponding unstimulated condition with $p \leq 0.05$ determined by student's t-test (n=4).

| | **control** | **cortisol [1 µM]** | **cortisol [1 µM] + Ze117** | | |
|---|---|---|---|---|---|
| | | | **[10 µg/ml]** | **[25 µg/ml]** | **[50 µg/ml]** |
| **Cer** | | | | | |
| double bonds | 1.33 ± 0.02 | 1.35 ± 0.02 | 1.34 ± 0.02 | 1.33 ± 0.01 | 1.32 ± 0.02 |
| chain length | 38.26 ± 0.08 | 38.20 ± 0.13 | 38.24 ± 0.10 | 38.22 ± 0.10 | 38.23 ± 0.11 |
| **PG** | | | | | |
| double bonds | 6.12 ± 0.68 | 5.58 ± 0.55 | 4.94 ± 0.28 | 4.50 ± 0.58 | 4.45 ± 0.47* |
| chain length | 39.00 ± 0.62 | 38.51 ± 0.55 | 37.87 ± 0.31 | 37.42 ± 0.39 | 37.41 ± 0.44* |

### 4.2.4 Effect of cortisol and cortisol/Ze117 combination on individual lipid species of PBMC

While the evaluation of lipidomic data showed significant effects on the average number of double bonds and on the average chain length of individual lipid classes after cortisol preincubation, no significant effect was found for individual lipid species (Figure 4-10).

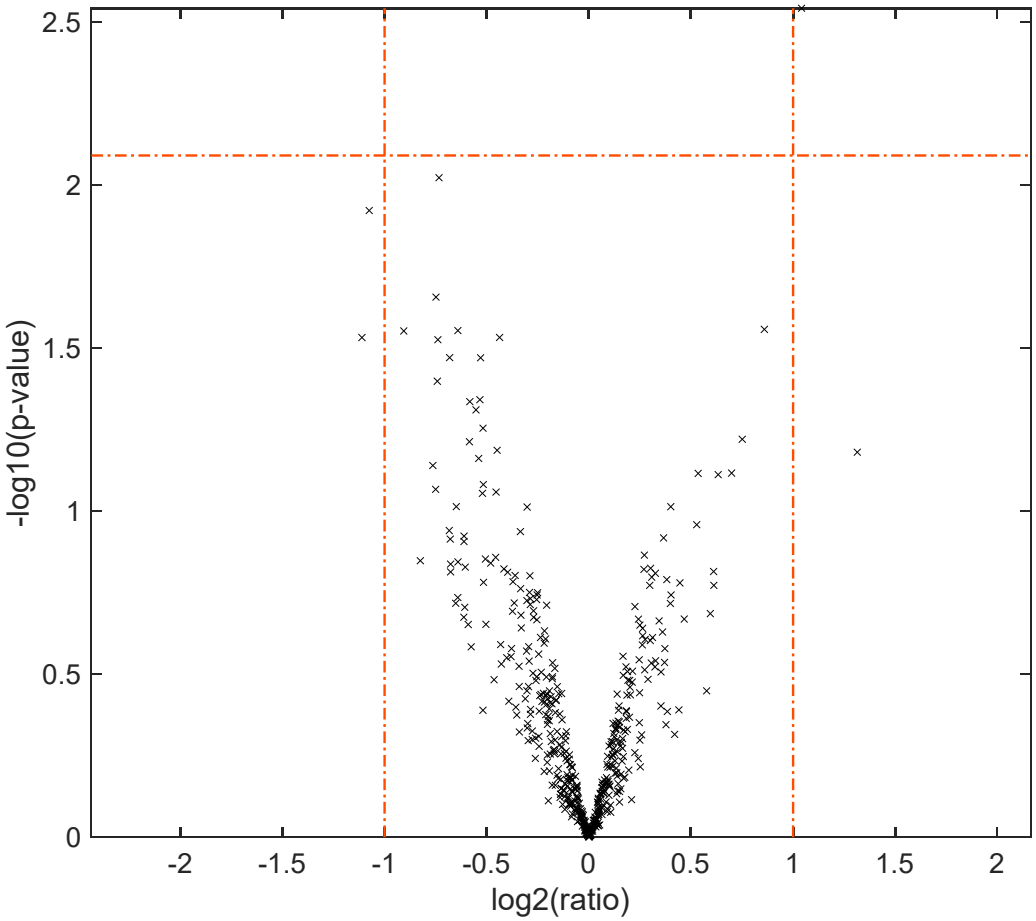


**Figure 4-10 Influence of cortisol on lipid ratios:** Volcano plot displaying lipid ratios between control and 1 µM cortisol pretreated PBMC. Each cross represents a single lipid species. A log2(ratio) < 0 corresponds to a decrease of the respective lipid species after cortisol preincubation. A log2(ratio) > 0 corresponds to an increase. The negative decadic logarithm of the p-value is plotted on the y-axis. The horizontal orange line shows the significance level corrected according to Benjamini-Hochberg. All lipid species below this line are considered as not significant (n=4).

In contrast, the combination of 1 µM cortisol and 25 µg/ml Ze117 significantly increased storage lipids, such as triacylglycerols (TAG) or diacylglycerols (DAG), compared to the cortisol condition (Figure 4-11). Similar results were found for the co-incubation of 1 µM cortisol with 10 µg/ml Ze117 and 50 µg/ml Ze117, respectively.

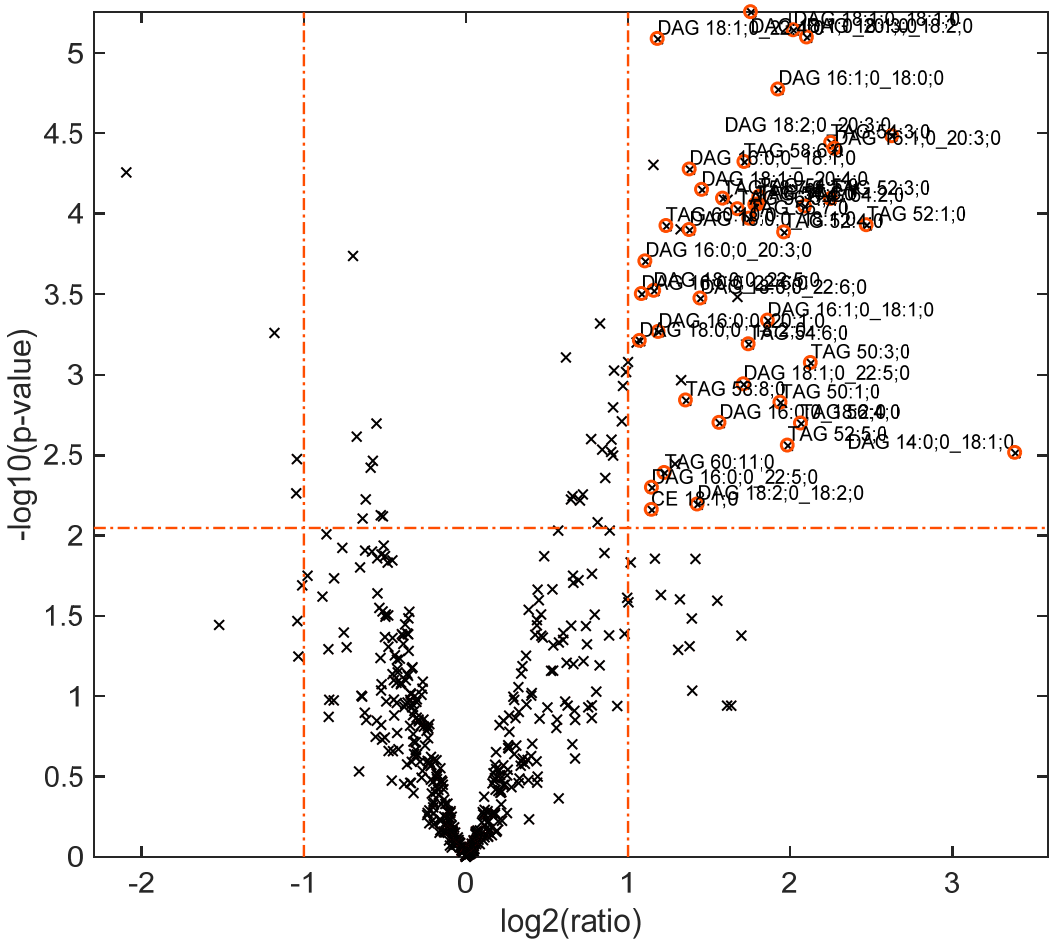


**Figure 4-11 Influence of cortisol and cortisol/Ze117 on lipid ratios with focus on storage lipids:** Volcano plot displaying lipid ratios between 1 µM cortisol and cortisol/Ze117 [1 µM/25µg/ml] pretreated PBMC. Each cross represents a single lipid species. Lipids with a log2(ratio) >0 were upregulated after Ze117 preincubation compared to the cortisol preincubation. Lipids with a log2(ratio) < 0 were accordingly downregulated. The negative decadic logarithm of the p-value is plotted on the y-axis. The horizontal orange line shows the significance level corrected according to Benjamini-Hochberg. All crosses below this line are considered as not significant. Storage lipids above the significance level and a log2(ratio) value below -1 and above 1, respectively, are marked with an orange circle (n=4).

Only a few lipid species apart from storage lipids changed their proportion significantly after a cortisol/Ze117 preincubation compared to cortisol (Figure 4-12). In order to determine the most relevant phospholipids, phospholipid species were selected

according to whose proportions increased or decreased significantly both at Ze117 concentrations of 0.025 mg/ml and 0.05 mg/ml. Phospholipid species which only were induced by one of two Ze117 concentration were not included.

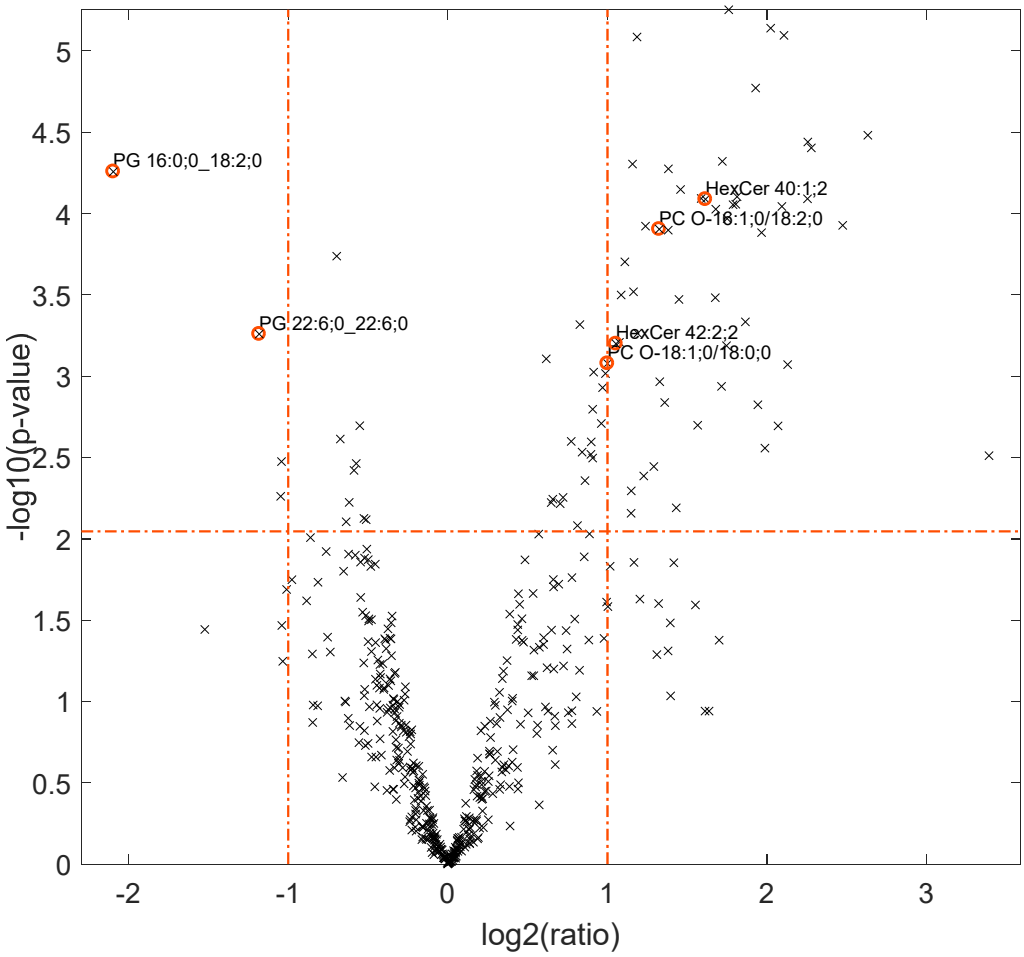


**Figure 4-12 Influence of cortisol and cortisol/Ze117 on lipid ratios with focus on selective lipids:** Volcano plot displaying lipid ratios between cortisol [1 µM] and cortisol/Ze117 [25µg/ml] pretreated PBMC. Each cross represents a single lipid species. A log2(ratio) < 0 corresponds to a decrease of the respective lipid species under cortisol/Ze117 [25µg/ml] preincubation. A log2(ratio) > 0 corresponds to an increase. The negative decadic logarithm of the p-value is plotted on the y-axis. The horizontal orange line shows the significance level corrected according to Benjamini-Hochberg. All lipid species below this line are considered not significant. Other lipid species than storage lipids above the significance level and a log2(ratio) value underneath -1 and above 1, respectively, are marked with an orange circle (n=4).

Under this specification six species whose proportions changed significantly after co-incubation with cortisol and Ze117 compared to cortisol (Table 4-7) were found. Two phosphatidylglycerol (PG) species were downregulated by the combination of

cortisol/Ze117. One of these species consisted of a PG head group with two docosanoic fatty acids with six double bonds each (PG 22:6/22:6). The other PG was composed by one hexadecanoic fatty acid without double bonds and one octadecanoic acid with two double bonds (PG 16:0/18:2).

Moreover, two hexosylceramides (HexCer) and phosphatidylcholine ethers (PC O) were found, whose proportions were significantly increased after co-incubation with cortisol and Ze117 compared to cortisol. The first HexCer was characterized by two fatty acids with 40 carbon atoms in total and one double bond (HexCer 40:1). The second HexCer was characterized by 42 carbon atoms in total and two double bonds (HexCer 42:2). One of the PC O consisted of a hexadecanoic fatty acid with one double bond and an octadecanoic acid with two double bonds (PC O-16:1/18:2). The other PC O was composed by two octadecanoic acids with one double bond (PC O-18:1/18:0).

**Table 4-7 Influence of cortisol and cortisol/Ze117 on lipid ratios with focus on selective lipids:** Lipid species other than storage lipids significantly induced by cortisol/Ze117 co-incubation compared to cortisol pretreatment as given in Figure 4-12.

| **Log2(ratio) < -1** | **Log2(ratio) > 1** |
|---|---|
| PG 22:6/22:6 | |
| PG 16:0/18:2 | |
| | HexCer 40:1 |
| | HexCer 42:2 |
| | PC O-16:1/18:2 |
| | PC O-18:1/18:0 |

## 4.3 Single particle tracking

### 4.3.1 Labeling of the $\beta_1$-adrenergic receptor

In this chapter the motion profile of the $\beta_1$-adrenergic receptor ($\beta_1$AR) on the plasma membrane of living cells will be described by single particle tracking (SPT). In order to make the target receptor accessible for fluorescence microscopy, a fluorescent label is needed. The fluorescent probe is thereby excited by light of a certain wavelength and then emits light of a slightly higher wavelength, which can be separated by optical filters. There are various possibilities to label receptors located in the plasma membrane. For example, fluorescent proteins such as GFP (green fluorescent protein) can be genetically attached to the target protein [62]. The disadvantages of GFP labeling are relatively rapid bleaching, blinking and possible altered receptor functioning.

For this reason, an alternative are smaller organic fluorophores with high quantum yields, which are available in a wide range of different photochemical properties [63]. Since the cell cannot produce these molecules autonomously, they must be applied in a different way. Possible techniques are e.g. fluorescently labeled ligands and antibodies. Another method is the use of protein tags. One of these tags is the SNAP-tag which is based on a genetic fusion of the target protein with a human DNA repair enzyme "$O^6$-alkylguanine-DNA alkyltransferase" (hAGT, the "SNAP-tag"). This enzyme has the ability to covalently bind $O^6$-benzylguanine derivatives with the elimination of guanine (Figure 4-13) [64]. To use this property *in vivo*, fluorophores are needed as benzylguanine (BG) conjugates. These conjugates are commercially available or can be prepared by simple chemical coupling reactions. This is to the advantage for SPT measurements: Depending on membrane permeability, photostability and the required wavelength, different fluorescent substrates can be selected. Membrane permeable fluorescent substrates are useful for observing intracellular processes [65]. Impermeable fluorescent substrates, on the other hand, are well suited for the purpose of this work, which is the staining of receptors on the plasma membrane. This is due to the fact that there is no intracellular interaction of the unbound fluorescent substrate, which could lead to phototoxicity and higher background signals.

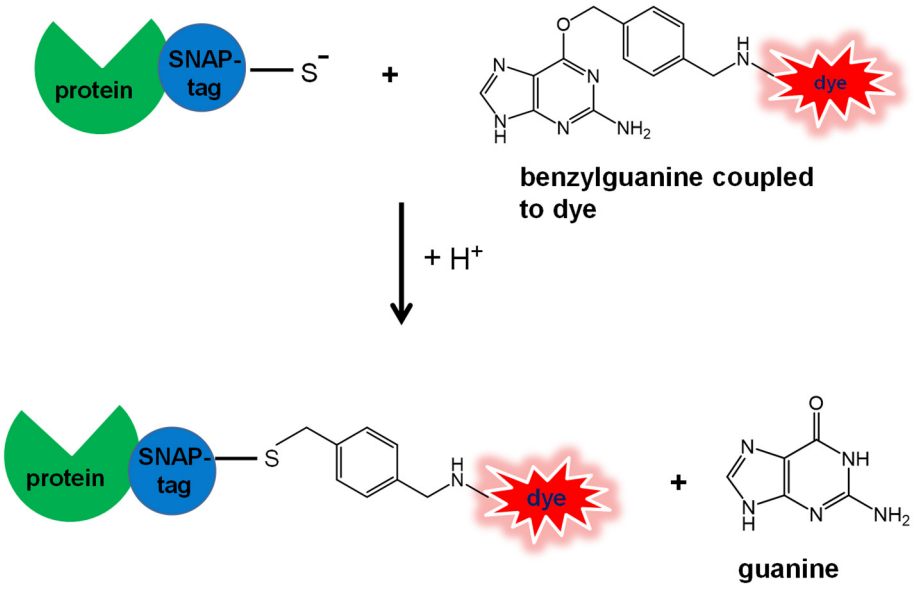


**Figure 4-13 Binding of a dye-labeled benzylguanine substrate to a SNAP-tag fusion protein**.

#### 4.3.1.1 Synthesis of BG-Dy549

The SPT setup used in this work is operated by a 532 nm laser. Benzylguanine coupled dyes of this excitation wavelength have been tested by Bosch et al. (2014) for their use in SPT experiments [63]. Brightness, photostability and nonspecific binding were considered for evaluation. Bosch et al. (2014) concluded that the dye Dy549 is best suited for a 532 nm laser as illustrated in Figure 4-14.

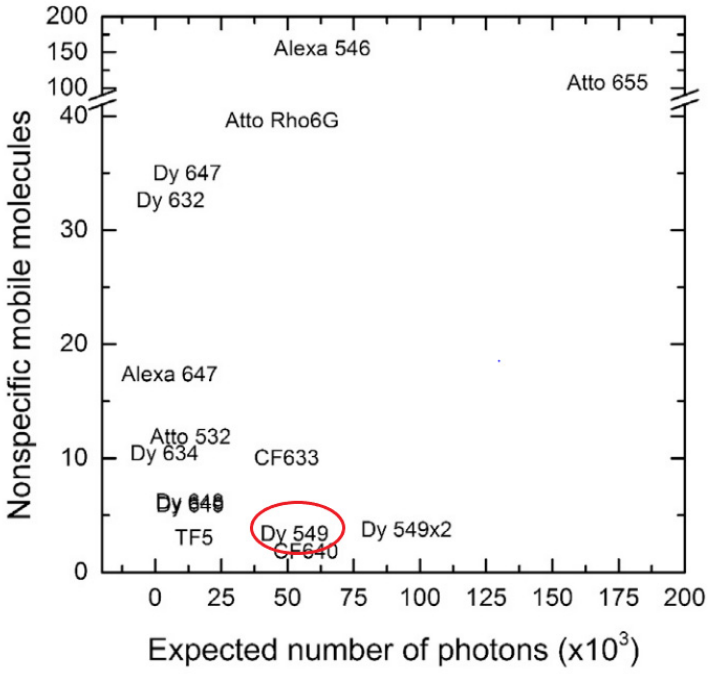


**Figure 4-14 Comparison of different benzylguanine coupled dyes for single particle tracking experiments:** The dyes were tested for nonspecific mobile molecules attached to the cell and expected number of photons. Fluorescent dyes in the lower right show lowest nonspecific binding to cells and best photostability. Figure from Bosch et al., 2014 [63].

Based on these results, it was decided to synthesize the SNAP-tag substrate by amide coupling of the NHS (N-hydroxysuccinimide) ester activated Dy549 and benzylguanine-$NH_2$ (BG-$NH_2$) as shown in Figure 4-15.

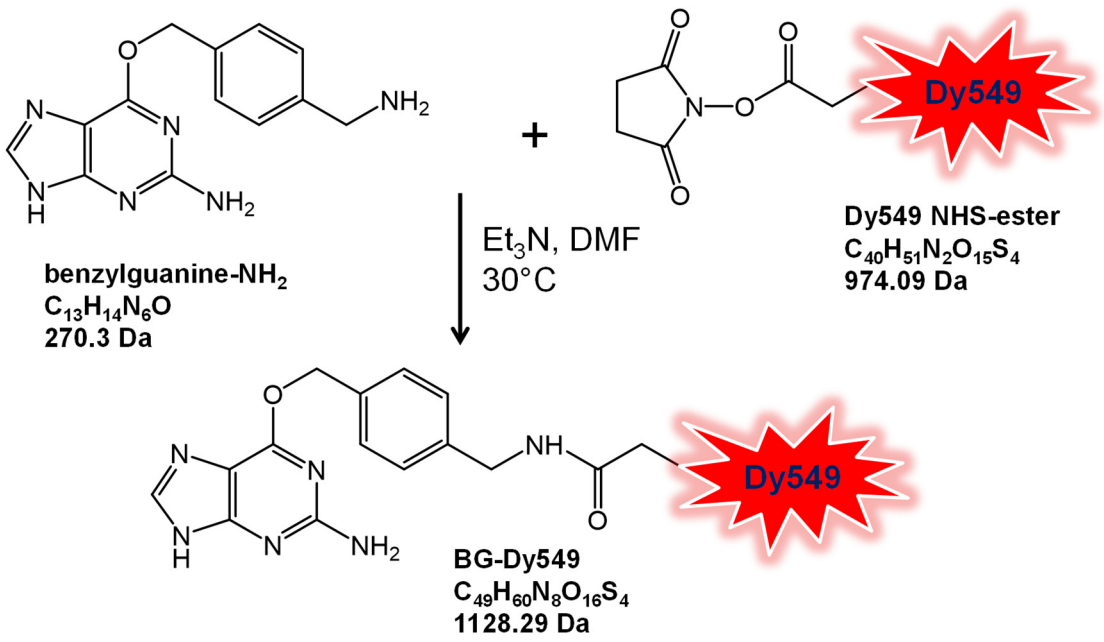


**Figure 4-15 Synthesis of BG-Dy549:** The structural formula of Dy549 is patented by the manufacturer and therefore cannot be specified.

The product was isolated by high-performance liquid chromatography (HPLC). As shown in Figure 4-16 the substance that eluated with a retention time of 11.03 min showed a UV spectrum, which matched to BG-Dy549.

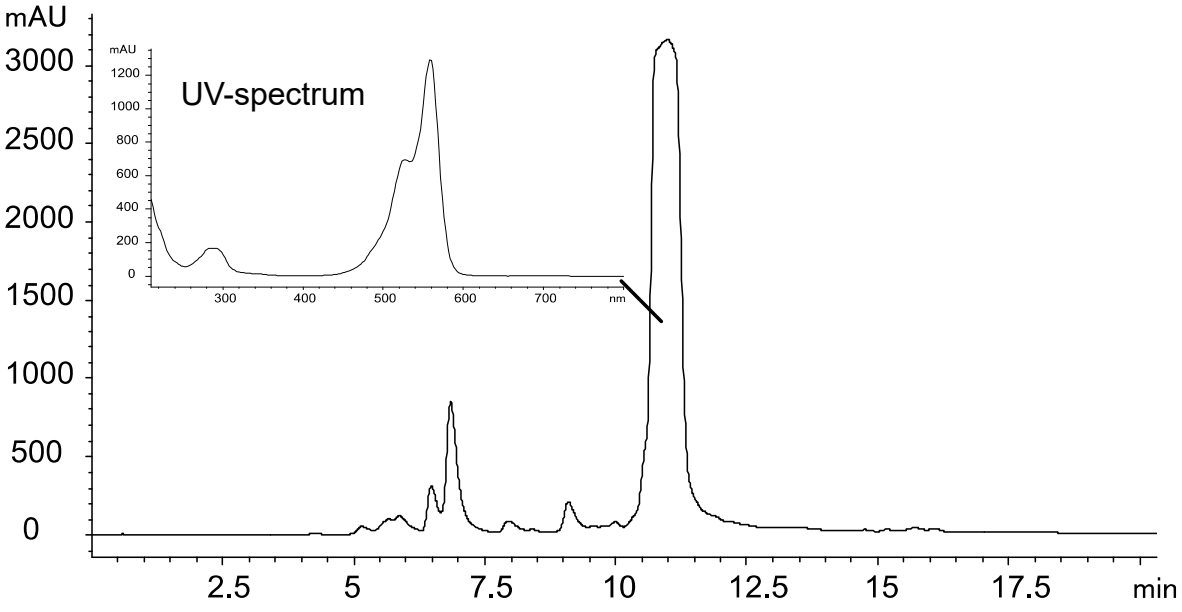


**Figure 4-16 HPLC chromatogram of the reaction mixture at 540 nm:** Insert shows the UV spectrum of BG-Dy549 with a retention time of 11.03 min.

To confirm that the eluate of the peak with a retention time of 11.03 min contained the desired product, matrix assisted laser desorption ionization-time of flight mass spectrometry (MALDI-TOF) analysis was performed. The spectrum is given in Figure 4-17 showing the strongest signal at m/z = 1129.237 which corresponded to the product BG-Dy549 with a theoretical mass of 1128.29 Da. The signal at m/z = 978.174 corresponded to a loss of guanine from the parent ion.

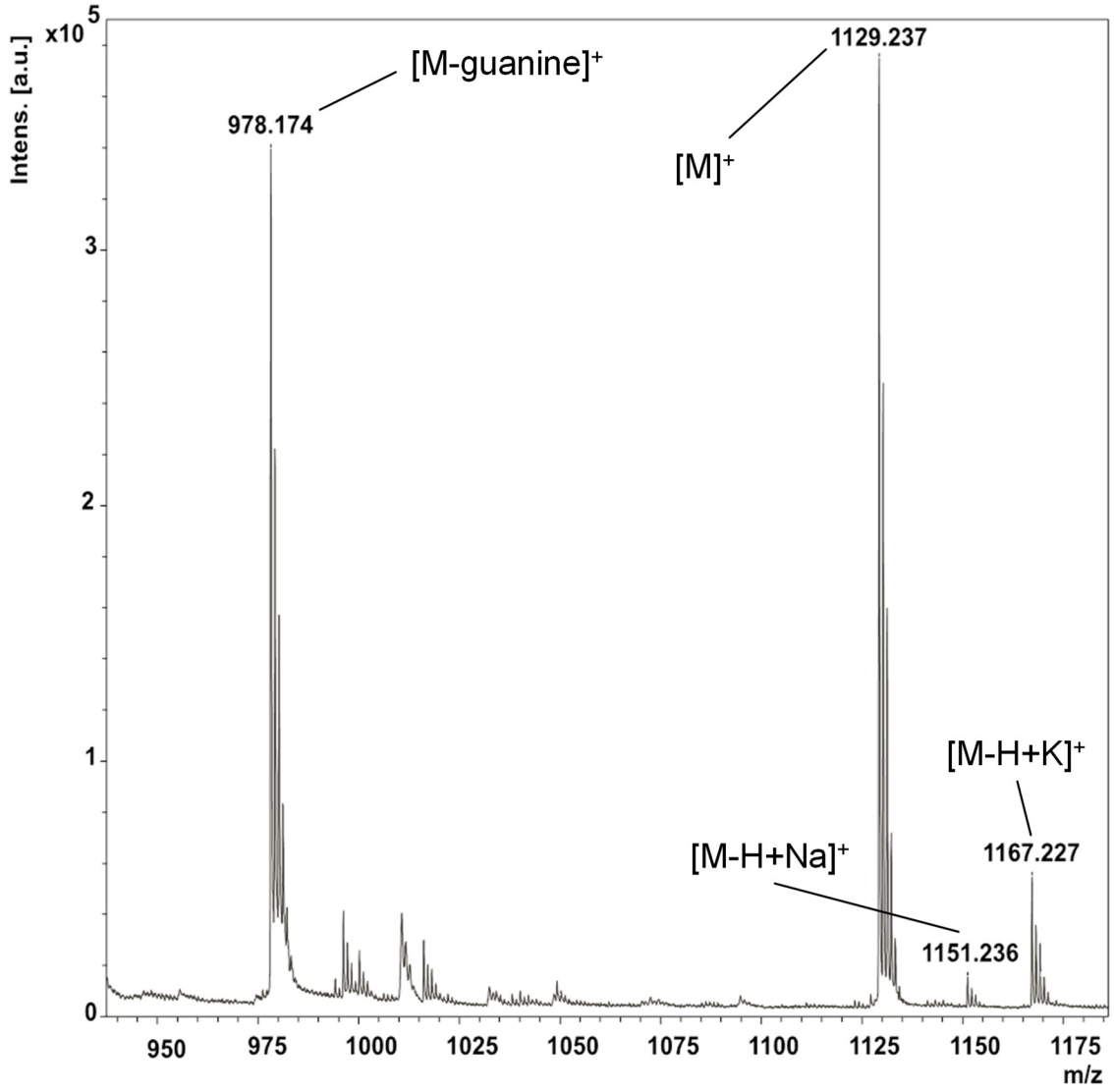


**Figure 4-17 MALDI-TOF analysis of the compound which eluated at 11.03 min:** The signal at m/z = 1128.237 fits to the expected mass of the product with 1128.29 Da ($C_{49}H_{60}N_8O_{16}S_4$).

The dye was tested for its function on living C6 cells expressing the SNAP-tagged $\beta_1$AR (SNAP-$\beta_1$AR). A membrane staining with low background signal was found by imaging with a wide field microscope (Figure 4-18). BG-Dy549 was added at a concentration of 2 µM on C6 cells expressing the SNAP-$\beta_1$AR.

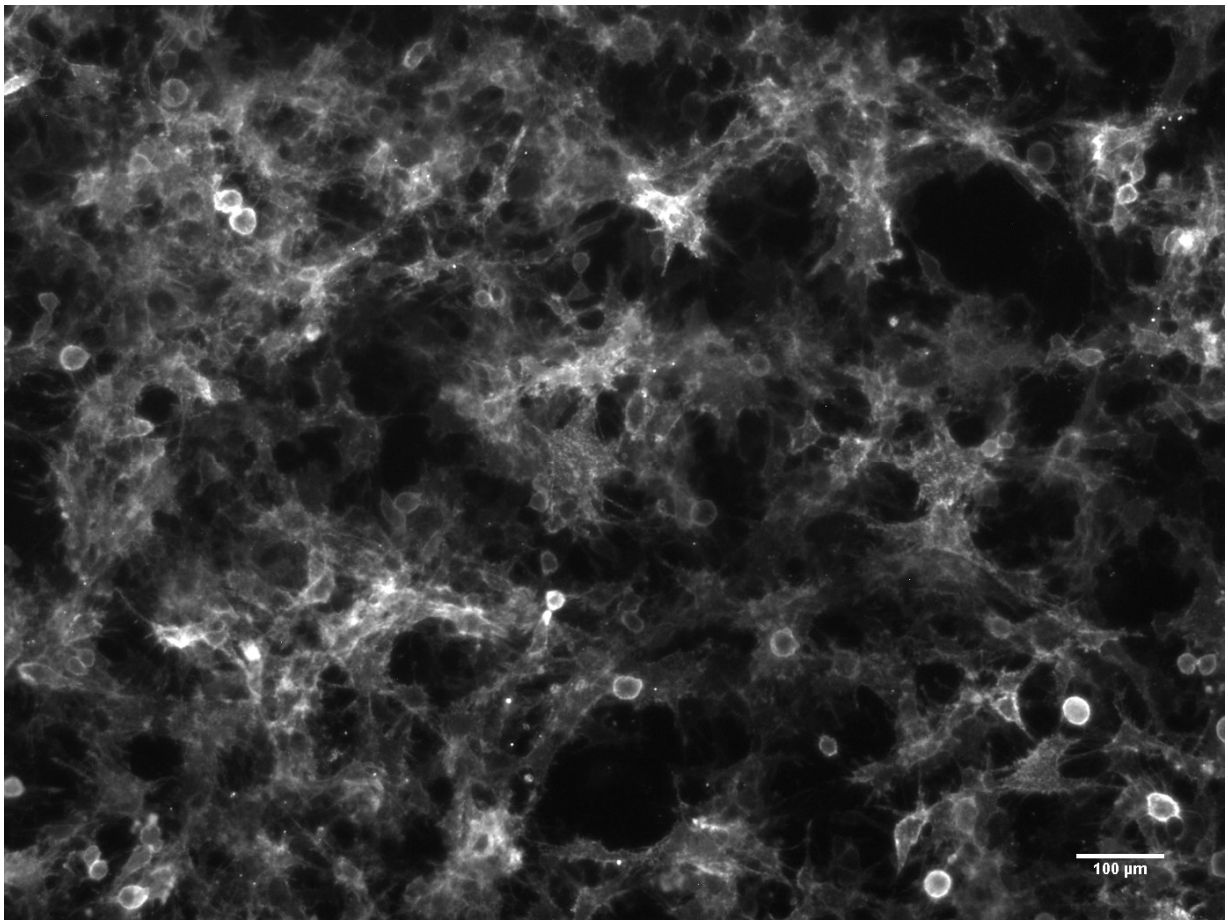


**Figure 4-18 Fluorescence image of C6 cells expressing the SNAP-$\beta_1$AR stained with BG-Dy549.**

#### 4.3.1.2 Cell line

The C6 rat glioma cell line was used for this work. For single particle tracking experiments a fluorescently labeled $\beta_1$AR was needed. Therefore, $\beta_1$AR was coupled to a SNAP-tag via its N-terminus and transfected into the C6 cells (C6 SNAP-$\beta_1$AR).

The expression of SNAP-$\beta_1$AR was confirmed by membrane staining with BG-Dy549 as seen in Figure 4-18.

### 4.3.2 Lateral diffusion behavior of $\beta_1$-adrenergic receptors

To be able to define the lateral diffusion behavior of $\beta_1$-adrenergic receptors ($\beta_1$AR), C6 cells expressing the SNAP-tagged $\beta_1$AR (C6 SNAP-$\beta_1$AR) were stained with 5 nM BG-Dy549. After positioning the focus on the upper cell membrane, image series of 1000 frames with a frame rate of 20 frames per second were taken. The dye labeled receptors were automatically detected by a uTrack software and the positions belonging to one trajectory were connected frame by frame. The resulting average track length was between 7 and 8 frames in every condition. For each condition at least three independent experiments were performed examining 5 to 10 cells each.

#### 4.3.2.1 Signal to noise ratio

In SPT experiments a high signal to noise ratio (SNR) should be achieved. The SNR depends on the brightness of the fluorescent dye and the background noise. In order to reduce the background noise before SPT analysis, SPT raw data was edited. The statical background in a series of images was captured by creating a projection of the average pixel intensity values over the entire series of SPT images. This projection ideally captured only the background, but not the moving particles. The background projection was eventually substracted from all images in the series (Figure 4-19). The procedure was automated by a self-written script in ImageJ and was executed for all images before initiating the tracking process.

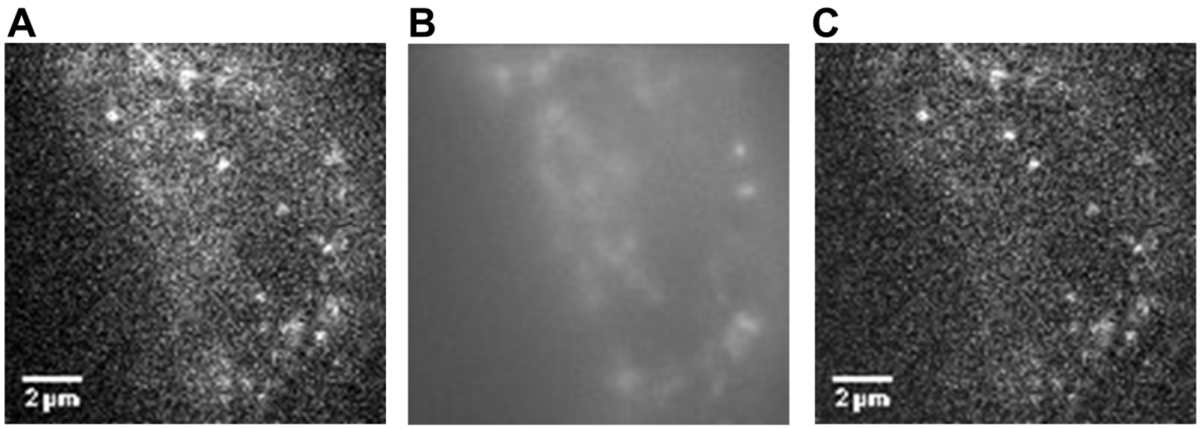


**Figure 4-19 SPT picture processing: A:** Fluorescent picture before processing. **B:** The statical background was captured by creating a projection of the average pixel intensity values over the entire series of SPT images **C:** Fluorescent picture with reduced background after substracting the statical background.

The SNR was calculated by the difference of the signal intensity and the background intensity divided by the standard deviation of the background [66]. This means for the example in Figure 4-20:

$$SNR = (1.6 – 1.1) / 0.07 = 7.1$$

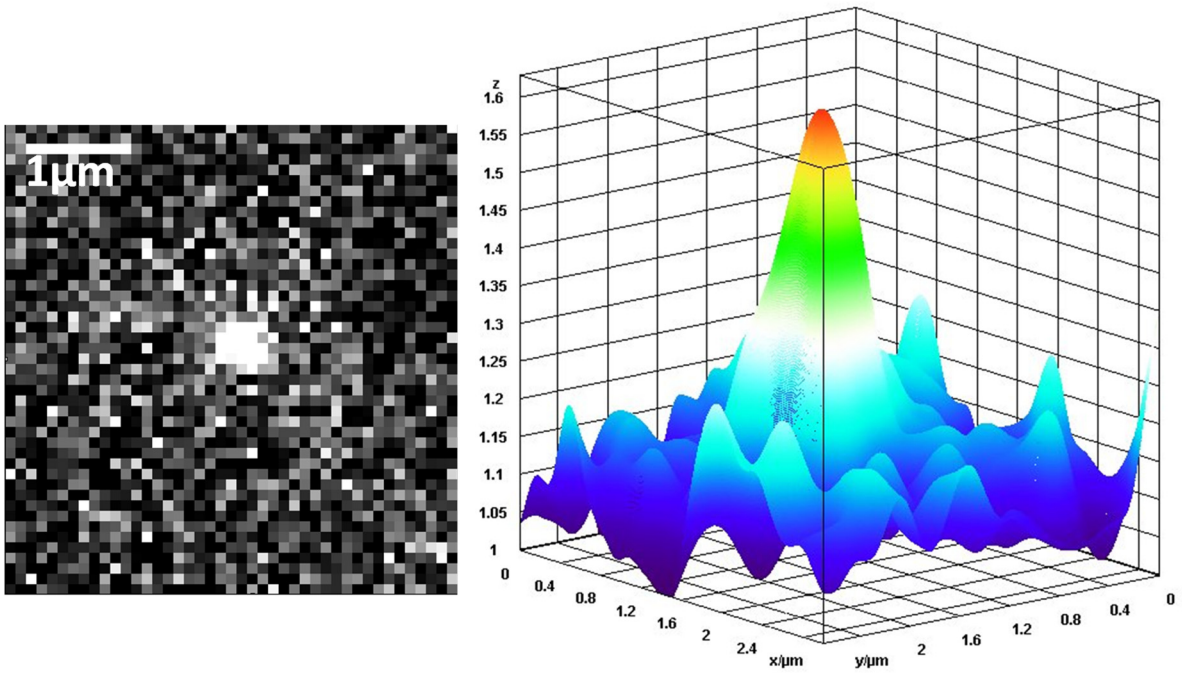


**Figure 4-20 Picture of SNAP-$\beta_1$AR vs 3D surface plot:** X and Y axes define the position of the receptor. Z axis shows the intensities of the pixels. The intensity maximum was 1.6. The mean intensity of the background noise was 1.1 with a standard deviation of 0.07.

To ensure accurate and robust automated spot tracking, a SNR of 4 should be reached [67]. With the used microscope setup, SNRs of BG-Dy549 label SNAP-$\beta_1$AR were distributed as shown in Figure 4-21. The mean signal to noise ratio of detected spots was 8.64 ± 3.30. A stable detection of the single particles could therefore be assumed.

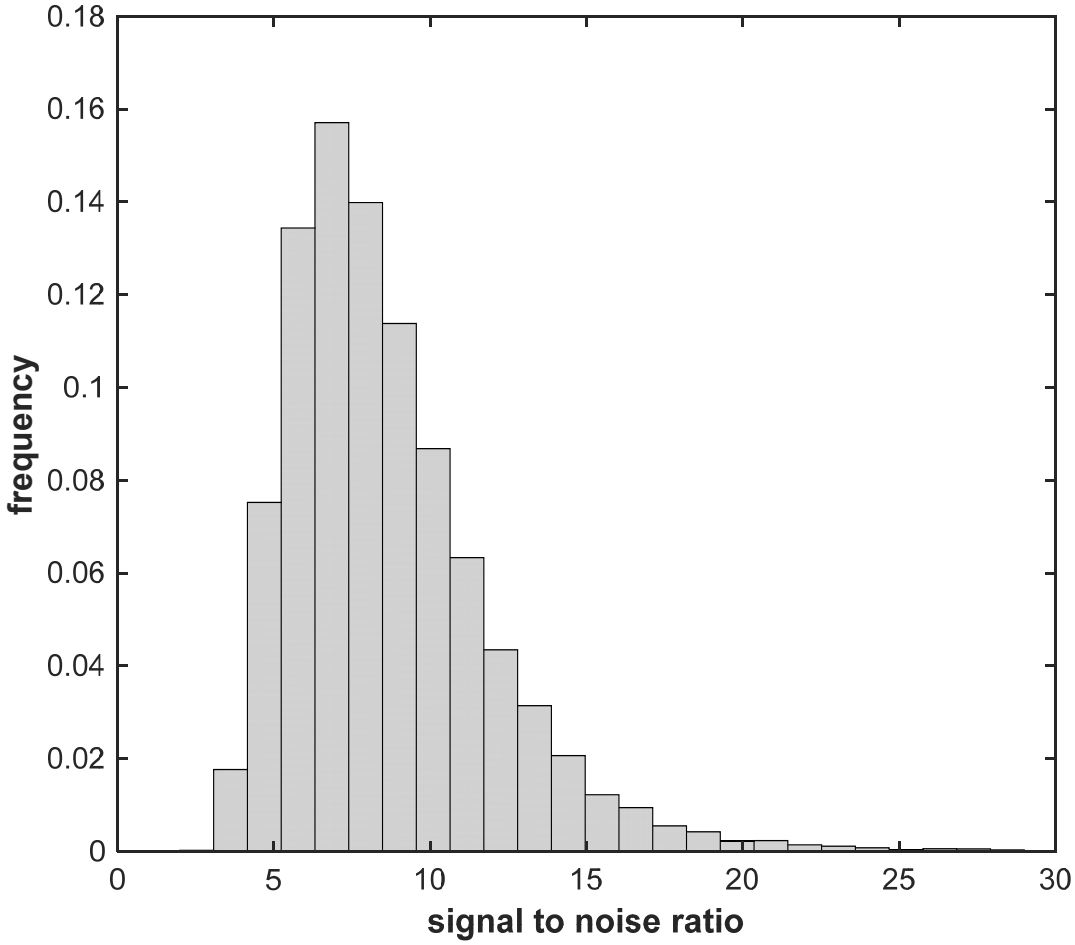


**Figure 4-21 Signal to noise ratio distribution of detected SNAP-$\beta_1$AR particles.** The mean signal to noise ratio was 8.64 ± 3.30.

#### 4.3.2.2 A three state diffusion model

To ensure a comprehensive data analysis, tracks from 2 frames upwards were considered. In order to analyze data sets with short trajectories the algorithm vbSPT was used, which is based on a variational Bayesian treatment of a hidden Markov model.

The vbSPT algorithm divided the trajectories into segments according to their momentary diffusion speed as described by Persson et al. [56]. The segments were then classified into three disctinct diffusive states (S1, S2, and S3). Each state was defined by a diffusion coefficient and a corresponding state occupancy value. The

algorithm was able to recognize higher order models, but it was decided to classify them into an immobile state S1, a slow diffusing state S2, and a fast diffusing state S3.

C6 SNAP-$\beta_1$AR control cells showed diffusion coefficients of 0.016 ± 0.001 µm²/s for S1, 0.034 ± 0.0002 µm²/s for S2 and 0.166 ± 0.013 µm²/s for S3. Stimulation with 10 µM isoprenaline did not affect the diffusion coefficients.

C6 SNAP-$\beta_1$AR were pretreated for 5 days with 0.25 mg/ml Ze117, 1 µM escitalopram, 1 µM desipramine, and 1 µM cortisol. One milimolar methyl-β-cyclodextrin (MβCD) was given to the cells 30 min prior to SPT measurements. Diffusion coefficients in all conditions except for Ze117 pretreated cells ranged from 0.015 ± 0.001 to 0.017 ± 0.002 µm²/s for S1, 0.031 ± 0.0015 to 0.036 ± 0.002 µm²/s for S2, and 0.132 ± 0.030 to 0.190 ± 0.017 µm²/s for S3 (Figure 4-22 and Table 4-8). Similar to the control cells, stimulation with 10 µM isoprenaline did not affect the diffusion coefficients.

SNAP-$\beta_1$AR of Ze117 pretreated cells, on the other hand, showed significantly altered diffusion coefficients of 0.013 ± 0.002 µm²/s for S1 and 0.127 ± 0.030 µm²/s for S3 compared to control cells. The diffusion coefficient for S2 did not change. Stimulation with 10 µM isoprenaline of control cells and cells pretreated with Ze117, cortisol, escitalopram, desipramine and MβCD, respectively, did not affect the diffusion coefficients compared to unstimulated cells of the respective preincubation condition.

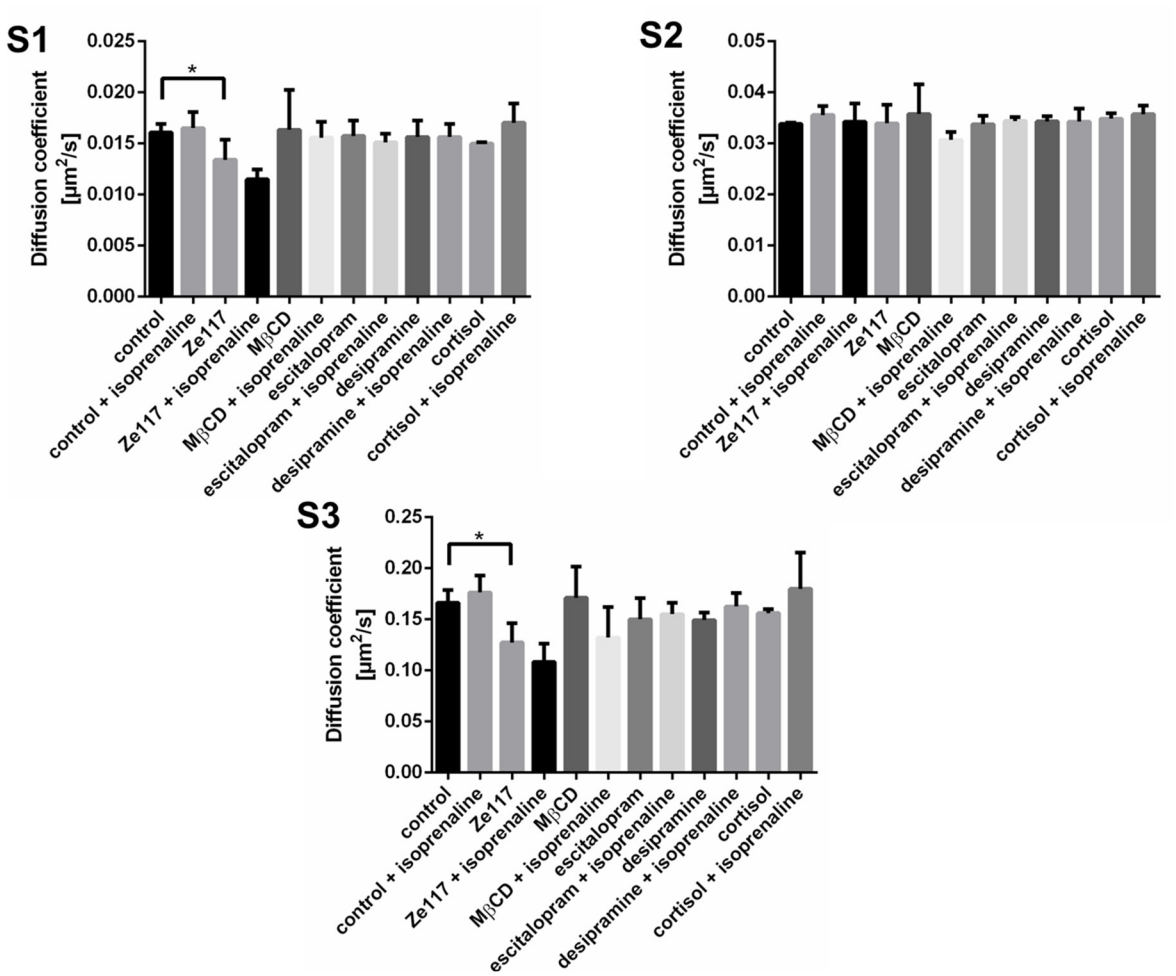


**Figure 4-22 Diffusion behaviour of SNAP-$\beta_1$AR:** Diffusion coefficients corresponding to states S1-S3 of SNAP-$\beta_1$AR on the plasma membrane of C6 SNAP-$\beta_1$AR before and after stimulation with 10 µM isoprenaline. Data was attained by vbSPT. Cells were pretreated for 5 days with 0.25 mg/ml Ze117, 1 µM escitalopram, 1 µM desipramine, and 1 µM cortisol, respectively. One milimolar methyl-β-cyclodextrin (MβCD) was given to the cells 30 min before SPT measurements. * Marked values with $p \leq 0.05$ are significantly different from their corresponding control determined by one-way ANOVA.

**Table 4-8 Corresponding values of Figure 4-22:** Diffusion coefficients corresponding to states S1-S3 of SNAP-$\beta_1$AR on the plasma membrane of SNAP-$\beta_1$AR cells before and after stimulation with 10 µM isoprenaline. Data was attained by vbSPT. Cells were pretreated for 5 days with 0.25 mg/ml Ze117, 1 µM escitalopram, 1 µM desipramine, and 1 µM cortisol, respectively. One milimolar methyl-β-cyclodextrin (MβCD) was given to the cells 30 min before SPT measurements. * Marked values with $p \leq 0.05$ are significantly different from their corresponding controls determined by one-way ANOVA.

| | **Diffusion coefficient for S1 [µm²/s]** | **Diffusion coefficient for S2 [µm²/s]** | **Diffusion coefficient for S3 [µm²/s]** |
|---|---|---|---|
| **control** | | | |
| unstimulated | 0.016 ± 0.001 | 0.034 ± 0.0002 | 0.166 ± 0.013 |
| stimulated | 0.017 ± 0.002 | 0.036 ± 0.002 | 0.176 ± 0.017 |
| **Ze117** | | | |
| unstimulated | 0.013 ± 0.002 * | 0.034 ± 0.004 | 0.127 ± 0.030 * |
| stimulated | 0.011 ± 0.001 | 0.034 ± 0.004 | 0.109 ± 0.018 |
| **MβCD** | | | |
| unstimulated | 0.016 ± 0.004 | 0.036 ± 0.006 | 0.171 ± 0.031 |
| stimulated | 0.016 ± 0.002 | 0.031 ± 0.002 | 0.132 ± 0.030 |
| **escitalopram** | | | |
| unstimulated | 0.016 ± 0.002 | 0.034 ± 0.002 | 0.150 ± 0.020 |
| stimulated | 0.015 ± 0.001 | 0.034 ± 0.001 | 0.155 ± 0.011 |
| **desipramine** | | | |
| unstimulated | 0.016 ± 0.002 | 0.034 ± 0.001 | 0.149 ± 0.007 |
| stimulated | 0.016 ± 0.001 | 0.034 ± 0.003 | 0.162 ± 0.013 |
| **cortisol** | | | |
| unstimulated | 0.015 ± 0.001 | 0.035 ± 0.002 | 0.168 ± 0.016 |
| stimulated | 0.017 ± 0.002 | 0.036 ± 0.001 | 0.190 ± 0.032 |

### 4.3.2.3 Agonist stimulation altered receptor state occupancy

The vbSPT algorithm was also capable of computing the relative number of particles in each state. The resulting state occupancies are shown in Figure 4-23 and Table 4-9. C6 SNAP-$\beta_1$AR were pretreated for 5 days with 0.25 mg/ml Ze117, 1 µM escitalopram, 1 µM desipramine, and 1 µM cortisol, respectively. One milimolar methyl-β-cyclodextrin (MβCD) was given to the cells 30 min prior SPT measurements. Ten minutes before the SPT measurements C6 SNAP-$\beta_1$AR in all pretreatment conditions were either stimulated with 10 µM isoprenaline or not stimulated. The results are given in Figure 4-23 and Table 4-9.

In C6 SNAP-$\beta_1$AR control cells the occupancy of the immobile state S1 increased significantly from 0.21 ± 0.01 under non-stimulating conditions to 0.29 ± 0.03 after stimulation with 10 µM isoprenaline. Under stimulating conditions, the fraction of receptors in S2 was significantly reduced from 0.73 ± 0.01 to 0.64 ± 0.03, whereas occupancy in S3 remained unchanged with 0.06 ± 0.01. C6 SNAP-$\beta_1$AR cells preincubated for 5 days with 1 µM escitalopram showed a similar response to isoprenaline stimulation in SNAP-$\beta_1$AR diffusion compared to stimulated control cells. The fraction of receptors in state S1 significantly increased from 0.21 ± 0.002 to 0.28 ± 0.01. The fraction of receptors in S2 was significantly reduced from 0.72 ± 0.010 to 0.67 ± 0.02. The receptor fraction in S3 did not change (Figure 4-23 and Table 4-9).

Cortisol did not show any effect on the cells under non-stimulating conditions. The values were almost identical compared to the control cells (Figure 4-23 and Table 4-9). Under isoprenaline stimulation significant effects for S1 and S2 were observed similar to stimulated control cells. Occupancy of S1 increased from 0.20 ± 0.01 to 0.31 ± 0.02, whereas occupancy of S2 decreased from 0.73 ± 0.01 to 0.64 ± 0.02.

Under the influence of desipramine the receptor fraction in S1 under non-stimulating conditions increased significantly from 0.21 ± 0.01 to 0.28 ± 0.02 compared to the control condition. Similarly, the receptor fraction in S2 decreased significantly from 0.73 ± 0.02 to 0.65 ± 0.02, whereas the receptor fraction in S3 was not affected. Under isoprenaline stimulation no changes in occupancies of SNAP-$\beta_1$AR were detected compared to corresponding unstimulated desipramine pretreated cells.

After a 5-day-incubation of the cells with 0.025 mg/ml Ze117, the fraction of receptors in S1 under non-stimulating conditions increased significantly from 0.21 ± 0.01 to 0.30 ± 0.01 compared to control cells. This was at the expense of the receptor fraction in S2 which decreased from 0.73 ± 0.02 to 0.61± 0.03. After isoprenaline stimulation no further changes in the occupancy of the diffusive states were observed.

Under the influence of 1 mM MβCD the occupancy of S1 increased significantly from 0.21 ± 0.01 to 0.38 ± 0.07, while the occupancy of S2 significantly decreased from 0.73 ± 0.02 to 0.56 ± 0.06 compared to control. After isoprenaline stimulation no significant changes in occupancy of the diffusive states were observed.

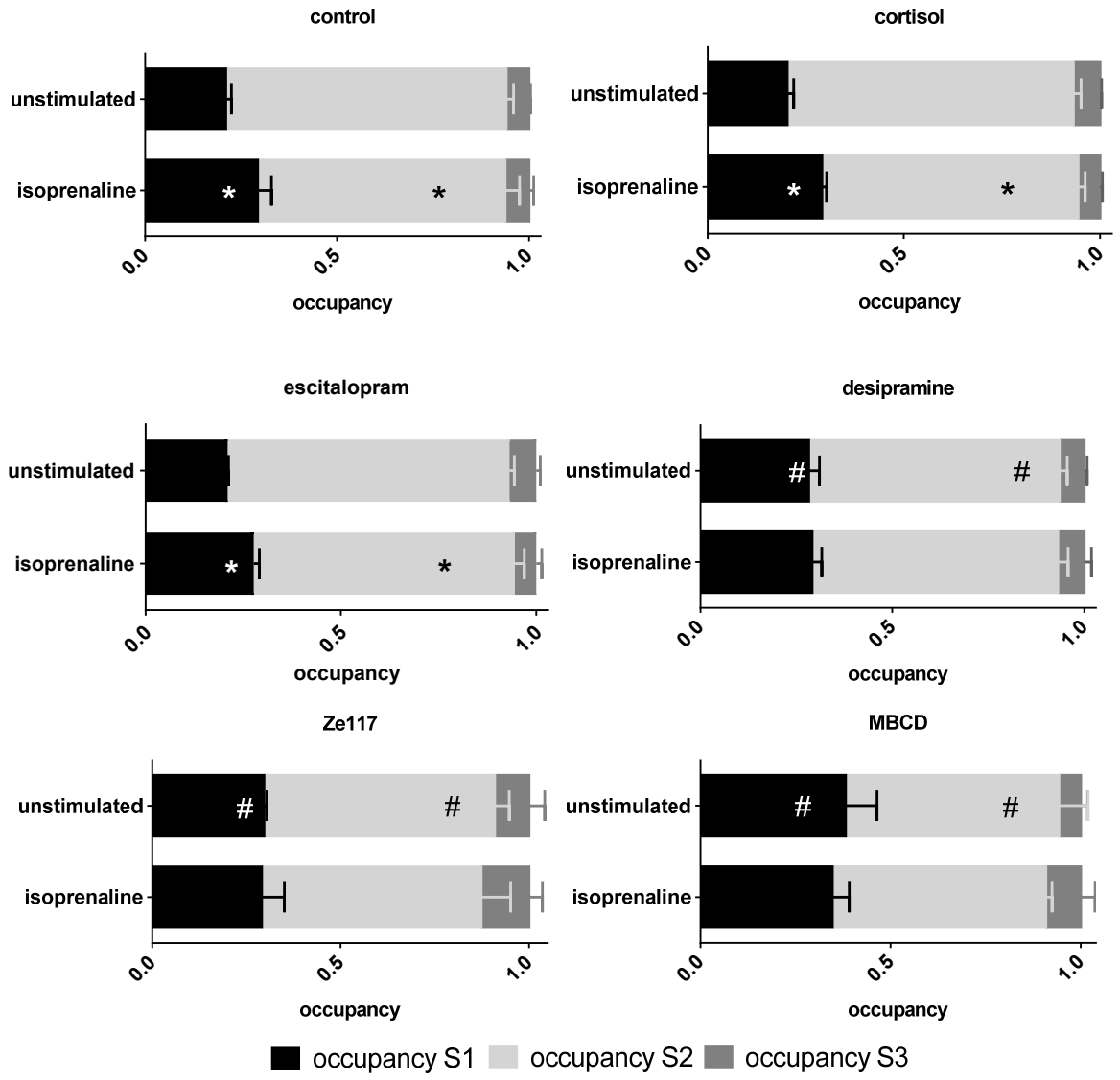


**Figure 4-23 Occupancies of diffusive states:** S1, S2, and S3 of SNAP-$\beta_1$AR on the plasma membrane of C6 SNAP-$\beta_1$AR cells before and after stimulation with 10 µM isoprenaline. Data was attained by vbSPT analysis. Cells were pretreated for 5 days with 0.25 mg/ml Ze117, 1 µM escitalopram, 1 µM desipramine, and 1 µM cortisol, respectively. One milimolar methyl-β-cyclodextrin (MβCD) was given to the cells 30 min before SPT measurements. * Marked values of occupancies are significantly different from corresponding unstimulated conditions with $p \leq 0.05$ determined by student's t-test. # Marked values of unstimulated conditions are significantly different from the unstimulated control condition with $p \leq 0.05$ determined by one-way ANOVA.

**Table 4-9 Corresponding values to Figure 4-23:** Occupancies of diffusive states S1, S2, and S3 of SNAP-$\beta_1$AR on the plasma membrane of C6 SNAP-$\beta_1$AR cells before and after stimulation with 10 µM isoprenaline. Data was attained by vbSPT analysis. Cells were pretreated for 5 days with 0.25 mg/ml Ze117, 1 µM escitalopram, 1 µM desipramine, and 1 µM cortisol, respectively. One milimolar methyl-β-cyclodextrin (MβCD) was given to the cells 30 min before SPT measurements. * Marked values of occupancies are significantly different from corresponding unstimulated conditions with $p \leq 0.05$ determined by student's t-test. # Marked values of unstimulated conditions are significantly different from the unstimulated control condition with $p \leq 0.05$ determined by one-way ANOVA.

| | **occupancy for S1** | **occupancy for S2** | **occupancy for S3** |
|---|---|---|---|
| **control** | | | |
| unstimulated | 0.21 ± 0.01 | 0.73 ± 0.02 | 0.06 ± 0.004 |
| stimulated | 0.29 ± 0.03 ***** | 0.64 ± 0.03 * | 0.06 ± 0.01 |
| **cortisol** | | | |
| unstimulated | 0.20 ± 0.01 | 0.73 ± 0.01 | 0.07 ± 0.003 |
| stimulated | 0.31 ± 0.02 ***** | 0.64 ± 0.02 * | 0.06 ± 0.008 |
| **escitalopram** | | | |
| unstimulated | 0.21 ± 0.002 | 0.72 ± 0.01 | 0.06 ± 0.003 |
| stimulated | 0.28 ± 0.01 * | 0.67 ± 0.02 * | 0.05 ± 0.01 |
| **desipramine** | | | |
| unstimulated | 0.28 ± 0.02 # | 0.65 ± 0.02 # | 0.06 ± 0.006 |
| stimulated | 0.29 ± 0.02 | 0.67 ± 0.02 | 0.07 ± 0.02 |
| **MβCD** | | | |
| unstimulated | 0.38 ± 0.07 # | 0.56 ± 0.06 # | 0.06 ± 0.02 |
| stimulated | 0.35 ± 0.04 | 0.56 ± 0.01 | 0.09 ± 0.03 |
| **Ze117** | | | |
| unstimulated | 0.30 ± 0.01 # | 0.61 ± 0.03 # | 0.09 ± 0.03 |
| stimulated | 0.29 ± 0.05 | 0.58 ± 0.06 | 0.09 ± 0.03 |

### 4.3.2.4 Packing coefficient analysis of spatial confinement

To further characterize the lateral diffusion of SNAP-$\beta_1$AR, the track segments corresponding to each state were extracted from full trajectories and subjected to a confinement analysis based on their state and packing coefficient (Pc) [57,68]. Every track segment in each state was classified as confined or freely diffusing based on its Pc. The Pc was then compared to a threshold derived from the 80$^{th}$ percentile of Pc in simulated data of free diffusion (Pc80). Track segments with an average Pc above that threshold were considered to be confined (Figure 4-24). Values were calculated for sufficiently long segments using a 10 frame (0.5 s) sliding window [57].

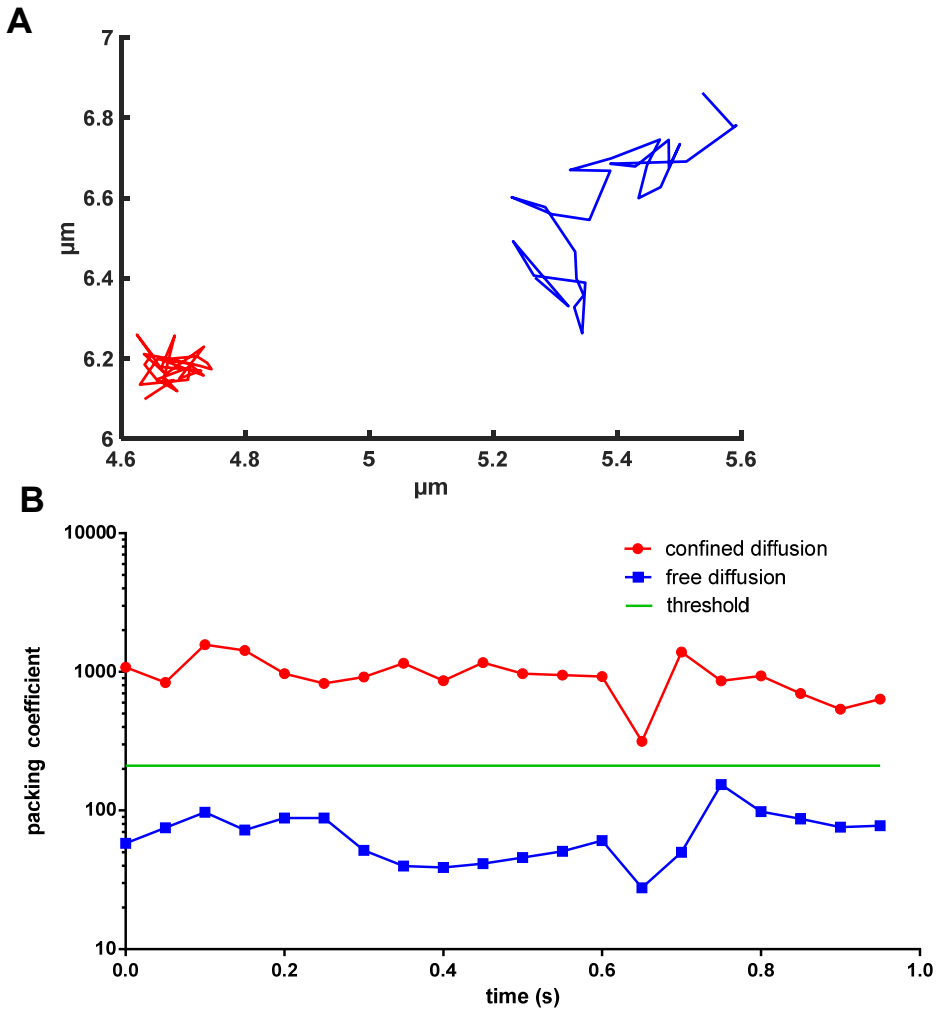


**Figure 4-24 Different diffusion behaviour of SNAP-$\beta_1$AR: A:** Representative trajectories of a confined diffusing particle in red and a free diffusing particle in blue. Both trajectories had a length of 20 frames (1.0 s). **B:** The trajectories were subjected to a confinement analysis based on their packing coefficients calculated with a 10 frames sliding window. A track was considered to be confined if its mean Pc-value was above the Pc80-threshold (=210, green line) of its corresponding state.

As can be seen in Figure 4-25-A, the trajectories were exponentially distributed mainly due to photobleaching. Only 25% of the unsegmented trajectories were longer than the average track length of 7.8 frames. The segmentation of the tracks by vbSPT resulted in different track length distributions for each state. Since the Pc-algorithm used a 10 frames sliding window, only trajectory segments that were visible for at least 0.5 s (10 frames) in SPT were included in the evaluation. In state S1 the average track length was 23.6 frames and 63% of the track segments were included in the confinement analysis. The average track length in S2 was 7.2 frames and 24% of the track segments were longer than 10 frames. The track segments in S3 were the shortest with an average of 3.0 frames (0.15 sec) and less than 1% could theoretically be included in the analysis. For this reason, statistically robust confinement analyses were only possible for S1 and S2.

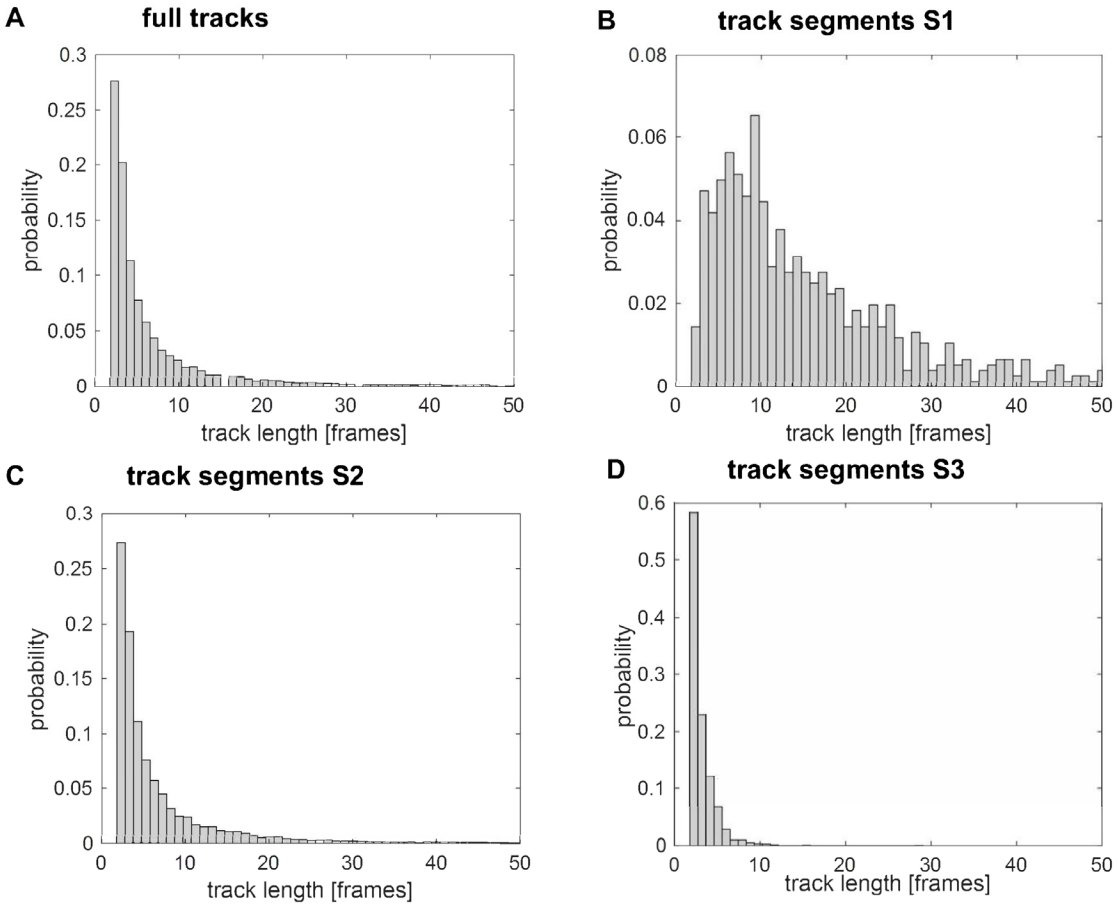


**Figure 4-25 Track length distributions: A:** Track length distribution of all detected SNAP-$\beta_1$AR trajectories in control cells before segmentation by vbSPT. Track length distributions of the trajectory segments in state S1 (**B**), S2 (**C**), and S3 (**D**).

The Pc80-values for S1 and S2 were set as 467 and 210, respectivly. For the control cells, 67.58 ± 6.52% of the evaluated trajectories in S1 were identified to be confined as shown in Figure 4-26. The mean confinement size, given as the square root of the convex hull area, was 79.4 ± 0.7 nm. After stimulation with 10 µM isoprenaline the confinement fraction remained approximately the same, whereas the confinement size was reduced to 78.7 ± 3.7 nm. Neither the pretreatment with 1 µM escitalopram, 1 µM desipramine, and 1 µM cortisol nor the treatment with 1 mM MβCD resulted in a significant change of confinement fractions or mean confinement sizes. Stimulation with 10 µM isoprenaline also did not change the confined fraction in S1. In these pretreatments the confined fraction ranged between 63.10 ± 4.89% and 74.51 ± 7.02%. In state S2 stimulation with 10 µM isoprenaline did not change the confinement in control cells compared to non-stimulated control cells. In the escitalopram, desipramine, and cortisol conditions, neither significant changes in the confined fraction nor in the mean confinement size were measured.

In C6 SNAP-$\beta_1$AR cells pretreated with 0.025 mg/ml Ze117, however, the confined fraction of S1 increased significantly to a value of 86.91 ± 11.05% compared to the control condition. The mean confinement size decreased to 68.1 ± 7.0 nm. Under isoprenaline stimulation the confined fraction in S1 increased further to 95.25 ± 4.59%, whereas the mean confinement size was significantly further reduced to 59.6 ± 1.4 nm. In S2 Ze117 preincubation significantly increased confined fraction in the non-stimulated condition to 73.08 ± 7.31%, compared to control cells. The mean confinement size decreased from 118 ± 2.6 nm to 103 ± 1.6 nm. After stimulation, this fraction rose significantly further to 88.68 ± 4.91%. The confinement size decreased from 107.8 ± 1.6 nm to 103.0 ± 2.1 nm.

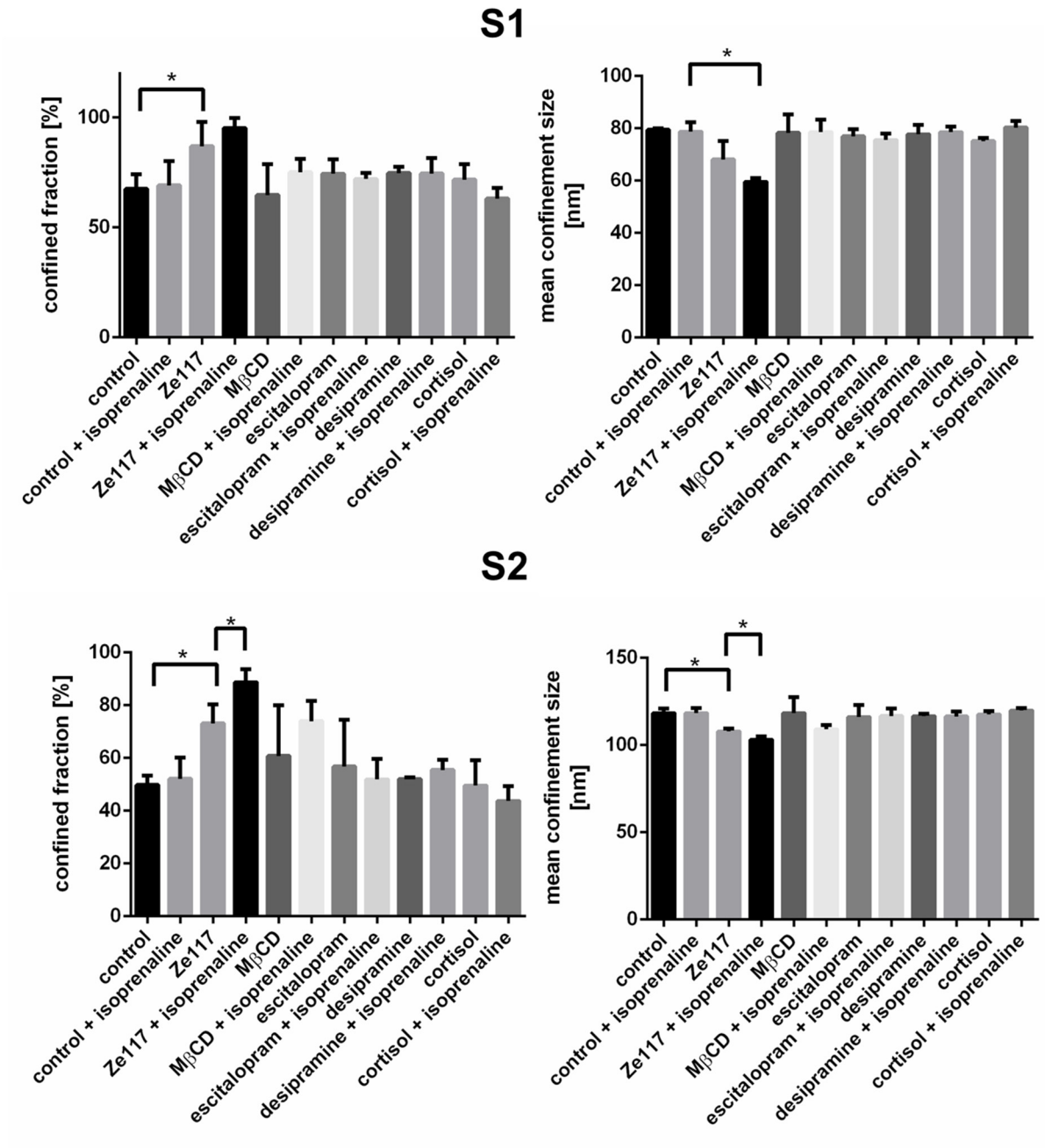


**Figure 4-26 Confinement of SNAP-$\beta_1$AR:** Percentages of confined trajectories and mean confinement sizes in the states S1 and S2 of SNAP-$\beta_1$AR on the plasma membrane of C6 SNAP-$\beta_1$AR cells. SPT measurements were performed with and without stimulation by 10 µM isoprenaline. Data were attained by packing coefficient analysis. Cells were pretreated for 5 days with 0.25 mg/ml Ze117, 1 µM escitalopram, 1 µM desipramine and 1 µM cortisol, respectively. One micromolar methyl-β-cyclodextrin (MβCD) was given to the cells 30 min before SPT measurements. * Marked values with $p \leq 0.05$ are significantly different from their corresponding control determined by one-way ANOVA.

**Table 4-10 Corresponding values to Figure 4-26:** Percentages of confined trajectories in the states S1 and S2 of SNAP-$\beta_1$AR on the plasma membrane of C6 SNAP-$\beta_1$AR cells. SPT measurements were performed with and without stimulation by 10 µM isoprenaline. Data were attained by packing coefficient analysis. Cells were pretreated for 5 days with 0.25 mg/ml Ze117, 1 µM escitalopram, 1 µM desipramine and 1 µM cortisol, respectively. One micromolar methyl-β-cyclodextrin (MβCD) was given to the cells 30 min before SPT measurements. * Marked values with $p \leq 0.05$ are significantly different from their corresponding control determined by one-way ANOVA.

| | **confined fraction in S1 [%]** | **confined fraction in S2 [%]** | **mean confinement size in S1 [nm]** | **mean confinement size in S2 [nm]** |
|---|---|---|---|---|
| **control** | | | | |
| unstimulated | 67.58 ± 6.52 | 49.80 ± 3.45 | 79.4 ± 0.7 | 118.3 ± 2.6 |
| stimulated | 69.12 ± 11.11 | 52.12 ± 8.08 | 78.7 ± 3.7 | 118.3 ± 3.0 |
| **cortisol** | | | | |
| unstimulated | 73.49 ± 7.03 | 49.52 ± 9.64 | 75.1 ± 1.2 | 117.6 ± 1.8 |
| stimulated | 63.10 ± 4.89 | 43.71 ± 5.50 | 80.3 ± 2.6 | 119.8 ± 1.6 |
| **escitalopram** | | | | |
| unstimulated | 74.49 ± 6.52 | 56.76 ± 17.72 | 77.0 ± 2.8 | 116.1 ± 7.0 |
| stimulated | 72.07 ± 2.76 | 51.88 ± 7.81 | 75.6 ± 2.4 | 116.7 ± 4.3 |
| **desipramine** | | | | |
| unstimulated | 74.79 ± 2.79 | 51.95 ± 0.74 | 77.7 ± 3.7 | 116.5 ± 1.4 |
| stimulated | 74.51 ± 7.02 | 55.48 ± 3.93 | 78.6 ± 2.0 | 116.4 ± 2.8 |
| **MβCD** | | | | |
| unstimulated | 64.77 ± 13.95 | 60.82 ± 19.22 | 78.3 ± 7.0 | 118.3 ± 9.2 |
| stimulated | 75.13 ± 6.12 | 74.00 ± 7.60 | 78.5 ± 4.8 | 109.1 ± 2.3 |
| **Ze117** | | | | |
| unstimulated | 86.91 ± 11.05 * | 73.08 ± 7.31 * | 68.1 ± 7.0 | 107.8 ± 1.6 * |
| stimulated | 95.25 ± 4.59 | 88.68 ± 4.91 * | 59.6 ± 1.4 * | 103.0 ± 2.1 * |

#### 4.3.2.5 Evaluation of vbSPT and packing coefficient analysis by computational simulations

To test the accuracy of the vbSPT and Pc algorithm, experimentally realistic track data was simulated inside a 10x10 µm square and subsequently evaluated by vbSPT. Three receptor states with diffusion coefficients of 0.016 µm²/s for S1, 0.034 µm²/s for S2, and 0.168 µm²/s for S3 were generated. For S1, S2, and S3 relative occupancy values of 0.21, 0.73, and 0.06 were simulated, respectively. The model values were based on the experimentally obtained data. 2000 trajectories were generated. To take photobleaching into account, an exponential distribution with the mean track length of 7.4 was assumed. All generated spots were subjected to a localization error by a normally distributed positional offset with $\sigma$ = 20 nm in each dimension.

Both the number of states and the diffusion coefficients (D) were determined accurately by vbSPT. Values for D1, D2, and D3 were calculated by vbSPT as 0.016 µm²/s, 0.035 µm²/s, and 0.170 µm²/s. The occupancy values were reproduced precisely by vbSPT and were calculated as 0.23 for S1, 0.70 for S2, and 0.07 for S3 (Table 4-11).

**Table 4-11 Evaluation of simulated data using vbSPT**

| Parameter | Simulated data | vbSPT data |
|---|---|---|
| Trajectory number | 2000 | 2000 |
| D1 (µm²/s) | 0.016 | 0.016 |
| D2 (µm²/s) | 0.034 | 0.035 |
| D3 (µm²/s) | 0.168 | 0.170 |
| S1 Occupancy | 0.21 | 0.23 |
| S2 Occupancy | 0.73 | 0.70 |
| S3 Occupancy | 0.06 | 0.07 |

Confinement was modeled for the respective track segments of each state with particles diffusing out of bounds being deflected towards the center. The mean confinement size was defined as the square root of a circular confinement area specified as 80 nm for S1 and 120 nm for S2. Confinement fractions were simulated with 50, 60, 70, 80 and 90% for each S1 and S2.

The data of the confined fraction were reproduced accurately for values between 50% and 70% (Table 4-12). If the simulated confined fractions exceeded 80%, the fractions determined by Pc analysis were underestimated. This was expectable, as a threshold was used, which derived from the 80$^{th}$ percentile of packing coefficients in simulated data of free diffusion.

The mean confinement sizes of SNAP-$\beta_1$AR in S1 were recognized with values between 88.7 nm and 89.3 nm (Table 4-12). The offset of 9 nm was probably due to the predefined localization accuracy of 20 nm. After Pc analysis the mean confinement sizes for S2 ranged from 114.9 nm to 115.6 nm and therefore showed an offset of 5 nm.

**Table 4-12** Evaluation of simulated data using packing coefficient analysis

| Parameter | Simulated data | Pc analysis data |
|---|---|---|
| S1 confined fraction (Mean confinement size) | 50% (80 nm) | 52% (89.3 nm ) |
| | 60% (80 nm) | 58% (88.8 nm ) |
| | 70% (80 nm) | 68% (88,8 nm) |
| | 80% (80 nm) | 74% (89.0 nm) |
| | 90% (80 nm) | 80% (88.7 nm) |
| S2 confined fraction (Mean confinement size) | 50% (120 nm) | 54% (115.6 nm) |
| | 60% (120 nm) | 60% (115.1 nm) |
| | 70% (120 nm) | 65% (115.1 nm) |
| | 80% (120 nm) | 74% (114.9 nm) |
| | 90% (120 nm) | 80% (114.9 nm) |

#### 4.3.2.6 Oligomerization states of SNAP-tagged $\beta_1$-adrenergic receptors

To study the oligomerization states of BG-Dy549 labeld SNAP-tagged $\beta_1$-adrenergic receptors (SNAP-$\beta_1$AR) on the cell surface, histogram analyses of the fluorescence intensities of all particles were performed for each condition.

The fluorescence intensities of monomeric receptors detected in SPT are normally distributed around the mean value $\mu$ corresponding to a single fluorophore. In the case of multimeric receptor complexes, the intensity distribution is the sum of $n$ components with the respective mean values $\mu \cdot n$. To determine the fractions and mean intensities of the corresponding oligomers and monomers, a mixed Gaussian fitting was performed on the underlying intensity distributions of the SPT data (Figure 4-27).

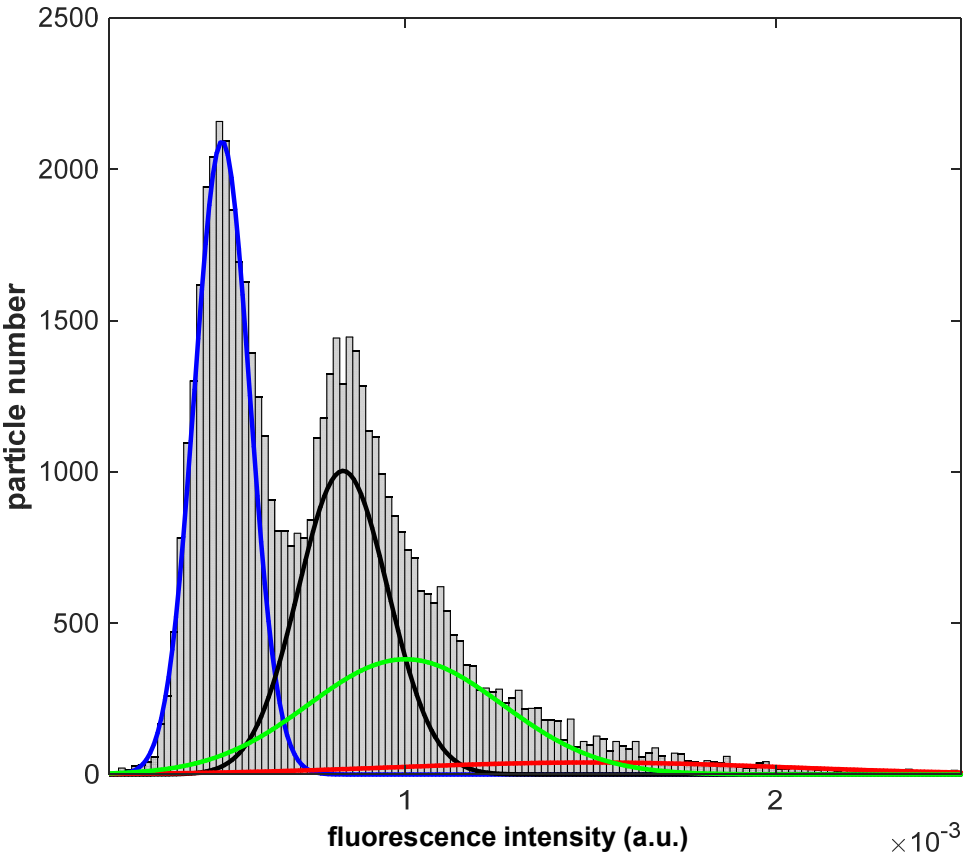


**Figure 4-27 Representative fluorescence intensity distribution of BG-Dy549 labeled SNAP-$\beta_1$AR:** Data were fitted with a mixed Gaussian model. The curve fitting was performed for four components corresponding to different oligomerization states: monomers (blue line), dimers (black line), trimers (green line) and tetramers (red line).

This analysis revealed that in all conditions four populations of different intensities corresponding to monomers, dimers, trimers, and tetramers were found. Figure 4-28 shows that the fractions of monomers or oligomers fluctuate strongly, which can be seen from standard deviations. Thus, significant differences of the oligomerization states within all conditions could not be seen.

The present data revealed that mainly monomers occur in fractions from 0.36 to 0.51. The receptor dimer complexes accounted for fractions between 0.32 and 0.42. Receptor trimer complexes represented smaller fractions with a relative occurrence between 0.14 and 0.28. Tetramers were even rarer and occured with proportions between 0.01 and 0.04. Values for each condition are given in Table 4-13.

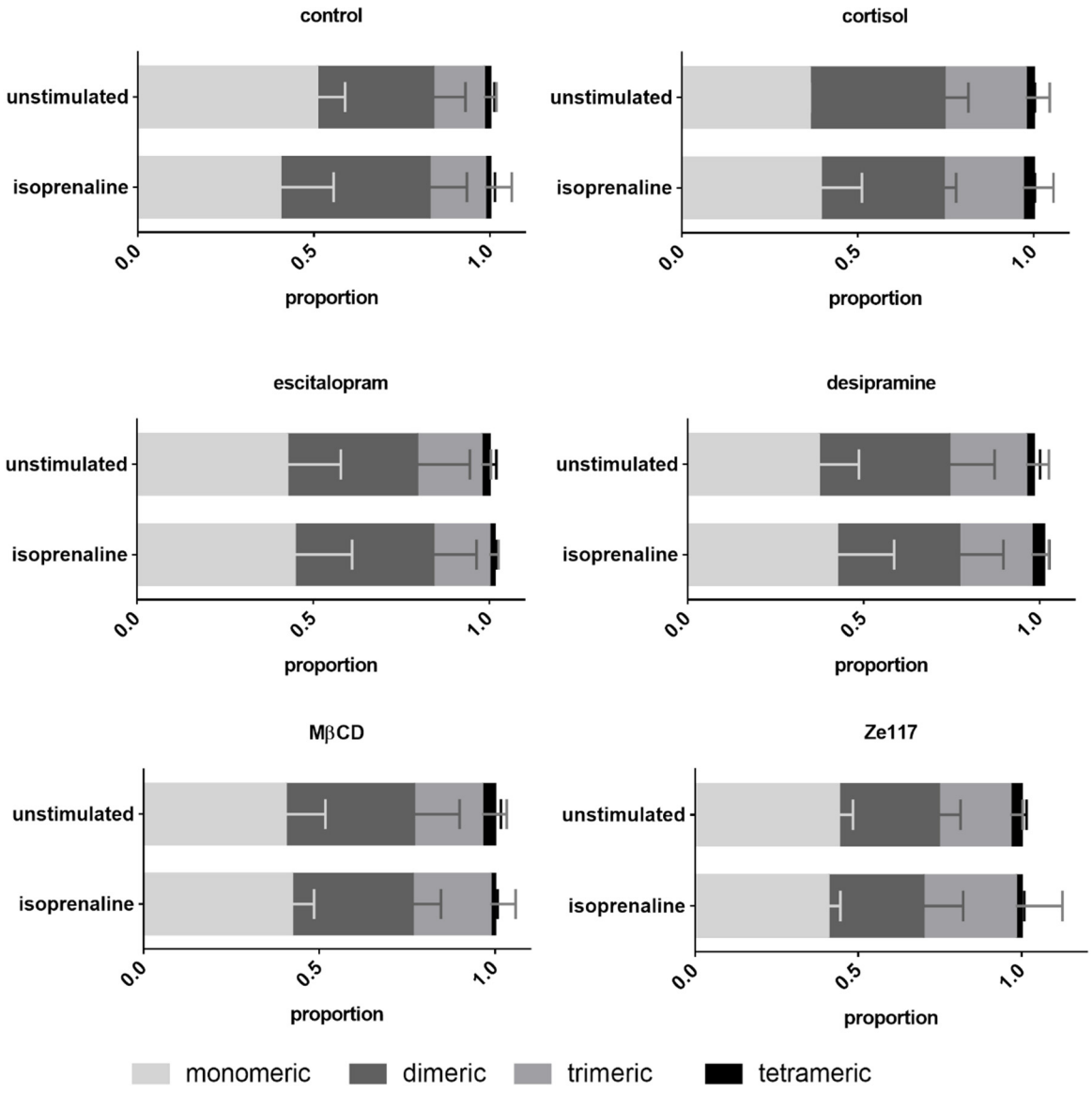


**Figure 4-28 Fractions of receptor mono- and oligomers of SNAP-$\beta_1$AR on the plasma membrane of C6 SNAP-$\beta_1$AR cells:** SPT measurements were performed with and without stimulation by 10 µM isoprenaline. Data was attained by fitting fluorescence intensities with a mixed Gaussian model. Cells were pretreated for 5 days with 0.25 mg/ml Ze117, 1 µM escitalopram, 1 µM desipramine, and 1 µM cortisol, respectively. One micromolar methyl-β-cyclodextrin (MβCD) was given to the cells 30 min before SPT measurements.

**Table 4-13 Corresponding values to Figure 4-28** Fractions of receptor mono- and oligomers of SNAP-β1AR on the plasma membrane of C6 SNAP-β1AR cells: SPT measurements were performed with and without stimulation by 10 µM isoprenaline. Data was attained by fitting fluorescence intensities with a mixed Gaussian model. Cells were pretreated for 5 days with 0.25 mg/ml Ze117, 1 µM escitalopram, 1 µM desipramine, and 1 µM cortisol, respectively. One micromolar methyl-β-cyclodextrin (MβCD) was given to the cells 30 min before SPT measurements.

| | **monomer proportion** | **dimer proportion** | **trimer proportion** | **tetramer proportion** |
|---|---|---|---|---|
| **control** | | | | |
| unstimulated | 0.51 ± 0.08 | 0.33 ± 0.09 | 0.14 ± 0.04 | 0.019 ± 0.012 |
| stimulated | 0.40 ± 0.15 | 0.42 ± 0.11 | 0.16 ± 0.08 | 0.015 ± 0.014 |
| **cortisol** | | | | |
| unstimulated | 0.36 ± 0.01 | 0.38 ± 0.07 | 0.23 ± 0.07 | 0.023 ± 0.003 |
| stimulated | 0.39 ± 0.12 | 0.35 ± 0.04 | 0.23 ± 0.09 | 0.031 ± 0.003 |
| **escitalopram** | | | | |
| unstimulated | 0.43 ± 0.15 | 0.37 ± 0.15 | 0.18 ± 0.03 | 0.023 ± 0.020 |
| stimulated | 0.45 ± 0.16 | 0.39 ± 0.12 | 0.16 ± 0.03 | 0.015 ± 0.004 |
| **desipramine** | | | | |
| unstimulated | 0.37 ± 0.12 | 0.37 ± 0.13 | 0.22 ± 0.07 | 0.022 ± 0.018 |
| stimulated | 0.42 ± 0.16 | 0.35 ± 0.13 | 0.21 ± 0.05 | 0.036 ± 0.015 |
| **MβCD** | | | | |
| unstimulated | 0.43 ± 0.11 | 0.36 ± 0.13 | 0.19 ± 0.07 | 0.037 ± 0.017 |
| stimulated | 0.40 ± 0.06 | 0.34 ± 0.08 | 0.22 ± 0.07 | 0.013 ± 0.007 |
| **Ze117** | | | | |
| unstimulated | 0.44 ± 0.04 | 0.31 ± 0.07 | 0.22 ± 0.04 | 0.035 ± 0.015 |
| stimulated | 0.41 ± 0.04 | 0.29 ± 0.12 | 0.28 ± 0.14 | 0.018 ± 0.008 |

# 5 Discussion

Depressive disorders are ranked in the top 10 priority list of public health significance [69]. It is predicted to become the second most important disease worldwide in 2030 [70]. Therefore, a better understanding of the molecular mechanisms of this disease and its successful treatment are of great interest. Although the exact pathology of depression is still unknown, it is generally acknowledged that chronic stress is an important factor in the development of depression [71]. Chronic stress leads to an increased formation of catecholamines and glucocorticoids (e.g. cortisol), resulting in hyperactivity of the hypothalamic-pituitary-adrenal (HPA) axis [43].

The treatment of a depressive disorder aims at relieving the depressive symptoms. The choice of the appropriate treatment alternative of depression depends on clinical factors such as the severity of the symptoms and the course of the illness, as well as the patient‘s preference. Basically, there are four primary treatment strategies: psychosocial interventions (“watchful waiting”), pharmacotherapy, psychotherapeutic care and and a combination therapy of the latter two [2]. Currently, selective serotonin reuptake inhibitors (SSRI) or tricyclic and related antidepressants are first line medication [2]. Nontheless, clinical studies show that the clinical effect is not far above placebo [72]. Even though SSRI show a better cardiovascular compatibility than tricyclic antidepressants, side effects occur. Among these are e.g. withdrawal symptoms as well as gastrointestinal and excitatory adverse events [2]. The German National Health Care Guideline for Unipolar Depression recommends St. John's wort (SJW) as a first therapeutic attempt for mild or moderate depressive disorders [2]. Also, the Committee on Herbal Medicinal Products (HMPC) grants Hypericum perforatum L., Herba the status “well established medical use” based on the clinical and preclinical data [73]. A Cochrane review by Linde et al. (2008), based on 29 trials with 5489 patients in total, showed that St. John's wort (SJW) preparations are as efficacious as synthetic antidepressants, but show fewer adverse effects [19].

However, the exact mechanism of action of SJW extracts is still not fully understood. One accepted hypothesis is that SJW preparations inhibit the reuptake of serotonin, norepinephrine and dopamine in the presynaptic cleft [24,74]. This increases the concentration of neurotransmitters in the presynaptic cleft and intensifies the signal

transduction to the postsynaptic neuron. A diminished activity of neurotransmitter pathways is a key factor in the pathophysiology of depression [75] and is counteracted by SJW. Another mechanism of action was identified by Keksel et al. (2019), who demonstrated a membrane fluidity increasing effect in C6 cells mediated by chronic incubation with the stress hormone cortisol. An opposite effect was found after chronic Ze117 treatment [53]. By co-incubation of cortisol with Ze117 it was observed that Ze117 counteracts a possible cortisol-induced change in the lipid composition of C6 cells.

In this work, alterations of the plasma membrane fluidity of peripheral blood mononuclear cells (PBMC) were assessed by fluorescence anisotropy measurements using 1,6-diphenyl-1,3,5-hexatriene (DPH) as probe. To test DPH in this work as a sensitive plasma membrane probe and the applicability of PBMC anistropy measurements, cholesterol depletion was performed in PBMC by using methyl-β-cyclodextrin (MβCD) [76,77]. By decreasing the cholesterol content of the plasma membrane a decreased fluorescence anisotropy value and therefore increased plasma membrane fluidity was observed (Figure 4-2). An explanation is provided by Chen et al. (1999) [78]. They found that an increase in plasma membrane cholesterol content sterically blocks large motions of fatty acyl chains of phospholipids. Cholesterol thereby rigidifies the plasma membranes by restricting the random diffusion of phospholipids.

Keksel et al. (2019) applied the same technique and the identical fluorescent probe, but used adherent C6 cells instead of soluble PBMC. One advantage of applying soluble cells in fluorescence anisotropy measurements is a lower background signal in a cell suspension compared to a monolayer on a glas coverslip. Another advantage is that in a cell suspension several million cells can be measured at the same time, which allows to generate more stable results. In contrast, by measuring cell monolayers on glas coverslips only several thousand cells are assessed at the same time.

In this work a decrease of fluorescence anisotropy after cortisol preincubation was found in PBMC, indicating an increased membrane fluidity (Figure 4-3). After preincubation with Ze117 plasma membrane fluidity decreased. The same membrane fluidity changing effects of cortisol and Ze117 on C6 cells which were shown by Keksel et al. (2019) were reproduced on primary PBMC in this work [53]. This is remarkable

because in contrast to brain tissues PBMC are easy to obtain and could therefore be used for diagnostic purposes.

Cortisol mediated increase in membrane fluidity was also found for DPH probed human lymphocytes [46]. This is interesting because in PBMC mainly lymphocytes occur.

A plasma membrane rigidification in murine microglia cells was also described by Kraus et al. (2007) after a 24 h incubation with a non commercial SJW extract [79]. They also applied fluorescence anisotropy measurements, but used pyrene decanoic acid instead of DPH as a fluorescent probe.

The plasma membrane consists mainly of different phospholipids, which are arranged in a bilayer. The polar, hydrophilic head groups are on the outside and the hydrophobic hydrocarbon chains are on the inside of the bilayer. The hydrocarbon chains consist of fatty acids, which can differ in length and saturation. In fact, plasma membrane fluidity partly depends on the chain length and the number of double bonds of the fatty acid moieties of phospholipids. Cis-configured double bonds are responsible for curvatures in unsaturated fatty acids. If phospholipids contain fatty acids with more double bonds, the resulting curvatures increase and van der Waal‘s interactions between acyl chains decrease, leading to a more fluid membrane. In contrast, pure saturated fatty acids can be packed more tightly leading to a more rigid plasma membrane [80]. Changes in the membrane fluidity were attributed by Keksel et al. (2019) to changes in molecular structures of fatty acid moieties and head groups of membranous phospholipids [53]. Thus, in the present work the fatty acid composition of phospholipids was further investigated by a comprehensive lipidomic analysis of cortisol and Ze117 preincubated PBMC.

Interestingly, numerous other studies have recently highlighted a relationship between major depressive disorders (MDD) and the lipidome [80–82]. Mocking et al. (2017) concluded in a review regarding fatty acids in psychiatric disorders, that fatty acid metabolism forms a complex neurometabolic network that seems to alter the vulnerability of psychiatric diseases [80].

Knowles et al. (2017) found that alterations in the lipidome are not necessarily secondary to the manifestation of MDD, but rather share etiology with the illness [41]. They concluded that lipids, their fatty acid moieties and their molecular pathways are

promising candidates when attempting to improve diagnostics and treatment efforts in MDD.

In this thesis the influences of cortisol and the cortisol/Ze117 combination, respectively, on the average chain length and the average number of double bonds of fatty acids were analyzed for several lipid classes. The evaluation was based on quantitative values of each lipid species relative to total amounts of the respective lipid classes assessed by mass spectometry analysis. In lipidomic studies both chain lengths and double bonds of fatty acids are described as robust and resilient parameters [60,61]. Thus, small differences indicate changes in the lipid metabolism of the cells.

Compared to the control, a significant increase in both the average chain length and the average number of double bonds within phosphatidylcholines (PC) was found for cortisol treated PBMC (Figure 4-5). In contrast, the average chain length after co-incubation with 1 µM cortisol and 50 µg/ml Ze117 was brought to control level, indicating a significant counteracting effect of Ze117. A similar counteracting effect of Ze117 compared to cortisol-treated cells was observed for the average chain length of phosphatidylinositols (PI) (Figure 4-7).

For other investigated lipid classes no significant effect of cortisol was observed. However, Ze117 showed a reduction of the average chain length and the average number of double bonds in most lipid classes, except for phosphatidylcholine ethers (PC O), phosphatidylserines (PS), and ceramides (Cer) compared to the cortisol condition.

The cortisol-induced increase of the average number of double bonds in the PC species could be due to an increased proportion of long chain polyunsaturated fatty acids (LC-PUFA). Otoki et al. (2017) investigated seasonal changes in the occurrence of fatty acids bound to phospholipids, triacylglycerols and cholesterol esters in the plasma of patients with winter depression [83]. They observed in phospholipids a non-significant but continuous increase of all LC-PUFA during winter season. It can be assumed that this is accompanied by an increase of the average number of double bonds and the average chain length. Surprisingly, this has not been investigated by the authors.

Mocking et al. (2015) investigated in a clinical trial whether alterations in fatty acid (FA) metabolism are associated with prospective response to the antidepressant paroxetine

in MDD. They compared 70 initially unmedicated MDD-patients with 51 age- and gender-matched controls, regarding salivary cortisol and erythrocyte membrane fatty acids. The authors found that, compared to controls, patients showed higher FA-chain length and FA-unsaturation. However, early paroxetine responders showed initial low FA-chain length, FA-peroxidation and eicosapentaenoic acid that increased during the study, while non-responders exhibited opposite patterns. The results demonstrate that FA-metabolism is altered in depressive patients and is also associated with prospective paroxetine response in MDD and may therefore be an early indicator of treatment effectiveness.

The decrease of the average number of double bonds of fatty acids after cortisol/ Ze117 co-incubation suggests a lower activity or expression of desaturases in PBMC mediated by Ze117. Δ-5 and Δ-6 desaturase are the rate limiting enzymes involved in the biological pathway of synthesis of polyunsaturated fatty acids (PUFA) [84,85]. Both desaturases are encoded in two, ‘head to head’ genes on chromosome 11: FADS1 and FADS2 [86]. Both desaturases together with elongase are involved in the transformation of the Ω6 fatty acid linoleic acid (18:2) to arachidonic acid (20:4). Arachidonic acid (AA) is a precursor of prostaglandins and leukotriens and thus strongly involved in inflammatory processes. Obukowicz et al. (1998) demonstrated in a mouse model, that inhibition of desaturases reduced arachidonic acid formation and decreased oedema and inflammation [87]. Higher AA levels in erythrocyte membranes of patients with MDD were also observed in a clinicial trial by Mocking et al. (2018) [88].

An inhibition of desaturases by SJW ingredients is not yet described in the literature. Still, SJW is also known for its anti-inflammatory effect [89], which could also partly be related to an inhibition of desaturases. Since increasing amounts of data suggest that inflammatory processes have an impact in the pathogenesis of depression, there could be a connection between antidepressant and anti-inflammatory properties of SJW. It has been shown that depressed patients have higher levels of proinflammatory cytokines, acute phase proteins, chemokines and cellular adhesion molecules [90]. Furthermore, therapeutic administration of the cytokine interferon-α leads to depressive symptoms in up to 50% of patients. Proinflammatory cytokines have been found to interact with many of the pathophysiological domains that characterize

depression, including neurotransmitter metabolism, neuroendocrine function, synaptic plasticity and behavior [90].

However, a distinction must be made between anti-inflammatory PUFA and proinflammatory PUFA. Ω3 PUFA are characterized by the presence of a double bond three atoms away from the terminal methyl group in their carbon chain. Ω6 PUFA, respectively, are characterized by the presence of a double bond six atoms away from the terminal methyl group. Ω6 PUFA are considered proinflammatory, as linoleic acid (18:2, Ω6) is a precursor of AA. In contrast, Ω3 PUFA α-linolenic acid (ALA, 18:3, Ω3) appears to attenuate inflammation. ALA can be metabolized into precursors for long-chain Ω3 PUFA such as eicosapentaenoic acid (EPA, 20:5, Ω3) and docosahexaenoic acid (DHA, 22:5, Ω3). Ω3 PUFA act as competitive substrate for Δ-5 and Δ-6 desaturases of the Ω6 PUFA metabolism and therefore show anti-inflammatory effects [91].

Thus, a general increase in the average number of double bonds and the average chain length can in principle not speak for a higher probability of depression. On the contrary, some studies show that a higher proportion of PUFA correlate with a lower depression probability. In a meta-analytic review by Lin et al. (2010) low levels of DHA and EPA were discussed to be involved in the pathogenesis of depression [40]. Higher levels of DHA and EPA were found in rodents treated with antipsychotics [92]. However, the results of the present work are in line with the connection of depression with fatty acid metabolism. It can be assumed that it might be useful to combine the St. John's wort therapy with the administration of Ω3 fatty acids to obtain a stronger antidepressant effect. This combination could lead to a mutual inhibition of AA synthesis.

An approach to treat depression directly through pharmaceutical intervention in the fatty acid metabolism is currently a topic of research [93]. Glitazones are usually prescribed for the treatment of type 2 diabetes. However, latest results of research indicate that the administering of this class of drugs seems to be a promising approach for the treatment of MDD. Glitazones are specific agonists of the peroxisome proliferator-activated receptor γ (PPARγ), which is an important transcription factor for various enzymes of lipid metabolism. Several studies have shown that they have a clinical benefit in the treatment of depression. In a review by Colle et al. (2016) 8 studies with 448 patients with major depression were included, of which 209 patients

received PPAR-γ agonists (pioglitazone or rosiglitazone) for 6–12 weeks, either alone or in add-on therapy to conventional treatments [93]. In 7 out of 8 studies PPAR-γ agonists had an antidepressant effect, demonstrated by improved depressive scores.

Like Ze117 on PBMC, a decrease in the average number of double bonds and average chain length was observed in hepatic tissues of rats after dietary treatment with a PPAR-pan agonist [94]. There is also evidence that St. John's wort preparations enhance the expression of PPARγ [95–97].

It is noteworthy that after evaluating lipidomic data of cortisol pretreated PBMC, on the one hand, significant effects on the global parameters like average number of double bonds and average chain length were found. On the other hand, no significant effect on the occurrence of individual lipid species was observed (Figure 4-10). Due to the lipid standards used for mass spectrometry in this lipidomics approach, shifts within one lipid species can only be statistically determined, if alterations of at least 15% to 50% occur. Obviously, the changes in the lipidome caused by cortisol are not large enough to be measured significantly for individual lipid species. In any case, the changes in membrane fluidity can be explained rather by global sum effects, such as the average number of double bonds, than by changes in the proportions of a few individual lipid species.

However, compared to PBMC pretreated with cortisol alone, co-incubation with cortisol/Ze117 mainly elevated storage lipids like triacylglycerides (TAG) and diacylglycerides (DAG) (Figure 4-11). It was also examined which lipids besides the storage lipids were subject to significant changes when comparing cortisol preincubated PBMC with PBMC co-incubated with cortisol and Ze117. A total of six individual lipid species from three different lipid classes with significant differences between the two conditions were found (Table 4-7). Two phosphatidylglycerol (PG) species were downregulated by the cortisol/Ze117 combination. In addition, two hexosylceramides (HexCer) and phosphatidylcholine ethers (PC O) were identified, whose proportions were significantly increased after co-incubation with cortisol and Ze117 compared to cortisol pretreatment. Since no pattern can be identified from these few single lipid species, this result is difficult to interpret. Some diagnostic markers of depression were also identified in literature. A rodent study examined the lipidome in plasma after subcutaneous injections of corticosterones [98]. A decrease of phosphatidylcholines and phosphatidylethanolamines was observed in plasma

samples. The proportion of lysophosphatidylcholines, ceramides, phosphatidic acids and phosphatidylglycerols increased.

In a study by Demirkan et al. (2013) 148 plasma phospho- and sphingolipid species of 742 individuals were examined [99]. They identified phosphatidylcholine ether, characterized by two fatty acids with 36 carbon atoms in total and 4 double bonds (PC O 36:4) as a lipid that correlates both with MDD and a target molecule of phospholipase A2 (PLA2). PLA2 catalyzes the cleavage of AA from PC O 36:4. AA is subsequently converted into inflammatory mediators. Additionally, AA increases membrane fluidity and activates protein kinase C [100]. However, Walther et al. (2018) concluded in a review, that the prediction power of individual lipid markers is still insufficient, as study results were inconsistent [42].

Nonetheless, in the present work a clear pattern was seen for elevated proportions of nearly all storage lipid species of the TAG and DAG classes.

In a serum lipidomic analysis of patients with MDD Kim et al. (2018) also identified several triglyceride species as possible diagnostic markers for MDD [82], next to lysophosphatidic acids and lysophosphatidylcholines.

The increase in storage lipids suggests an activation of PPAR. Many of the proteins relevant for fatty acid uptake, such as acyl-CoA-binding protein, apolipoproteins, fatty acid binding proteins, and Δ-6-desaturase are regulated by PPARα, PPARδ or PPARγ. [101,102]. Another reason for the increase in storage lipids could be a cortisol/Ze117 mediated activation of PLA2. PLA2 hydrolyzes the fatty acid at the sn-2 position of the glycerol moiety of the head group. The released fatty acids are then available for further metabolic pathways, which may lead to an increase in DAG and TAG levels [103]. Lee et al. (2009) conducted a study in which rats were treated with various antidepressants for four weeks [104]. Subsequently, lipidome analysis of the prefrontal cortex revealed a decrease in long-chain fatty acids in the phosphatidyl choline species and an increase in lysophosphatidylcholine species with short fatty acids after administration of the antidepressants maprotiline and paroxetine. This finding was attributed to an activation of PLA2, specifically hydrolyzing long-chain fatty acids. In a further study by the same working group on the same maprotiline pretreated rats a behavioral test was conducted. The test confirmed a less pronounced depressive behavior. The antidepressive effect of maprotiline was again reduced by PLA2 suppression. [105].

Another reason for an exposed position of PLA2 in the context of depression is that lithium, often used for the treatment of bipolar depressive disorders and unipolar depression, was shown to inhibit the over-activity of arachidonic acid-specific PLA2 in the brain *in vivo* [106].

In a study by Kim et al. (2018) serum lipidomic analyses of patients with MDD were compared to those of healthy patients. Interestingly, they found decreased levels of several TAG and DAG species in patients with MDD. The SSRI fluoxetine also caused an increase in storage lipids in liver cells [107], similarly to Ze 117 as described in this work. Feng et al. (2012) attributed this finding to an activation of sterol regulatory element binding protein (SREBP). SREBP is a master regulator of lipid homeostasis and its activation leads to triglycerides accumulation through increasing lipid synthesis and decreasing lipid oxidation [108]. In another study cultured human glioma cells (GaMg) were exposed to the antidepressants imipramine, amitriptyline, clomipramine, citalopram, fluoxetine, mirtazapine, and bupropion. Although to different extents, all antidepressants activated the SREBP system [109].

It has also been described in literature that the lipid composition has a direct influence on neuronal receptors, which are embedded in the plasma membrane [33,59]. Thus, in the present work the lateral diffusion behavior of $\beta_1$-adrenergic receptors ($\beta_1$AR) in the plasma membrane of cortisol, escitalopram, desipramine, MβCD and Ze117 pretreated cells was observerd.

The $\beta_1$AR belongs to the family of G-protein-coupled receptors (GPCR). For a successful transduction of an external signal into the cell interior, a GPCR must bind a G-protein and activate it by exchanging a bound GDP with a GTP. After activation, the heterotrimeric G-protein splits into α and βγ subunits. The α subunit in turn activates effector proteins such as adenylyl cyclase (AC). These protein-protein interactions all take place at the plasma membrane and are significantly influenced by the lateral mobility of the individual components in the membrane. This theory is known as the "mobile receptor hypothesis" [110]. The mobility of the receptor depends on many factors. According to the "membrane skeleton fence model", the membrane is divided by a network of actin filaments, which is part of the cytoskeleton of the cells and is located in close proximity to the plasma membrane [111]. In addition, various transmembrane proteins anchored to the actin-based membrane skeleton meshwork act as rows of pickets that temporarily represent diffusion barriers within the plasma

membrane [112]. The phospholipid bilayer also contains membrane regions which are particularly rich in cholesterol and are characterized by an increased membrane rigidity and density of signal proteins. The resulting microdomains of the cell membrane represent semi-permeable diffusion barriers for receptors. Interestingly, receptors and signal proteins are not evenly distributed in these microdomains but are more or less preferentially located in individual microdomains. This modulates the probability of protein-protein interaction and allows the cell to regulate receptor mediated signals [113]. Receptors either diffuse within the microdomain or can leave it by "hop diffusion" [112]. Consequently, each receptor trajectory would have two different diffusion behaviors: a hindered diffusion within microdomains and a more or less free diffusion outside the microdomain. However, the receptor also interacts with other proteins, such as G-proteins, which also has an impact on the receptor's diffusion. Sunkgaworn et al. (2017) found that during interaction with $G\alpha_i$-proteins, the diffusion of $\alpha_{2A}$-adrenergic receptors is significantly hindered [114]. The different receptor states described in this work are therefore due to the interactions of receptors with their micro-environment in the cell membrane. If one of the test substances influences the balance between the different receptor states, e.g. by direct interaction with the receptors, changes in membrane properties or receptor activities, the probability of the receptor to be in a certain diffusive state changes.

In order to observe the lateral mobility of $\beta_1$AR, SNAP-tagged receptors were fluorescently labeled with a SNAP-tag-dye (Figure 4-18). Calebiro et al. (2013) were the first authors demonstrating the usability of SNAP-tagged receptors for single particle tracking [37]. They used direct receptor labeling with SNAP-tag to dynamically monitor $\beta_1$AR, $\beta_2$AR and $GABA_B$ receptors on living cells, and compared their spatial arrangement, mobility and supramolecular organization. Several following studies used SNAP-tagged receptors for single particle tracking [68,114,115]. Schwenzer et al. (2018) investigated the lateral mobility of SNAP-tagged $\beta_2$AR in HEK wild type and HEK β-arrestin knock out cells with and without isoprenaline stimulation. Sunkgaworn et al. (2017) investigated receptor-G-protein interactions by staining the receptor and G-protein with different colored fluorescent dyes [114]. Ibach et al.(2015) used single particle tracking techniques and SNAP-tagged epidermal growth factor receptors (EGFR) to relate mobility and aggregation of EGFR to its signaling activity [115].

For keeping bleaching as low as possible and at the same time obtaining a high brightness after laser excitation at a wavelength of 532 nm, the fluorescent dye Dy549 was chosen for the present work [63]. This dye was coupled to the SNAP-tag substrate benzylguanine (BG) by a simple amide coupling reaction. As Meijering et al. (2012) pointed out, a signal to noise ratio of at least 4 should be reached to ensure accurate and robust automated spot tracking [67]. The mean signal noise ratio of BG-Dy549 stained receptors in the SPT experiments of this work was 8.64 ± 3.30 (Figure 4-21). Furthermore, in a publication by Bosch et al. (2014) BG-Dy549 was found to be among the best choices to label SNAP-tag fusion proteins for single-molecule tracking in terms of low unspecific membrane binding and high photostability [63]. BG-Dy549 was therefore considered suitable for single particle tracking experiments in the present work.

After localizing the SNAP-tagged $\beta_1$AR (SNAP-$\beta_1$AR) in different positions over time and merging the single spots to trajectories with uTrack, the vbSPT algorithm divided the trajectories into segments according to their momentary diffusion speed as described by Persson et al. (2013) [56]. Thus, different diffusion states can be detected within a single trajectory. In contrast to other hidden Markov model approaches in single molecule tracking [116,117], vbSPT is able to extract useful information, such as diffusion coefficients and occupancy values, even from data sets with short trajectories. This is important as fluorescent dyes bleach out due to irradiation by a laser, which statistically results in a higher proportion of short trajectories (Figure 4-25).

The vbSPT generated segments were then classified into three disctinct receptor diffusion states (S1, S2, and S3). Each state was defined by a diffusion coefficient and a corresponding state occupancy value. The states were classified as an immobile state S1, a slow diffusing state S2, and a fast diffusing state S3. However, the vbSPT algorithm was able to detect more than three states, but the introduction of a fourth state to the model led to an additionally immobile receptor state, and the detection of higher diffusion coefficients in the other three states. A mean square displacement analysis of a four-state model showed that S1 and S2 were extremely similar und could therefore be subsumed to a single state, resulting in a three-state model.

In the present study, for SNAP-$\beta_1$AR overexpressed in C6 cells three individual diffusion coefficients were detected (Figure 4-22). Calebiro et al. (2013) also investigated the lateral diffusion of SNAP-$\beta_1$AR using SPT [37]. The authors calculated

diffusion coefficients of individual SNAP-$\beta_1$AR by using MSD analysis. However, the receptor population was not examined for the occurrence of different states as in the present thesis by using a statistic evaluation algorithm like vbSPT. The peak of the frequency distribution of diffusion coefficients was between 0.032 and 0.043 µm²/s, which corresponds almost exactly to the state S2 with 0.034 ± 0.0002 µm²/s found in the present work, which accounted for the largest proportion of receptor states with 73% (Figure 4-22, Figure 4-23). The median diffusion coefficient in the analysis by Calebiro et al. (2013) did not change significantly after stimulation with isoprenaline.

In the present study the three diffusion coefficients of the respective $\beta_1$AR states were not significantly changed by preincubation with cortisol, citalopram, desipramine, and MβCD (Figure 4-22). Even after stimulation with isoprenaline there was no change in the diffusion coefficients under the mentioned preincubations. After preincubation with Ze117, however, the diffusion coefficients of the diffusive receptor states S1 and S2 decreased significantly. Hypericin as a constituent of Ze117 is known to be incorporated into the membrane and, as a fluorescent and immobile component, could therefore distort the tracking results. However, a significant direct detection of hypericin in the SPT experiment can be excluded. Hypericin has a molar extinction coefficient of 40,000 $M^{-1}cm^{-1}$ and a quantum yield of 0.3 [118]. In comparison, the molar extinction coefficient of BG-Dy549 is 150,000 $M^{-1}cm^{-1}$ [122]. Thus, BG-Dy549 is many times brighter than hypericin. Additionally, by using a laser with a wavelength of 532 nm the excitiation of BG-Dy549 with an absorption maximum of 549 nm is more efficient compared to hypericin with an absorption maximum of 590 nm. The lower excitation of hypericin should lead to an even weaker brightness of hypericin compared to BG-Dy549. Brightness of possibly detected hypericin molecules in the plasma membrane would therefore fall below the threshold value set for uTrack evaluation and was consequently not considered for the generation of trajectories.

However, hypericin accumulates in the plasma membrane and could therefore represent a diffusion barrier for SNAP-$\beta_1$AR in the cell membrane, which is difficult to overcome and thus could have caused the increase in the proportion of immobile receptors. The observed change in lipid composition and the Ze117 induced rigidification of the plasma membrane are also likely to contribute to a slower receptor diffusion. By using fluorescence correlation spectroscopy (FCS) Jakobs et al. (2013) found two diffusion states for the $\beta_1$AR in control C6 cells with diffusion coefficients of

11.6 $\mu m^2/s$ und 0.07 $\mu m^2/s$ [27]. FCS is capable to detect diffusing particles that diffuse very fast. However, over the measurement time of e.g. 60 s very slow or immobile receptors do not leave the focus of the microscope. Since FCS registers fluctuations in fluorescence, particles that do not leave the focus are not detected. Thus, very slow or almost immobile receptors, as found in this work, cannot be detected by FCS. Nevertheless, it is interesting that after a preincubation with the St. John's wort ingredients hyperforin and hyperoside, a slight reduction of the diffusion coefficients could also be observed by Jacobs et al. (2013). They concluded, that hyperforin and hyperoside mediate a redistribution of active $\beta_1$AR from functional microdomains to coated pits.

Keksel et al. (2019) also investigated the lateral diffusion of $\beta_1$AR in C6 cells after chronic preincubation of cortisol and Ze117, but only under unstimulated conditions [53]. They also found three states with diffusion coefficients of D1=0.0136 $\mu m^2/s$, D2=0.0517 $\mu m^2/s$, and D3=0.3470 $\mu m^2/s$. The higher diffusion coefficient of D3, compared to the result in this work, can be explained due to different expression levels of SNAP-$\beta_1$AR, since a different clone of C6 cells expressing SNAP-$\beta_1$AR was used. After cortisol preincubation no changes in the lateral mobility of $\beta_1$AR was observed. However, after Ze117 preincubation the diffusion coefficients of the three diffusive states decreased to 0.0084 $\mu m^2/s$, 0.0420 $\mu m^2/s$ and 0.2560 $\mu m^2/s$, respectively.

In contrast to the rather small changes in the diffusion coefficients of the individual receptor states, significant influences on the occupancy values of the receptor states were observed in the present study. After isoprenaline stimulation a significant increase of the proportion of receptor state S1 was observed in control cells (Figure 4-23). This occurred at the expense of the occupancy of S2, which decreased significantly. Similar findings were observed after isoprenaline stimulation of cortisol and citalopram pretreated cells. Thus, both cortisol and escitalopram had no effect on the lateral mobility of SNAP-$\beta_1$AR.

The increase of the fraction of the receptor diffusion state S1 after stimulation suggests regulatory responses of the cell. It is possible that more receptors enter clathrin coated pits to be internalized where they move at a slower diffusion speed. It is also plausible that the receptors interact more often with downstream enzymes, such as β-arrestin, adenylyl cyclase or Gsα, which leads to a slower receptor diffusion. Sungkaworn et al. (2017) investigated the lateral diffusion of fluorescently labeled $\alpha_{2a}$-adrenergic

receptors and $G\alpha_i$ subunits [114]. They also used vbSPT for data evaluation and found 4 individual diffusive states. They observed that during the time of $\alpha_{2a}$-adrenergic receptor and $G\alpha_i$ subunit interactions, the fraction of the immobile state S1 and the slow diffusion state S2 increased. In contrast, less receptors were detected in states defined by faster diffusion coefficients.

As mentioned above, Calebiro et al. (2013) could not detect any significant changes in the median diffusion coefficient of SNAP-$\beta_1$AR after stimulation with isoprenaline [37], but in their study no differential analysis of individual states was performed.

Ibach et al. (2015) found a similar redistribution of SNAP-tagged epidermal growth factor receptors in MCF-7 cells to slower diffusive states after agonist stimulation [115]. They also used the vbSPT algorithm for data evaluation and found 3 distinct diffusive states similar to the results of this work, defined by diffusion coefficients of 0.0019 µm²/s, 0.022 µm²/s and 0.1 µm²/s, respectively.

Schwenzer et al. (2019) investigated the lateral diffusion behavior of SNAP-tagged $\beta_2$-adrenergic receptors in HEK wild type cells and HEK β-arrestin knock out cells with and without agonist stimulation [68]. Interestingly, they also found three diffusive states for $\beta_2$-adrenergic receptors after vbSPT analysis. In HEK wild type cells they also found a redistribution of receptors from a fast diffusing states to immobile state after agonist stimulation. However, this was not observed in HEK β-arrestin KO cells indicating that slower diffusive receptors are due to receptor interactions with other proteins, like β-arrestins, or β-arrestin dependent internalization processes.

Surprisingly, a comparable increase in the proportions of SNAP-$\beta_1$AR in the state S1 and a decrease of S2 occupany was found after the treatment of unstimulated C6 cells with MβCD (Figure 4-23). Pucadyil et al. (2007) performed FRAP (fluorescence recovery after photobleaching) experiments on EYFP coupled serotonin$_{1a}$-receptors before and after cholesterol depletion by MβCD [119]. They also found that after cholesterol depletion the fraction of immobile serotonin$_{1a}$-receptors was higher in comparison to control cells. MβCD removes cholesterol from the plasma membranes and thus generally leads to a more fluid plasma membrane, as shown in the anisotropy experiments (Figure 4-2). Certain membrane regions that are high in cholesterol are called lipid rafts, which often also contain downstream proteins like adenylyl cylclase. In cardiomyocytes it could be shown that the $\beta_1$AR is mainly located outside of these

regions [113]. Therefore, raft disruption due to cholesterol depletion would not have a direct impact on the lateral mobility of $\beta_1$AR under non-stimulating conditions. However, MβCD mediated disruption of cholesterol-rich raft regions, in which e.g. adenylyl cyclase or Gsα are located, increases the probability of interaction with $\beta_1$AR, which in turn would lead to both a slower diffusion and a switching of states. Rybin et al. (2000) showed that through the disruption of lipid rafts by MβCD, the cAMP accumulation in cardiomyocyte cells increased after $\beta_1$AR agonist stimulation, which supports this hypothesis [113].

Interestingly, a similar effect was observed in the present study after a six-day preincubation with the antidepressants desipramine and Ze117 (Figure 4-23). After subsequent stimulation with isoprenaline there was no further change in the proportions of the receptor states. Remarkably, the occupancy values were almost identical as of agonist stimulated control cells.

Keksel et al. (2019) also found three diffusive states for SNAP-$\beta_1$AR in C6 cells. They found occupancies for controls cells of 17% for S1, 41% for S2 and 42% for S3. In the present work, the occupancy for S3 was clearly lower, whereas the occupancy of S1 was higher. As mentioned above, this could be due to the usage of a different cell clone of SNAP-$\beta_1$AR expressing C6 cells and other cell culture conditions. Similarly to the results of this work, after cortisol preincubation, no alteration in lateral mobility was observed. However, an increase of the occupancy in S1 after chronic Ze117 preincubation was also observed by the authors. This was accompanied by a decrease of the occupancy in S3.

Jakobs et al. (2013) also observed a significant redistribution of receptors to a slow diffusing receptor state after preincubation of C6 cells with the St. John's wort ingredients hyperforin and hyperoside by using fluorescence correlation spectroscopy [27].

Interestingly, Singh et al. (2018) proved that SSRI and tricyclic antidepressants destroy lipid raft localized $G_s\alpha$/tubulin complexes [120]. Donati et al. (2005) found that a chronic treatment of C6 cells with two functionally and structurally different antidepressants, desipramine and fluoxetine, reduced the $G_s\alpha$ content of the lipid raft domains down to 60% [121]. Postmortem studies reveal an increased lipid raft localization of $G_s\alpha$ in suicide victims compared to age-matched control subjects [122]. Considering that in

the present work $\beta_1$AR are preferently located outside of lipid rafts, it is reasonable to assume that there is an increased interaction of SNAP-$\beta_1$AR with $G_s\alpha$ after treatment with antidepressants, such as Ze117 which leads to more pronounced fraction of receptors in a slowly diffusing receptor state. Another explanation for a higher fraction of receptors in a slow diffusive state could be that an increased number of SNAP-$\beta_1$AR are located in clathrin coated pits prior endocytosis or that diffusion is attenuated by changes in the plasma membrane composition. If this was the case for SNAP-$\beta_1$AR, one might expect that the spatial confinement of the receptors would be more pronounced. Accordingly, the confined fraction of receptors in the respective states should increase.

In basal condition, about two-thirds (68%) of track segments of SNAP-$\beta_1$AR in S1 showed a confined diffusion with a mean confinement size of 79 nm, depicted by the square root of convex hull area. SNAP-$\beta_1$AR in S2 were less often confined (49%) and restricted diffusion was observed in a larger confinement size of 118 nm on average. Stimulation did neither change confinement size nor confined fraction.

Similar results at basal conditions were found for $\beta_2$-adrenergic receptors ($\beta_2$AR) by Schwenzer et al. (2018) [68]. However, they found for $\beta_2$AR a significant increase of the confined fraction in each state after agonist stimulation. This is not surprising as $\beta_2$AR are recovered along with a substantial amount of $G_s\alpha$ in caveolin-3-enriched membrane domains at basal conditions. $\beta_2$AR translocate out of this compartment upon stimulation with isoprenaline and as activated $\beta_2$ARs undergo clathrin-dependent endocytosis [123]. In contrast, $\beta_1$AR are also less susceptible to agonist-mediated internalization than the $\beta_2$-subtype, and their endocytic route, which is unknown, may be different [124]. Rybin et al. (2000) found that the vast majority of total cellular $\beta_1$AR are excluded from certain membrane microdomains called caveolae, wheras $\beta_2$AR are mostly located within caveolae [113]. A partitioning of $\beta_1$AR between membrane microdomains was also not observed after treatment with isoprenaline in these studies. The failure to detect an agonist-induced change in $\beta_1$AR partitioning between different membrane microdomains also suggests that the tempo and possibly the mode of regulation for $\beta_1$ARs and $\beta_2$ARs are quite different. This would explain the differences between confinement data for $\beta_2$ARs by Schwenzer et al. (2019) and $\beta_1$AR shown in this work.

Differences in the spatial distributions of $\beta_1$AR and $\beta_2$AR might physiologically contribute to different signal transduction intensities induced by $\beta_2$AR and $\beta_1$AR agonists. Interestingly, it was demonstrated that physical and functional coupling of $\beta_2$AR to $G_s\alpha$ after stimulation with isoprenaline is more efficient than for $\beta_1$AR and $G_s\alpha$ [125]. This has been attributed to structural differences in the receptor's third intracellular loop [125]. However, co-localization of $\beta_2$AR along with G-proteins in the same membrane raft regions provides an additional explanation for the "more efficient" coupling of $\beta_2$AR to AC, relative to $\beta_1$AR [123].

Preincubation with MβCD, cortisol, desipramine, and escitalopram did not alter the confined fraction within the individual states. Likewise, no alteration in the mean confinement size was found.

Surprisingly, after Ze117 preincubation a significant increase of the confined fraction in S1 and S2 was observed. This is not surprising, since the receptor's microenvironment has changed drastically considering the lipidomics results and the reduction in membrane fluidity caused by Ze117.

This also leads to the assumption that isoprenaline stimulation, desipramine and Ze117 preincubation leads to a changed likelihood of receptor-protein interaction and therefore to altered state occupancies. Ze117 additionally leads to a changed microenvironment of the receptor, which can be seen by altered lipid compositions in PBMC and altered confinement values in C6 cells.

Considering that isoprenaline stimulation and preincubation with Ze117, desipramine and MβCD, respectively, all lead to an altered likelihood of receptor and downstream-protein interaction whereas Ze117 also changed the lipid-microenvironment of the receptor, the following can be assumed: While interactions of receptors with downstream proteins influence the state occupancy, the composition of the membrane environment influences the confinement of the receptor.

It is most likely, that such alterations in the lateral mobility of the $\beta_1$AR correlate with influences in signal transduction. Keksel et al. (2018) showed, that chronic treatment with Ze117 lead to a decreased cAMP level in C6 cells [53]. Jakobs et al. (2013) also showed that the preincubation with the St. John's wort constituents hyperoside and hyperforin lead to less pronounced cAMP level in C6 cells after agonist stimulation compared to untreated control cells [27].

Oligomerization states of $\beta_1$AR were analyzed by fluorescence intensity histogram analysis and curve fitting with a mixed Gaussian model leading to different monomer, dimer, trimer, and tetramer fractions of SNAP-tagged $\beta_1$AR in C6 cells. The respective proportions decreased with increasing oligomerization which was not significantly influenced by any of the pretreatments.

Calebiro et al. (2013) analyzed oligomerization and lateral mobility of $\beta_1$AR using single particle TIRF (total internal reflection fluorescence) microscopy [37]. For overexpressed SNAP-$\beta_1$AR in CHO cells they found fractions of mono-, di-, tri-, and tetramers with respective abundances of approx. 20%, 60%, 15%, and 5%. Remarkably, the distribution of the oligomerization states in CHO cells is not exactly the same as in C6 cells presented in the present work (Figure 4-28). In particular, the presence of monomers was more pronounced in C6 cells. Similar to the given results Calebiro et al. (2013) did not find an impact on the oligomerization states of $\beta_1$ARs after agonistic stimulation, which was also observed in isoprenaline stimulated C6 cells.

The high standard deviations of the oligomerization fractions obtained from the experiments of the present work indicate large fluctuations in oligomerization. As Calebiro et al. (2013) were able to show, the probability of finding mono, di-, tri- or tetramers strongly depends on the receptor density in the membrane. The higher the receptor density, the more pronounced is the fraction of higher oligomerization levels. Since this may vary greatly from cell to cell, this would be one explanation for the variability of the oligomerization data.

To confirm the accuracy of the data generated by vbSPT and Pc algorithms, experimentally realistic track data was generated by a computational simulation and subsequently evaluated by vbSPT and Pc algorithms. The input data for simulation was based on the measured data obtained from SPT experiments. The underlying number of states, diffusion coefficients and occupancy values were calculated correctly by vbSPT, which is in line with the accuracy of the experimental data. With the help of the packing coefficient, the confined fraction was calculated accurately with an offset of 5%. The mean confinement sizes in S1 were simulated with 80 nm, but were calculated by Pc algorithm with an offset of 9 nm, probably due to the localization error of 20 nm. In state S2, the mean confinement size was calculated with an average of

115 nm instead of the correct 120 nm. This underestimated value could also be explained by the simulated localization error.

# 6 Conclusion and outlook

This thesis aimed to identify alterations in the lipidome of peripheral blood mononuclear cells (PBMC) after preincubation with the antidepressant St. John's wort extract Ze117 and the stress hormone cortisol. It was also investigated whether Ze117 had an influence on the lateral mobility of $\beta_1$-adrenergic receptors ($\beta_1$AR), an important receptor in the pathogenesis of depression.

The data generated by fluorescence anisotropy measurements demonstrate that cortisol and Ze117 show opposite effects on plasma membrane fluidity. Considering the results of the lipidomic analysis, altered plasma membrane fluidity is caused by parallel changes in the fatty acid composition of the lipidome. Most likely alterations of the physicochemical properties of the plasma membrane caused by Ze117 also have an effect on the lateral mobility of the $\beta_1$AR. This in turn should have an impact on the likelihood of downstream interactions of $\beta_1$AR with $G_s\alpha$ and therefore on the processing of neurotransmitter signals.

It is widely accepted that depression is caused, among other things, by an abnormal signal transduction within certain neurotransmitter systems [11]. Until now it has been assumed that this could be caused, for example, by hyperactivity of the HPA axis, mutations of certain receptor genes or altered receptor expression as observed in postmortem studies on depressive subjects [43,126,127]. However, the findings of this work suggest another probable cause of depressive disorders: Changes in the membrane environment alter the location and the diffusion behavior of membranous receptors and therefore also the receptor signaling.

In this work, no changes in homo-oligomerization of $\beta_1$AR after Ze117 or cortisol treatment was observed. One assumption is that not only individual receptor systems are relevant for the pathogenesis of depression, but also receptor complexes consisting of different receptor species. Future studies should also focus on the formation and modulation of homo- and hetero-receptor-complexes in connection with depression. It has already been shown for 5-$HT_{1a}$ and the 5-$HT_7$ receptors that the formation of heterodimers plays an important role in the regulation of receptor-mediated signaling and internalization, suggesting the implication of heterodimerization in the development and maintenance of depression [39].

Furthermore, it can be assumed that the interaction of different receptor classes can be modulated by changes in the membrane composition and by the formation or disruption of membranous microdomains and therefore modulate receptor signaling. Conclusively, the modulation of the membrane composition may represent another therapy approach for depression. First approaches in this direction already exist, e.g. the application of dietary supplements rich in unsaturated fatty acids for the therapy and prevention of depression [128].

Most likely, the membrane composition also has effects on other receptor systems not yet discussed in connection with depression, such as orphan G-protein coupled receptors (GPCRs) which are relevant for signaling in cognitive processes. Although the Hamilton Depression Score only reflects the mood of the patient, cognitive aspects seem to be important for the disease pattern of depression but are highly underestimated [129]. Further research in this area could provide interesting insights into the development and treatment of depression.

To obtain more detailed lateral diffusion data of the $\beta_1$AR, it will be useful for following experiments to use a single particle tracking microscope with total internal reflection fluorescence (TIRF) technology. In contrast to the wide field microscope used in this work, TIRF technology would allow an even more precise receptor localization and a faster frame rate. A wider camera chip with e.g. 512x512 pixels instead of 128x128 pixels would also provide better localization and a larger recordable area. As a result, several cells could be recorded in one measurement, which would lead to a bigger amount of evaluable data. By using a TIRF microscope with high frame rates and equipped with two or more lasers it would also be possible to observe interactions of parallel fluorescently labeled receptors and G-proteins.

Another approach for future research could be to conduct a lipidomic and proteomic analysis in parallel and within the same cell type in order to identify possible protein targets of Ze117. Probable results of such an experiment could be PPARγ, as well as Δ-5 and Δ-6 desaturases. In order to make more precise statements about the membrane composition, it would also be useful to perform lipidomic analyses on membrane preparations instead of examining the entire lipidome of the cell.

The membrane fluidity or the lipid composition of the cell membrane could also serve as a diagnostic parameter for depression. This would enable the possibility to monitor

the success of therapy by fluorescence anisotropy measurements and lipidome analysis.

GPCR signaling is an exceptionally complex process and it takes place in an equally complex biomembrane. The comprehensive description of these fundamental processes, particularly in the pharmaceutical perspective, requires further research. Further SPT experiments and a deeper understanding of the plasma membrane composition are therefore necessary.

# 7 References


[1] P. Cassano, M. Fava, Depression and public health, J. Psychosom. Res. 53 (2002) 849–857. https://doi.org/10.1016/S0022-3999(02)00304-5.

[2] DGPPN, S3-Leitlinie / Nationale VersorgungsLeitlinie Unipolare Depression Langfassung, Ärztliches Zent. Für Qual. Der Medizin. (2015). https://doi.org/10.6101/AZQ/000266.

[3] K.P. Ebmeier, C. Donaghey, J.D. Steele, Recent developments and current controversies in depression, Lancet. 367 (2006) 153–167. https://doi.org/10.1016/S0140-6736(06)67964-6.

[4] R. V. Bijl, A. Ravelli, G. Van Zessen, Prevalence of psychiatric disorder in the general population: Results of the Netherlands Mental Health Survey and Incidence Study (NEMESIS), Soc. Psychiatry Psychiatr. Epidemiol. 33 (1998) 587–595. https://doi.org/10.1007/s001270050098.

[5] M.A. Busch, U.E. Maske, L. Ryl, R. Schlack, U. Hapke, Prävalenz von depressiver Symptomatik und diagnostizierter Depression bei Erwachsenen in Deutschland: Ergebnisse der Studie zur Gesundheit Erwachsener in Deutschland (DEGS1), Bundesgesundheitsblatt - Gesundheitsforsch. - Gesundheitsschutz. 56 (2013) 733–739. https://doi.org/10.1007/s00103-013-1688-3.

[6] F. Jacobi, M. Höfler, J. Strehle, S. Mack, A. Gerschler, L. Scholl, M.A. Busch, U. Maske, U. Hapke, W. Gaebel, W. Maier, M. Wagner, J. Zielasek, H.U. Wittchen, Psychische störungen in der allgemeinbevölkerung. Studie zur gesundheit erwachsener in Deutschland und ihr zusatzmodul psychische gesundheit (DEGS1-MH), Nervenarzt. 85 (2014) 77–87. https://doi.org/10.1007/s00115-013-3961-y.

[7] L.S. Kahn, U. Halbreich, The effect of estrogens on depression, Estrogen Eff. Psychiatr. Disord. (2005) 145–173. https://doi.org/10.1007/3-211-27063-9_7.

[8] D.S. Bennett, P.J. Ambrosini, D. Kudes, C. Metz, H. Rabinovich, Gender differences in adolescent depression: Do symptoms differ for boys and girls?, J. Affect. Disord. 89 (2005) 35–44. https://doi.org/10.1016/j.jad.2005.05.020.

[9] C. Kuehner, Gender differences in unipolar depression: An update of epidemiological findings and possible explanations, Acta Psychiatr. Scand. 108 (2003) 163–174. https://doi.org/10.1034/j.1600-0447.2003.00204.x.

[10] J. Ormel, M. Vonkorff, A.J. Oldehinkel, G. Simon, B.G. Tiemens, T.B. Üstün, Onset of disability in depressed and non-depressed primary care patients, Psychol. Med. 29 (1999) 847–853. https://doi.org/10.1017/S0033291799008600.

[11] G.R. Villas Boas, R. Boerngen de Lacerda, M.M. Paes, P. Gubert, W.L. da C. Almeida, V.C. Rescia, P.M.G. de Carvalho, A.A.V. de Carvalho, S.A. Oesterreich, Molecular aspects of depression: A review from neurobiology to treatment, Eur. J. Pharmacol. 851 (2019) 99–121. https://doi.org/10.1016/j.ejphar.2019.02.024.

[12] P.K. Gillman, Tricyclic antidepressant pharmacology and therapeutic drug interactions updated, Br. J. Pharmacol. 151 (2007) 737–748. https://doi.org/10.1038/sj.bjp.0707253.

[13] I.M. Anderson, Selective serotonin reuptake inhibitors versus tricyclic antidepressants: a meta-analysis of efficacy and tolerability, J. Affect. Disord. 58 (2000) 19–36. https://doi.org/10.1016/S0165-0327(99)00092-0.

[14] N.P.V. Nair, S.K. Ahmed, N.M.K. Ng Ying Kin, Biochemistry and pharmacology of reversible inhibitors of MAO-A agents: Focus on moclobemide, J. Psychiatry Neurosci. 18 (1993) 214–225.

[15] Council of Europe, Hyperici herbae extractum siccum quantificatum, Eur. Pharmacopoeia. 8.0 (2013) 1391–1395.

[16] E. Schrader, B. Meier, A. Brattström, Hypericum treatment of mild-moderate depression in a placebo-controlled study. A prospective, double-blind, randomized, placebo-controlled, multicentre study, Hum. Psychopharmacol. 13 (1998) 163–169. https://doi.org/10.1002/(SICI)1099-1077(199804)13:3<163::AID-HUP5>3.0.CO;2-I.

[17] H. Woelk, Comparison of St John's wort and imipramine for treating depression: Randomised controlled trial, Br. Med. J. 321 (2000) 536–539. https://doi.org/10.1136/bmj.321.7260.536.

[18] K. Behnke, G.S. Jensen, H.J. Graubaum, J. Gruenwald, Hypericum perforatum versus fluoxetine in the treatment of mild to moderate depression, Adv. Ther. 19 (2002) 43–52. https://doi.org/10.1007/BF02850017.

[19] K. Linde, M.M. Berner, L. Kriston, St John's wort for major depression, Cochrane Database Syst. Rev. 5 (2008) 144. https://doi.org/10.1002/14651858.CD000448.pub3.

[20] A. Qaseem, M.J. Barry, D. Kansagara, Nonpharmacologic Versus Pharmacologic Treatment of Adult Patients With Major Depressive Disorder: A Clinical Practice Guideline From the American College of Physicians, Ann. Intern. Med. 164 (2016) 350. https://doi.org/10.7326/M15-2570.

[21] A. V. Ravindran, L.G. Balneaves, G. Faulkner, A. Ortiz, D. McIntosh, R.L. Morehouse, L. Ravindran, L.N. Yatham, S.H. Kennedy, R.W. Lam, G.M. MacQueen, R. V. Milev, S. V. Parikh, Canadian Network for Mood and Anxiety Treatments (CANMAT) 2016 clinical guidelines for the management of adults with major depressive disorder: Section 5. Complementary and Alternative Medicine Treatments, Can. J. Psychiatry. 61 (2016) 576–587. https://doi.org/10.1177/0706743716660290.

[22] M. Schmidt, V. Butterweck, The mechanisms of action of St. John's wort: an update, Wiener Medizinische Wochenschrift. 165 (2015) 229–235. https://doi.org/10.1007/s10354-015-0372-7.

[23] Y. Chang, S.J. Wang, Hypericin, the active component of St. John's wort, inhibits glutamate release in the rat cerebrocortical synaptosomes via a mitogen-activated protein kinase-dependent pathway, Eur. J. Pharmacol. 634 (2010) 53–61. https://doi.org/10.1016/j.ejphar.2010.02.035.

[24] C. Ruedeberg, U.N. Wiesmann, A. Brattstroem, U.E. Honegger, Hypericum perforatum L. (St John's wort) extract Ze 117 inhibits dopamine re-uptake in rat striatal brain slices. An implication for use in smoking cessation treatment?, Phyther. Res. 22 (2009) n/a-n/a. https://doi.org/10.1002/ptr.2921.

[25] G.M. De Marchis, S. Bürgi, U. Kientsch, U.E. Honegger, Vitamin E reduces antidepressant-related β-adrenoceptor down-regulation in cultured cells. Comparable effects on St. John's Wort and tricyclic antidepressant treatment, Planta Med. 72 (2006) 1436–1437. https://doi.org/10.1055/s-2006-951727.

[26] L. Prenner, A. Sieben, K. Zeller, D. Weiser, H. Häberlein, Reduction of high-affinity beta2-adrenergic receptor binding by hyperforin and hyperoside on rat C6 glioblastoma cells measured by fluorescence correlation spectroscopy., Biochemistry. 46 (2007) 5106–13. https://doi.org/10.1021/bi6025819.

[27] D. Jakobs, A. Hage-Hülsmann, L. Prenner, C. Kolb, D. Weiser, H. Häberlein, Downregulation of β1-adrenergic receptors in rat C6 glioblastoma cells by hyperforin and hyperoside from St John's wort, J. Pharm. Pharmacol. 65 (2013) 907–915. https://doi.org/10.1111/jphp.12050.

[28] L.A. Hu, Y. Tang, W.E. Miller, M. Cong, A.G. Lau, R.J. Lefkowitz, R.A. Hall, β1-adrenergic receptor association with PSD-95: Inhibition of receptor internalization and facilitation of β1-adrenergic receptor interaction with N-methyl-D-aspartate receptors, J. Biol. Chem. 275 (2000) 38659–38666. https://doi.org/10.1074/jbc.M005938200.

[29] P. Zill, T.C. Baghai, R. Engel, P. Zwanzger, C. Schüle, C. Minov, S. Behrens, R. Bottlender, M. Jäger, R. Rupprecht, H.J. Möller, M. Ackenheil, B. Bondy, Beta-1-adrenergic receptor gene in major depression: Influence on antidepressant treatment response, Am. J. Med. Genet. - Neuropsychiatr. Genet. 120 B (2003) 85–89. https://doi.org/10.1002/ajmg.b.20017.

[30] S.P. Banerjee, L.S. Kung, S.J. Riggi, S.K. Chanda, Development of β-adrenergic receptor subsensitivity by antidepressants, Nature. 268 (1977) 455–456. https://doi.org/10.1038/268455a0.

[31] G.A. Ordway, C. Gambarana, A. Frazer, Quantitative autoradiography of central beta adrenoceptor subtypes: Comparison of the effects of chronic treatment with desipramine or centrally administered l-isoproterenol, J. Pharmacol. Exp. Ther. 247 (1988) 379–389.

[32] S. Bürgi, K. Baltensperger, U.E. Honegger, Antidepressant-induced switch of β1-adrenoceptor trafficking as a mechanism for drug action, J. Biol. Chem. 278 (2003) 1044–1052. https://doi.org/10.1074/jbc.M209972200.

[33] D. Calebiro, T. Sungkaworn, Single-Molecule Imaging of GPCR Interactions, Trends Pharmacol. Sci. 39 (2018) 109–122. https://doi.org/10.1016/j.tips.2017.10.010.

[34] A. De Lean, J.M. Stadel, R.J. Lefkowitz, A ternary complex model explains the agonist-specific binding properties of the adenylate cyclase-coupled β-adrenergic receptor, J. Biol. Chem. 255 (1980) 7108–7117.

[35] P. Samama, S. Cotecchia, T. Costa, R.J. Lefkowitz, A mutation-induced activated state of the β2-adrenergic receptor. Extending the ternary complex model, J. Biol. Chem. 268 (1993) 4625–4636.

[36] S. Terrillon, M. Bouvier, Roles of G-protein-coupled receptor dimerization, EMBO Rep. 5 (2004) 30–34. https://doi.org/10.1038/sj.embor.7400052.

[37] D. Calebiro, F. Rieken, J. Wagner, T. Sungkaworn, U. Zabel, A. Borzi, E. Cocucci, A. Zürn, M.J. Lohse, A. Zurn, M.J. Lohse, Single-molecule analysis of fluorescently labeled G-protein-coupled receptors reveals complexes with distinct dynamics and organization., Proc. Natl. Acad. Sci. U. S. A. 110 (2013) 743–8. https://doi.org/10.1073/pnas.1205798110.

[38] G. Milligan, G Protein-Coupled Receptor Dimerization: Function and Ligand Pharmacology, Mol. Pharmacol. 66 (2004) 1–7. https://doi.org/10.1124/mol.104.000497.

[39] V.S. Naumenko, N.K. Popova, E. Lacivita, M. Leopoldo, E.G. Ponimaskin, Interplay between serotonin 5-HT1A and 5-HT7 receptors in depressive disorders, CNS Neurosci. Ther. 20 (2014) 582–590. https://doi.org/10.1111/cns.12247.

[40] P.Y. Lin, S.Y. Huang, K.P. Su, A meta-analytic review of polyunsaturated fatty acid compositions in patients with depression, Biol. Psychiatry. 68 (2010) 140–147. https://doi.org/10.1016/j.biopsych.2010.03.018.

[41] E.E.M. Knowles, K. Huynh, P.J. Meikle, H.H.H. Göring, R.L. Olvera, S.R. Mathias, R. Duggirala, L. Almasy, J. Blangero, J.E. Curran, D.C. Glahn, The lipidome in major depressive disorder: Shared genetic influence for ether-phosphatidylcholines, a plasma-based phenotype related to inflammation, and disease risk, Eur. Psychiatry. 43 (2017) 44–50. https://doi.org/10.1016/j.eurpsy.2017.02.479.

[42] A. Walther, C.V. Cannistraci, K. Simons, C. Durán, M.J. Gerl, S. Wehrli, C. Kirschbaum, Lipidomics in major depressive disorder, Front. Psychiatry. 9 (2018). https://doi.org/10.3389/fpsyt.2018.00459.

[43] G.P. Chrousos, Stress and disorders of the stress system, Nat. Rev. Endocrinol. 5 (2009) 374–381. https://doi.org/10.1038/nrendo.2009.106.

[44] C. Rabasa, S.L. Dickson, Impact of stress on metabolism and energy balance, Curr. Opin. Behav. Sci. 9 (2016) 71–77. https://doi.org/10.1016/j.cobeha.2016.01.011.

[45] M. Van Bodegom, J.R. Homberg, M.J.A.G. Henckens, Modulation of the hypothalamic-pituitary-adrenal axis by early life stress exposure, Front. Cell. Neurosci. 11 (2017) 1–33. https://doi.org/10.3389/fncel.2017.00087.

[46] M. V. Tolentino, M.M. Sarasua, O.A. Hill, D.B. Wentworth, D. Franceschi, R.B. Fratianne, Peripheral lymphocyte membrane fluidity after thermal injury, J. Burn Care Rehabil. 12 (1991) 498–504. https://doi.org/10.1097/00004630-199111000-00002.

[47] D. Johnston, G. Melnykovych, Effects of dexamethasone on the fluorescence polarization of diphenylhexatriene in HeLa cells, BBA - Biomembr. 596 (1980) 320–324. https://doi.org/10.1016/0005-2736(80)90365-X.

[48] T.A. Brasitus, P.K. Dudeja, R. Dahiya, A. Halline, Dexamethasone-induced alterations in lipid composition and fluidity of rat proximal-small-intestinal brush-border membranes, Biochem. J. 248 (1987) 455–461. https://doi.org/10.1042/bj2480455.

[49] J.R. Lakowicz, Principles of fluorescence spectroscopy, 3rd Edition, Joseph R. Lakowicz, editor, 2006. https://doi.org/10.1007/978-0-387-46312-4.

[50] B. Aricha, I. Fishov, Z. Cohen, N. Sikron, S. Pesakhov, I. Khozin-Goldberg, R. Dagan, N. Porat, Differences in membrane fluidity and fatty acid composition between phenotypic variants of Streptococcus pneumoniae, J. Bacteriol. 186 (2004) 4638–4644. https://doi.org/10.1128/JB.186.14.4638-4644.2004.

[51] J. Repáková, J.M. Holopainen, M.R. Morrow, M.C. McDonald, P. Čapková, I. Vattulainen, Influence of DPH on the structure and dynamics of a DPPC bilayer, Biophys. J. 88 (2005) 3398–3410. https://doi.org/10.1529/biophysj.104.055533.

[52] L.M.S. Loura, J.P.P. Ramalho, Recent developments in molecular dynamics simulations of fluorescent membrane probes, Molecules. 16 (2011) 5437–5452. https://doi.org/10.3390/molecules16075437.

[53] N. Keksel, H. Bussmann, M. Unger, J. Drewe, G. Boonen, H. Häberlein, S. Franken, St John's wort extract influences membrane fluidity and composition of phosphatidylcholine and phosphatidylethanolamine in rat C6 glioblastoma cells, Phytomedicine. 54 (2019) 66–76. https://doi.org/10.1016/j.phymed.2018.06.013.

[54] C.S. Ejsing, J.L. Sampaio, V. Surendranath, E. Duchoslav, K. Ekroos, R.W. Klemm, K. Simons, A. Shevchenko, Global analysis of the yeast lipidome by quantitative shotgun mass spectrometry, Proc. Natl. Acad. Sci. U. S. A. 106 (2009) 2136–2141. https://doi.org/10.1073/pnas.0811700106.

[55] K. Jaqaman, D. Loerke, M. Mettlen, H. Kuwata, S. Grinstein, S.L. Schmid, G. Danuser, Robust single-particle tracking in live-cell time-lapse sequences, Nat. Methods. 5 (2008) 695–702. https://doi.org/10.1038/nmeth.1237.

[56] F. Persson, M. Lindén, C. Unoson, J. Elf, Extracting intracellular diffusive states and transition rates from single-molecule tracking data, Nat. Methods. 10 (2013) 265–269. https://doi.org/10.1038/nmeth.2367.

[57] M. Renner, L. Wang, S. Levi, L. Hennekinne, A. Triller, A Simple and Powerful Analysis of Lateral Subdiffusion Using Single Particle Tracking, Biophys. J. 113 (2017) 2452–2463. https://doi.org/10.1016/j.bpj.2017.09.017.

[58] G.E. Tafet, C.B. Nemeroff, The links between stress and depression: Psychoneuroendocrinological, genetic, and environmental interactions, J. Neuropsychiatry Clin. Neurosci. 28 (2016) 77–88. https://doi.org/10.1176/appi.neuropsych.15030053.

[59] T.J. McIntosh, S.A. Simon, Roles of bilayer material properties in function and distribution of membrane proteins, Annu. Rev. Biophys. Biomol. Struct. 35 (2006) 177–198. https://doi.org/10.1146/annurev.biophys.35.040405.102022.

[60] C. Chitraju, M. Trötzmüller, J. Hartler, H. Wolinski, G.G. Thallinger, G. Haemmerle, R. Zechner, R. Zimmermann, H.C. Köfeler, F. Spener, The impact of genetic stress by ATGL deficiency on the lipidome of lipid droplets from murine hepatocytes, J. Lipid Res. 54 (2013) 2185–2194. https://doi.org/10.1194/jlr.m037952.

[61] C. Thiele, K. Wunderling, P. Leyendecker, Multiplexed and single cell tracing of lipid metabolism, Nat. Methods. 16 (2019) 1123–1130. https://doi.org/10.1038/s41592-019-0593-6.

[62] R. Iino, I. Koyama, A. Kusumi, Single Molecule Imaging of Green Fluorescent Proteins in Living Cells: E-\rCadherin Forms Oligomers on the Free Cell Surface, Biophys. J. 80 (2001) 2667–2677.

[63] P.J. Bosch, I.R. Corrêa, M.H. Sonntag, J. Ibach, L. Brunsveld, J.S. Kanger, V. Subramaniam, Evaluation of fluorophores to label SNAP-Tag fused proteins for multicolor single-molecule tracking microscopy in live cells, Biophys. J. 107 (2014) 803–814. https://doi.org/10.1016/j.bpj.2014.06.040.

[64] A. Keppler, S. Gendreizig, T. Gronemeyer, H. Pick, H. Vogel, K. Johnsson, A general method for the covalent labeling of fusion proteins with small molecules in vivo, Nat. Biotechnol. 21 (2002) 86–89. https://doi.org/10.1038/nbt765.

[65] J.P. Siebrasse, I. Djuric, U. Schulze, M.A. Schl??ter, H. Pavenst??dt, T. Weide, U. Kubitscheck, Trajectories and single-particle tracking data of intracellular vesicles loaded with either SNAP-Crb3A or SNAP-Crb3B, Data Br. 7 (2016) 1665–1669. https://doi.org/10.1016/j.dib.2016.04.058.

[66] B. Shuang, J. Chen, L. Kisley, C.F. Landes, Troika of single particle tracking programing: SNR enhancement, particle identification, and mapping, Phys. Chem. Chem. Phys. 16 (2014) 624–634. https://doi.org/10.1039/c3cp53968g.

[67] E. Meijering, O. Dzyubachyk, I. Smal, Methods for cell and particle tracking, 1st ed., Elsevier Inc., 2012. https://doi.org/10.1016/B978-0-12-391857-4.00009-4.

[68] N. Schwenzer, H. Bussmann, S. Franken, H. Haeberlein, Live-cell single-molecule analysis of β2-adrenergic receptor diffusion dynamics and confinement, BioRxiv. 3 (2018). https://doi.org/10.1101/406488.

[69] T.B. Üstün, J.L. Ayuso-Mateos, S. Chatterji, C. Mathers, C.J.L. Murray, Global burden of depressive disorders in the year 2000, Br. J. Psychiatry. 184 (2004) 386–392. https://doi.org/10.1192/bjp.184.5.386.

[70] C.D. Mathers, D. Loncar, Projections of global mortality and burden of disease from 2002 to 2030, PLoS Med. 3 (2006) 2011–2030. https://doi.org/10.1371/journal.pmed.0030442.

[71] R. Faria, M.M. Santana, C.A. Aveleira, C. Simões, E. Maciel, T. Melo, D. Santinha, M.M. Oliveira, F. Peixoto, P. Domingues, C. Cavadas, M.R.M. Domingues, Alterations in phospholipidomic profile in the brain of mouse model of depression induced by chronic unpredictable stress, Neuroscience. 273 (2014) 1–11. https://doi.org/10.1016/j.neuroscience.2014.04.042.

[72] E.H. Turner, A.M. Matthews, E. Linardatos, R.A. Tell, R. Rosenthal, Selective Publication of Antidepressant Trials and Its Influence on Apparent Efficacy, N. Engl. J. Med. 358 (2008) 252–260. https://doi.org/10.1056/NEJMsa065779.

[73] C. Herbal, M. On, H. Perforatum, Committee on Herbal Medicinal Products (HMPC), Community Herbal Monograph on Hypericum Perforatum L., Herba (Well-established medicinal use), Reproduction. (2009) 1–9. https://doi.org/EMA/HMPC/101304/2008.

[74] U. Kientsch, S. Bürgi, C. Ruedeberg, S. Probst, U.E. Honegger, St. John's wort extract Ze 117 (Hypericum perforatum) inhibits norepinephrine and serotonin uptake into rat brain slices and reduces β-adrenoceptor numbers on cultured rat brain cells, Pharmacopsychiatry. 34 (2001) 56–60. https://doi.org/10.1055/s-2001-15452.

[75] C. Ménard, G.E. Hodes, S.J. Russo, Pathogenesis of depression: Insights from human and rodent studies, Neuroscience. 321 (2016) 138–162. https://doi.org/10.1016/j.neuroscience.2015.05.053.

[76] S. Hebbar, E. Lee, M. Manna, S. Steinert, G.S. Kumar, M. Wenk, T. Wohland, R. Kraut, A fluorescent sphingolipid binding domain peptide probe interacts with sphingolipids and cholesterol-dependent raft domains[s], J. Lipid Res. 49 (2008) 1077–1089. https://doi.org/10.1194/jlr.M700543-JLR200.

[77] R. Zidovetzki, I. Levitan, Use of cyclodextrins to manipulate plasma membrane cholesterol content: Evidence, misconceptions and control strategies, Biochim. Biophys. Acta - Biomembr. 1768 (2007) 1311–1324. https://doi.org/10.1016/j.bbamem.2007.03.026.

[78] Q. Chen, J. Amaral, P. Biancani, J. Behar, Excess membrane cholesterol alters human gallbladder muscle contractility and membrane fluidity, Gastroenterology. 116 (1999) 678–685. https://doi.org/10.1016/S0016-5085(99)70190-3.

[79] B. Kraus, H. Wolff, J. Heilmann, E.F. Elstner, Influence of Hypericum perforatum extract and its single compounds on amyloid-β mediated toxicity in microglial cells, Life Sci. 81 (2007) 884–894. https://doi.org/10.1016/j.lfs.2007.07.020.

[80] R.J.T. Mocking, J. Assies, H.G. Ruhé, A.H. Schene, Focus on fatty acids in the neurometabolic pathophysiology of psychiatric disorders, J. Inherit. Metab. Dis. 41 (2018) 597–611. https://doi.org/10.1007/s10545-018-0158-3.

[81] X. Liu, J. Li, P. Zheng, X. Zhao, C. Zhou, C. Hu, X. Hou, H. Wang, P. Xie, G. Xu, Plasma lipidomics reveals potential lipid markers of major depressive disorder, Anal. Bioanal. Chem. 408 (2016) 6497–6507. https://doi.org/10.1007/s00216-016-9768-5.

[82] E.Y. Kim, J.W. Lee, M.Y. Lee, S.H. Kim, H.J. Mok, K. Ha, Y.M. Ahn, K.P. Kim, Serum lipidomic analysis for the discovery of biomarkers for major depressive disorder in drug-free patients, Psychiatry Res. 265 (2018) 174–182. https://doi.org/10.1016/j.psychres.2018.04.029.

[83] Y. Otoki, M. Hennebelle, A.J. Levitt, K. Nakagawa, W. Swardfager, A.Y. Taha, Plasma Phosphatidylethanolamine and Triacylglycerol Fatty Acid Concentrations are Altered in Major Depressive Disorder Patients with Seasonal Pattern, Lipids. 52 (2017) 559–571. https://doi.org/10.1007/s11745-017-4254-1.

[84] E. Lattka, T. Illig, J. Heinrich, B. Koletzko, Do FADS genotypes enhance our knowledge about fatty acid related phenotypes?, Clin. Nutr. 29 (2010) 277–287. https://doi.org/10.1016/j.clnu.2009.11.005.

[85] F. Tosi, F. Sartori, P. Guarini, O. Olivieri, N. Martinelli, Delta-5 and Delta-6 Desaturases: Crucial Enzymes in Polyunsaturated Fatty Acid-Related Pathways with Pleiotropic Influences in Health and Disease, in: Adv. Exp. Med. Biol., 2014: pp. 61–81. https://doi.org/10.1007/978-3-319-07320-0_7.

[86] H.P. Cho, M.T. Nakamura, S.D. Clarke, Cloning, expression, and nutritional regulation of the mammalian Δ-6 desaturase, J. Biol. Chem. 274 (1999) 471–477. https://doi.org/10.1074/jbc.274.1.471.

[87] M.G. Obukowicz, D.J. Welsch, W.J. Salsgiver, C.L. Martin-Berger, K.S. Chinn, K.L. Duffin, A. Raz, P. Needleman, Novel, selective Δ6 or Δ5 fatty acid desaturase inhibitors as antiinflammatory agents in mice, J. Pharmacol. Exp. Ther. 287 (1998) 157–166. https://doi.org/10.1007/bf02562269.

[88] R.J.T. Mocking, T.S. Nap, A.M. Westerink, J. Assies, F.M. Vaz, M.W.J. Koeter, H.G. Ruhé, A.H. Schene, Biological profiling of prospective antidepressant response in major depressive disorder: Associations with (neuro)inflammation, fatty acid metabolism, and amygdala-reactivity, Psychoneuroendocrinology. 79 (2017) 84–92. https://doi.org/10.1016/j.psyneuen.2017.02.019.

[89] A.C. Sevastre-Berghian, V.A. Toma, B. Sevastre, D. Hanganu, L. Vlase, D. Benedec, I. Oniga, I. Baldea, D. Olteanu, R. Moldovan, N. Decea, G.A. Filip, S. V. Clichici, Characterization and biological effects of hypericum extracts on experimentally-induced - Anxiety, oxidative stress and inflammation in rats, J. Physiol. Pharmacol. 69 (2018) 789–800. https://doi.org/10.26402/jpp.2018.5.13.

[90] C.L. Raison, L. Capuron, A.H. Miller, Cytokines sing the blues: Inflammation and the pathogenesis of depression, Trends Immunol. 27 (2006) 24–31. https://doi.org/10.1016/j.it.2005.11.006.

[91] R. Marion-Letellier, G. Savoye, S. Ghosh, Polyunsaturated fatty acids and inflammation, IUBMB Life. 67 (2015) 659–667. https://doi.org/10.1002/iub.1428.

[92] R.K. McNamara, R. Jandacek, T. Rider, P. Tso, A. Cole-Strauss, J.W. Lipton, Differential effects of antipsychotic medications on polyunsaturated fatty acid biosynthesis in rats: Relationship with liver delta6-desaturase expression, Schizophr. Res. 129 (2011) 57–65. https://doi.org/10.1016/j.schres.2011.03.006.

[93] R. Colle, D. De Larminat, S. Rotenberg, F. Hozer, P. Hardy, C. Verstuyft, B. Fève, E. Corruble, PPAR-γ Agonists for the Treatment of Major Depression: A Review, Pharmacopsychiatry. 50 (2017) 49–55. https://doi.org/10.1055/s-0042-120120.

[94] Z. Ament, J.A. West, E. Stanley, T. Ashmore, L.D. Roberts, J. Wright, A.W. Nicholls, J.L. Griffin, PPAR-pan activation induces hepatic oxidative stress and lipidomic remodelling, Free Radic. Biol. Med. 95 (2016) 357–368. https://doi.org/10.1016/j.freeradbiomed.2015.11.033.

[95] D.M. Abd El Motteleb, D.I. Abd El Aleem, Renoprotective effect of Hypericum perforatum against diabetic nephropathy in rats: Insights in the underlying mechanisms, Clin. Exp. Pharmacol. Physiol. 44 (2017) 509–521. https://doi.org/10.1111/1440-1681.12729.

[96] T. Hatano, Y. Sameshima, M. Kawabata, S. Yamada, K. Shinozuka, T. Nakabayashi, H. Mizuno, St. John's Wort Promotes Adipocyte Differentiation and Modulates NF-κB Activation in 3T3-L1 Cells, Biol. Pharm. Bull. 37 (2014) 1132–1138. https://doi.org/10.1248/bpb.b13-00989.

[97] S. Krusekopf, I. Roots, St. John's wort and its constituent hyperforin concordantly regulate expression of genes encoding enzymes involved in basic cellular pathways, Pharmacogenet. Genomics. 15 (2005) 817–829. https://doi.org/10.1097/01.fpc.0000175597.60066.3d.

[98] T.G. Oliveira, R.B. Chan, F. V. Bravo, A. Miranda, R.R. Silva, B. Zhou, F. Marques, V. Pinto, J.J. Cerqueira, G. Di Paolo, N. Sousa, The impact of chronic stress on the rat brain lipidome, Mol. Psychiatry. 21 (2016) 80–88. https://doi.org/10.1038/mp.2015.14.

[99] A. Demirkan, A. Isaacs, P. Ugocsai, G. Liebisch, M. Struchalin, I. Rudan, J.F. Wilson, P.P. Pramstaller, U. Gyllensten, H. Campbell, G. Schmitz, B.A. Oostra, C.M. van Duijn, Plasma phosphatidylcholine and sphingomyelin concentrations are associated with depression and anxiety symptoms in a Dutch family-based lipidomics study, J. Psychiatr. Res. 47 (2013) 357–362. https://doi.org/10.1016/j.jpsychires.2012.11.001.

[100] A.A. Farooqui, L.A. Horrocks, Brain phospholipases A2: A perspective on the history, Prostaglandins Leukot. Essent. Fat. Acids. 71 (2004) 161–169. https://doi.org/10.1016/j.plefa.2004.03.004.

[101] M.A. de la Rosa Rodriguez, S. Kersten, Regulation of lipid droplet-associated proteins by peroxisome proliferator-activated receptors, Biochim. Biophys. Acta - Mol. Cell Biol. Lipids. 1862 (2017) 1212–1220. https://doi.org/10.1016/j.bbalip.2017.07.007.

[102] T. Varga, Z. Czimmerer, L. Nagy, PPARs are a unique set of fatty acid regulated transcription factors controlling both lipid metabolism and inflammation, Biochim. Biophys. Acta - Mol. Basis Dis. 1812 (2011) 1007–1022. https://doi.org/10.1016/j.bbadis.2011.02.014.

[103] J.E. Burke, E.A. Dennis, Phospholipase A 2 structure/function, mechanism, and signaling, J. Lipid Res. 50 (2009) 237–242. https://doi.org/10.1194/jlr.R800033-JLR200.

[104] L.H.W. Lee, G. Shui, A.A. Farooqui, M.R. Wenk, C.H. Tan, W.Y. Ong, Lipidomic analyses of the mouse brain after antidepressant treatment: Evidence for endogenous release of long-chain fatty acids?, Int. J. Neuropsychopharmacol. 12 (2009) 953–964. https://doi.org/10.1017/S146114570900995X.

[105] L.H.W. Lee, C.H. Tan, G. Shui, M.R. Wenk, W.Y. Ong, Role of prefrontal cortical calcium independent phospholipase A2 in antidepressant-like effect of maprotiline, Int. J. Neuropsychopharmacol. 15 (2012) 1087–1098. https://doi.org/10.1017/S1461145711001234.

[106] M.C.J. Chang, C.R. Jones, Chronic lithium treatment decreases brain phospholipase A2 activity, Neurochem. Res. 23 (1998) 887–892. https://doi.org/10.1023/A:1022415113421.

[107] X.M. Feng, J. Xiong, H. Qin, W. Liu, R.N. Chen, W. Shang, R. Ning, G. Hu, J. Yang, Fluoxetine Induces Hepatic Lipid Accumulation Via Both Promotion of the SREBP1c-Related Lipogenesis and Reduction of Lipolysis in Primary Mouse Hepatocytes, CNS Neurosci. Ther. 18 (2012) 974–980. https://doi.org/10.1111/cns.12014.

[108] D. Eberlé, B. Hegarty, P. Bossard, P. Ferré, F. Foufelle, SREBP transcription factors: Master regulators of lipid homeostasis, Biochimie. 86 (2004) 839–848. https://doi.org/10.1016/j.biochi.2004.09.018.

[109] M.B. Raeder, J. Fernø, M. Glambek, C. Stansberg, V.M. Steen, Antidepressant drugs activate SREBP and up-regulate cholesterol and fatty acid biosynthesis in human glial cells, Neurosci. Lett. 395 (2006) 185–190. https://doi.org/10.1016/j.neulet.2005.10.096.

[110] S. Jacobs, P. Cuatrecasas, The mobile receptor hypothesis for cell membrane receptor action, Trends Biochem. Sci. 2 (1977) 280–282. https://doi.org/10.1016/0968-0004(77)90281-X.

[111] A. Kusumi, Y. Sako, Cell surface organization by the membrane skeleton, Curr. Opin. Cell Biol. 8 (1996) 566–574. https://doi.org/10.1016/S0955-0674(96)80036-6.

[112] T. Fujiwara, K. Ritchie, H. Murakoshi, K. Jacobson, A. Kusumi, Phospholipids undergo hop diffusion in compartmentalized cell membrane, J. Cell Biol. 157 (2002) 1071–1081. https://doi.org/10.1083/jcb.200202050.

[113] V.O. Rybin, X. Xu, M.P. Lisanti, S.F. Steinberg, Differential targeting of β-adrenergic receptor subtypes and adenylyl cyclase to cardiomyocyte caveolae: A mechanism to functionally regulate the cAMP signaling pathway, J. Biol. Chem. 275 (2000) 41447–41457. https://doi.org/10.1074/jbc.M006951200.

[114] T. Sungkaworn, M.-L. Jobin, K. Burnecki, A. Weron, M.J. Lohse, D. Calebiro, Single-molecule imaging reveals receptor–G protein interactions at cell surface hot spots, Nature. (2017). https://doi.org/10.1038/nature24264.

[115] J. Ibach, Y. Radon, M. Gelléri, M.H. Sonntag, L. Brunsveld, P.I.H.H. Bastiaens, P.J. Verveer, Single particle tracking reveals that EGFR signaling activity is amplified in clathrin-coated pits, PLoS One. 10 (2015) 1–22. https://doi.org/10.1371/journal.pone.0143162.

[116] I. Chung, R. Akita, R. Vandlen, D. Toomre, J. Schlessinger, I. Mellman, Spatial control of EGF receptor activation by reversible dimerization on living cells, Nature. 464 (2010) 783–787. https://doi.org/10.1038/nature08827.

[117] R. Das, C.W. Cairo, D. Coombs, A hidden Markov model for single particle tracks quantifies dynamic interactions between LFA-1 and the actin cytoskeleton, PLoS Comput. Biol. 5 (2009). https://doi.org/10.1371/journal.pcbi.1000556.

[118] D.S. English, K. Das, K.D. Ashby, J. Park, J.W. Petrich, E.W. Castner, Confirmation of excited-state proton transfer and ground-state heterogeneity in hypericin by fluorescence upconversion, J. Am. Chem. Soc. 119 (1997) 11585–11590. https://doi.org/10.1021/ja9721071.

[119] T.J. Pucadyil, A. Chattopadhyay, Cholesterol depletion induces dynamic confinement of the G-protein coupled serotonin1A receptor in the plasma membrane of living cells, Biochim. Biophys. Acta - Biomembr. 1768 (2007) 655–668. https://doi.org/10.1016/j.bbamem.2007.01.002.

[120] H. Singh, N. Wray, J.M. Schappi, M.M. Rasenick, Disruption of lipid-raft localized Gαs/tubulin complexes by antidepressants: A unique feature of HDAC6 inhibitors, SSRI and tricyclic compounds, Neuropsychopharmacology. 43 (2018) 1481–1491. https://doi.org/10.1038/s41386-018-0016-x.

[121] R.J. Donati, M.M. Rasenick, Chronic antidepressant treatment prevents accumulation of Gsα in cholesterol-rich, cytoskeletal-associated, plasma membrane domains (lipid rafts), Neuropsychopharmacology. 30 (2005) 1238–1245. https://doi.org/10.1038/sj.npp.1300697.

[122] R.J. Donati, Y. Dwivedi, R.C. Roberts, R.R. Conley, G.N. Pandey, M.M. Rasenick, Postmortem brain tissue of depressed suicides reveals increased Gsα localization in lipid raft domains where it is less likely to activate adenylyl cyclase, J. Neurosci. 28 (2008) 3042–3050. https://doi.org/10.1523/JNEUROSCI.5713-07.2008.

[123] S.F. Steinberg, β2-Adrenergic receptor signaling complexes in cardiomyocyte caveolae/lipid rafts, J. Mol. Cell. Cardiol. 37 (2004) 407–415. https://doi.org/10.1016/j.yjmcc.2004.04.018.

[124] W. Liang, P.K. Curran, Q. Hoang, R.T. Moreland, P.H. Fishman, Differences in endosomal targeting of human β1- and β2-adrenergic receptors following clathrin-mediated endocytosis, J. Cell Sci. 117 (2004) 723–734. https://doi.org/10.1242/jcs.00878.

[125] S.A. Green, B.D. Holt, S.B. Liggett, Beta 1- and beta 2-adrenergic receptors display subtype-selective coupling to Gs., Mol. Pharmacol. 41 (1992) 889–93. http://www.ncbi.nlm.nih.gov/pubmed/1350321.

[126] M. Shadrina, E.A. Bondarenko, P.A. Slominsky, Genetics factors in major depression disease, Front. Psychiatry. 9 (2018) 1–18. https://doi.org/10.3389/fpsyt.2018.00334.

[127] L.J. Steinberg, M.D. Underwood, M.J. Bakalian, S.A. Kassir, J.J. Mann, V. Arango, 5-HT1A receptor, 5-HT2A receptor and serotonin transporter binding in the human auditory cortex in depression, J. Psychiatry Neurosci. 44 (2019) 294–302. https://doi.org/10.1503/jpn.180190.

[128] G. Deacon, C. Kettle, D. Hayes, C. Dennis, J. Tucci, Omega 3 polyunsaturated fatty acids and the treatment of depression, Crit. Rev. Food Sci. Nutr. 57 (2017) 212–223. https://doi.org/10.1080/10408398.2013.876959.

[129] L.B. Dehn, T. Beblo, Depressed, biased, forgetful: The interaction of emotional and cognitive dysfunctions in depression, Neuropsychiatrie. 33 (2019) 123–130. https://doi.org/10.1007/s40211-019-0307-4.

# 8 Danksagung

An dieser Stelle sollen all die jenigen Erwähnung finden, die wesentlich zum Gelingen dieser Arbeit beigetragen haben. Ich bedanke mich ganz herzlich bei

Prof. Dr. Hanns Häberlein, dafür, dass ich diese Arbeit unter seiner Leitung anfertigen durfte, die freundschaftliche Atmosphäre in seinem Arbeitskreis und seinen engagierten Einsatz.

Prof. Dr. Gabriele König für die freundliche Übernahme des Koreferats.

PD Dr. Sebastian Franken für die vielen guten Ideen, hilfreichen Diskussionen, sowie wertvollen Ratschläge.

der Firma Max Zeller Söhne AG aus Romanshorn, Prof. Dr. Veronika Butterweck und Dr. Georg Boonen für die finanzielle Unterstützung dieser Arbeit.

PD Dr. Jan-Peter Siebrasse für die wertvollen Diskussionen zum Thema Einzelmolekülmikroskopie und dafür, dass es mir möglich war, Fluoreszenz-Anistropie-Messungen durchzuführen.

Niko, ohne den die Etablierung der Matlab-Skripte nicht möglich gewesen wäre.

meinen Arbeitskollegen in der Arbeitsgruppe Häberlein, für die gute Hilfe und den freundschaftlichen Umgang miteinander und den vielen Spaß innerhalb und außerhalb der Labore.

allen Mitarbeitern des Instituts für die gute Zusammenarbeit.

Elisabeth Kruse, für die verwandtschaftliche Hilfe am Ende dieser Arbeit.

meinen Eltern Werner und Marlene, meinen Geschwistern Anke und Johannes und all den neuen Familienmitgliedern in meiner schönen Heimat für die Unterstützung zu jeder Zeit.

meinen Freunden aus Bonn für die schöne gemeinsame Zeit in unserer gemeinsamen Wahlheimat.

Und Antonia, für den ganzen Rest.